

QC852  
C6  
ATSL

no. 326

# GESTROPHIC ADJUSTMENT IN A STRATIFIED ATMOSPHERE

ATMOSPHERIC SCIENCE  
LABORATORY COLLECTION

SCOTT R. FULTON  
WAYNE H. SCHUBERT



Atmospheric Science  
PAPER NO.

ATMOSPHERIC SCIENCE  
LABORATORY COLLECTION

326

US ISSN 0067-0340

DEPARTMENT OF ATMOSPHERIC SCIENCE  
COLORADO STATE UNIVERSITY  
FORT COLLINS, COLORADO

GESTROPHIC ADJUSTMENT  
IN A STRATIFIED ATMOSPHERE

by

Scott R. Fulton

Wayne H. Schubert

This research was supported by the  
Global Atmospheric Research Program,  
National Science Foundation  
under Grant Nos. ATM-7808125  
and ATM-8009799.

Department of Atmospheric Science  
Colorado State University  
Fort Collins, Colorado  
80523

August, 1980

Atmospheric Science Paper No. 326

## ABSTRACT

The geostrophic adjustment process in a compressible atmosphere with arbitrary vertical stratification is studied as an initial value problem. The governing equations are the adiabatic quasi-static equations on an  $f$ -plane linearized about a motionless basic state. A rigid lid upper boundary condition is assumed which permits the use of a discrete eigenfunction expansion in the vertical. Using Fourier transforms in the horizontal a general solution is obtained for both the transient and final states.

The general solution is evaluated for several simple experiments with axisymmetric initial conditions in the mass and vorticity fields which have horizontal variations on the tropical cloud cluster scale. These experiments assume a basic state characterized by constant static stability in log-pressure coordinates and a Coriolis parameter corresponding to  $20^{\circ}\text{N}$  latitude. Results are presented which illustrate the nature of the transient adjustment process. Comparison of the initial and final states indicates that the inclusion of vertical structure does not alter the basic conclusion from previous barotropic studies that in the tropics the mass field tends to adjust to the wind field. However, it is found that the extent of this adjustment depends strongly on the vertical structure of the initial conditions. These results are interpreted in terms of the projection of the initial conditions onto the vertical modes.

## ACKNOWLEDGEMENTS

The authors are grateful to Duane E. Stevens, James J. Hack, Pedro L. Silva Dias and Mark DeMaria for their valuable suggestions and comments on this work. We also wish to thank Odilia Panella who typed the manuscript.

The research reported here has been supported by the National Science Foundation under Grant ATM-7808125. Computer time was provided by the National Center for Atmospheric Research, which is sponsored by the National Science Foundation.

## TABLE OF CONTENTS

	<u>Page</u>
ABSTRACT .....	iii
ACKNOWLEDGEMENTS.....	iv
TABLE OF CONTENTS.....	v
1. INTRODUCTION.....	1
2. GENERAL SOLUTION.....	4
2.1 Governing equations.....	4
2.2 Solution by eigenfunction expansion in the vertical...	8
2.3 Solution of the horizontal structure equation by Fourier transforms.....	15
2.4 Potential vorticity and the final adjusted state.....	20
3. EXPERIMENTS.....	24
3.1 Basic state, phase speeds and vertical structure functions.....	24
3.2 Numerical evaluation of the solution for axisymmetric perturbations.....	33
3.3 Results.....	38
3.3.1 experiment 1: initial condition in the mass field.....	38
3.3.2 experiment 2: initial condition in the vorticity field.....	59
3.4 Discussion.....	72
4. CONCLUSIONS.....	76
REFERENCES.....	79
APPENDIX A: The nature of the phase speed spectrum.....	82
APPENDIX B: Properties of the eigenvalues and eigenfunctions.....	85
APPENDIX C: Asymptotic solution of the horizontal structure equation.....	88
APPENDIX D: Principal symbols.....	95

## 1. INTRODUCTION

A fundamental feature of the tropical atmosphere is that it is continually being perturbed away from a quasi-balanced state by sources and sinks of energy and momentum such as radiation, the release of latent heat in clouds and momentum mixing by convective scale motions. The atmosphere responds to such perturbations by developing gravity-inertia waves which carry away energy and momentum and leave behind a state of approximate pressure-wind balance. In a linearized model where the final balanced state is geostrophic this process is known as geostrophic adjustment. The objective of this research is to study the geostrophic adjustment process as it occurs in a stratified atmosphere.

As indicated in the comprehensive review of the subject by Blumen (1972), the geostrophic adjustment problem has been studied extensively. Rossby (1938) first considered the relationship between the initial unbalanced and final balanced states of a simple one-dimensional current system in an incompressible fluid. His work was later refined by Mihaljan (1963), who derived exact expressions for the solution and energetics, and extended by Cahn (1945), who considered the linear transient aspects of the problem. Obukhov (1949) first treated the adjustment of two-dimensional barotropic flows, obtaining results for both the transient and final adjusted states. Other investigations of the adjustment problem since these initial studies have included consideration of the effect of a variable Coriolis parameter (Geisler and Dickinson, 1972; Silva Dias and Schubert, 1979), the effect of a basic flow with horizontal shear (Blumen and Washington, 1969) and the effects of transient forcing (Paegle, 1978). Recently, Schubert et al. (1980) have considered the geostrophic adjustment of axisymmetric

vortices and have clarified how the horizontal scale of the initial perturbation determines the nature and energetics of the adjustment process.

The studies cited above are primarily barotropic; i.e., they utilize simple models with little or no vertical structure. In the real atmosphere, however, initial perturbations may have various vertical structures and gravity-inertia waves can propagate vertically. Thus the effects of vertical stratification must be considered in order to more fully understand the adjustment process. Several investigators have studied this problem. Some (e.g., Monin, 1958; Kibel, 1963) have obtained solutions for certain specified basic states in terms of Green's functions in three dimensions. Although this approach yields general solutions, the evaluation and interpretation of these solutions is quite difficult due to their complexity and hence few examples have been studied. Other investigations (e.g., Bolin, 1953; Fjelsted, 1958; Fischer, 1963) have utilized spectral expansions in the vertical. This spectral approach reduces the solution to a superposition of solutions of the corresponding barotropic problem (each for a different depth of incompressible fluid) and thereby simplifies both the evaluation and the interpretation of the solution. In the past this approach has been used with basic states consisting of stratified incompressible fluids and an isothermal compressible atmosphere, and again only a few examples have been studied.

In this research we extend this spectral approach to study the geostrophic adjustment of a general stratified atmosphere and present results which illustrate the important features of the adjustment process. In chapter 2 we derive a general solution to the problem;

in order to make it mathematically tractable we consider linear perturbations about a basic state at rest. A general spectral expansion is used in the vertical which allows the consideration of any basic state stratification and vertical boundary conditions, subject only to the restriction that the corresponding vertical structure problem be of the Sturm-Liouville type. The initial value problem for the horizontal structure is solved by the method of Fourier transforms to obtain Obukhov's solution. In chapter 3 the general solution is evaluated for several simple experiments with axisymmetric initial conditions, using a basic state with constant static stability in log-pressure coordinates as a reasonable first approximation to the real atmosphere. Initial conditions in both the mass and wind fields are studied, concentrating on the effects of the vertical structure of these initial conditions. In chapter 4 we discuss the implications of the results of this study for tropical dynamics and suggest topics for further investigation.

## 2. GENERAL SOLUTION

In this chapter we derive a formal solution to the problem of the transient geostrophic adjustment of a compressible atmosphere on an  $f$ -plane. We consider only the case where the vertical structure of the basic state and the boundary conditions in the vertical give rise to a countably infinite set of vertical modes with a discrete phase speed spectrum. In section 2.1 the governing equations are linearized about a motionless basic state and reduced to a single equation in the geopotential tendency. The horizontal and vertical structure of the problem are separated in section 2.2 using an eigenfunction expansion in the vertical, and the transient solutions for the various field variables are expressed as superpositions of the resulting horizontal and vertical structure functions. In section 2.3 the horizontal structure equation is solved using Fourier transforms. The final adjusted state is obtained in section 2.4 by solving the potential vorticity equation.

### 2.1 Governing equations

We consider the adiabatic motions of an inviscid, compressible atmosphere in hydrostatic balance on an  $f$ -plane. The assumption of hydrostatic balance, valid for large-scale motions (e.g., Charney, 1948), eliminates vertically propagating acoustic waves and allows the convenient use of pressure as an independent variable. We choose as the vertical coordinate the logarithm of pressure

$$z^* \equiv \ln \left( \frac{p_0}{p} \right), \quad (2.1)$$

where  $p$  is pressure and  $p_0$  is the constant surface pressure.

Neglecting the horizontal component of the earth's rotation vector

(Phillips, 1966), the horizontal momentum, mass continuity, hydrostatic and adiabatic thermodynamic equations may be written as

$$\frac{D\tilde{\mathbf{y}}}{Dt} + f\hat{\mathbf{k}}\times\tilde{\mathbf{y}} + \nabla\phi = 0, \quad (2.2a)$$

$$\frac{\partial w^*}{\partial z^*} - w^* + \nabla \cdot \tilde{\mathbf{y}} = 0, \quad (2.2b)$$

$$\frac{\partial\phi}{\partial z^*} - RT = 0, \quad (2.2c)$$

$$c_p \frac{DT}{Dt} + RTw^* = 0. \quad (2.2d)$$

Here  $t$  is time,  $\tilde{\mathbf{y}} = D\tilde{\mathbf{x}}/Dt$  is the horizontal velocity vector, where  $\tilde{\mathbf{x}}$  is the horizontal position vector,  $w^* \equiv Dz^*/Dt$  is the "vertical velocity" in log-pressure coordinates,  $\phi$  is the geopotential,  $T$  is the absolute temperature,  $\hat{\mathbf{k}}$  is the vertical unit vector,  $f$  is the constant Coriolis parameter,  $R$  and  $c_p$  are the gas constant and specific heat at constant pressure, respectively, for dry air,  $\nabla$  is the del operator at constant  $z^*$ , and

$$\frac{D}{Dt} \equiv \frac{\partial}{\partial t} + \tilde{\mathbf{y}} \cdot \nabla + w^* \frac{\partial}{\partial z^*} \quad (2.3)$$

is the time derivative following the motion.

We now linearize the system (2.2) about a motionless, horizontally homogeneous basic state. Denoting the basic state quantities by over-bars we have

$$\left. \begin{aligned} \bar{\tilde{\mathbf{y}}} &= 0, \\ \bar{w}^* &= 0, \\ \bar{\phi} &= \bar{\phi}(z^*), \\ \bar{T} &= \bar{T}(z^*), \end{aligned} \right\} \quad (2.4)$$

where  $\bar{\Phi}(z^*)$  and  $\bar{T}(z^*)$  are assumed to be specified. Requiring that (2.4) satisfy the governing equations (2.2) leads to

$$\frac{d\bar{\Phi}}{dz^*} = R\bar{T} , \quad (2.5)$$

which is the hydrostatic relation for the basic state. Denoting perturbations from the basic state (2.4) by primes, we write

$$\left. \begin{aligned} \underline{v}(\underline{x}, z^*, t) &= \underline{v}'(\underline{x}, z^*, t) , \\ w^*(\underline{x}, z^*, t) &= w^{*'}(\underline{x}, z^*, t) , \\ \Phi(\underline{x}, z^*, t) &= \bar{\Phi}(z^*) + \Phi'(\underline{x}, z^*, t) , \\ T(\underline{x}, z^*, t) &= \bar{T}(z^*) + T'(\underline{x}, z^*, t) . \end{aligned} \right\} \quad (2.6)$$

Substituting (2.6) into (2.2), making use of (2.3) and (2.5) and assuming that the perturbation amplitudes are small enough so that products of perturbation quantities may be neglected, we obtain the linearized system of governing equations

$$\frac{\partial \underline{v}}{\partial t} + f\hat{k} \times \underline{v} + \nabla \Phi' = 0 , \quad (2.7a)$$

$$\frac{\partial w^*}{\partial z^*} - w^* + \nabla \cdot \underline{v} = 0 , \quad (2.7b)$$

$$\frac{\partial \Phi'}{\partial z^*} - R T' = 0 , \quad (2.7c)$$

$$\frac{\partial T'}{\partial t} + \Gamma w^* = 0 , \quad (2.7d)$$

where

$$\Gamma(z^*) \equiv \frac{d\bar{T}(z^*)}{dz^*} + \kappa \bar{T}(z^*) \quad (2.8)$$

is the static stability parameter and  $\kappa \equiv R/c_p$ .

The system (2.7) may be reduced to a single equation in one dependent variable as follows. Applying the operators  $(\nabla \cdot)$  and

$[\hat{k} \cdot (\nabla \times \quad)]$  to (2.7a) we obtain the divergence and vorticity equations

$$\frac{\partial \delta}{\partial t} - f\zeta + \nabla^2 \Phi' = 0 \quad (2.9)$$

and

$$\frac{\partial \zeta}{\partial t} + f\delta = 0, \quad (2.10)$$

where

$$\delta \equiv \nabla \cdot \underline{y} \quad (2.11)$$

and

$$\zeta \equiv \hat{k} \cdot (\nabla \times \underline{y}) \quad (2.12)$$

are the horizontal divergence and the vertical component of relative vorticity, respectively. Eliminating the vorticity  $\zeta$  between (2.9) and (2.10) results in

$$\frac{\partial^2 \delta}{\partial t^2} + f^2 \delta + \nabla^2 \left( \frac{\partial \Phi'}{\partial t} \right) = 0. \quad (2.13)$$

Eliminating  $T'$  between (2.7c) and (2.7d) yields

$$\frac{\partial}{\partial z^*} \left( \frac{\partial \Phi'}{\partial t} \right) + R\Gamma w^* = 0. \quad (2.14)$$

Using this result to eliminate  $w^*$  in (2.7b) we obtain

$$\left( \frac{\partial}{\partial z^*} - 1 \right) \left[ \frac{1}{R\Gamma} \frac{\partial}{\partial z^*} \left( \frac{\partial \Phi'}{\partial t} \right) \right] - \delta = 0. \quad (2.15)$$

We can then use (2.15) to eliminate  $\delta$  in (2.13), obtaining

$$\left( \frac{\partial^2}{\partial t^2} + f^2 \right) \left[ \left( \frac{\partial}{\partial z^*} - 1 \right) \left[ \frac{1}{R\Gamma} \frac{\partial}{\partial z^*} \left( \frac{\partial \Phi'}{\partial t} \right) \right] + \nabla^2 \left( \frac{\partial \Phi'}{\partial t} \right) \right] = 0. \quad (2.16)$$

Finally, defining the geopotential tendency  $\chi \equiv \partial \Phi' / \partial t$  we can write the tendency equation (2.16) in the form

$$\left( \frac{\partial^2}{\partial t^2} + f^2 \right) \left[ e^{z^*} \frac{\partial}{\partial z^*} \left( \frac{e^{-z^*}}{R\Gamma} \frac{\partial \chi}{\partial z^*} \right) \right] + \nabla^2 \chi = 0. \quad (2.17)$$

In the following two sections we derive a general solution of (2.17); the initial and boundary conditions on  $\chi(x, z^*, t)$  which are necessary to guarantee the uniqueness of the solution will be discussed as they naturally arise.

## 2.2 Solution by eigenfunction expansion in the vertical

The tendency equation (2.17) may be solved by separating the horizontal and vertical dependence of  $\chi(x, z^*, t)$  as follows. First, we look for solutions of the form

$$\chi(x, z^*, t) = X(x, t) Z(z^*) \quad (2.18)$$

With this substitution (2.17) becomes

$$\left[ \left( \frac{\partial^2}{\partial t^2} + f^2 \right) X \right] \left[ e^{z^*} \frac{d}{dz^*} \left( \frac{e^{-z^*}}{R\Gamma} \frac{dZ}{dz^*} \right) \right] + Z \nabla^2 \chi = 0, \quad (2.19)$$

which may be written in the form

$$\frac{\nabla^2 \chi}{\left( \frac{\partial^2}{\partial t^2} + f^2 \right) X} = - \frac{e^{z^*} \frac{d}{dz^*} \left( \frac{e^{-z^*}}{R\Gamma} \frac{dZ}{dz^*} \right)}{Z}. \quad (2.20)$$

Since the left-hand side of (2.20) is independent of  $z^*$  while the right-hand side depends only on  $z^*$ , both sides must in fact equal a constant, which we will denote by  $c^{-2}$ . In this manner (2.20) yields two equations: the horizontal structure equation

$$\frac{\partial^2 \chi}{\partial t^2} + f^2 \chi - c^2 \nabla^2 \chi = 0 \quad (2.21)$$

and the vertical structure equation

$$\frac{d}{dz^*} \left( \frac{e^{-z^*}}{R\Gamma} \frac{dZ}{dz^*} \right) + \frac{e^{-z^*}}{c^2} Z = 0. \quad (2.22)$$

Given the basic state stability profile  $\Gamma(z^*)$  and any suitable boundary conditions, the vertical structure equation (2.22) forms an eigenvalue problem with eigenvalue  $c^{-2}$  and eigenfunction  $Z(z^*)$ . We will refer to  $Z(z^*)$  as a vertical structure function and  $c$  as the phase speed associated with it; the motivation for the term phase speed will be clarified below. The set of phase speeds  $c$  for which (2.22) has non-trivial solutions  $Z(z^*)$  will be referred to as the phase speed spectrum. As discussed in Appendix A, this set may be empty, finite, countably infinite or uncountably infinite, depending on the boundary conditions in the vertical and the vertical structure of the basic state as expressed by  $\Gamma(z^*)$ .

In this study only the case where the phase speed spectrum is countably infinite will be considered. As a particular example of this case we consider the following boundary conditions. At the lower boundary we require that  $w=0$ , where  $w \equiv Dz/Dt$  is the vertical velocity in height coordinates and  $z \equiv \Phi/g$  is the geopotential height. If the earth's surface is taken to be flat, this condition should be applied at  $z=0$ . This is difficult to do in log-pressure coordinates because in general  $z=0$  does not coincide with a  $z^*$  surface. Therefore, following Monin (1958) and Siebert (1961), we will apply the approximate lower boundary condition

$$w = 0 \quad \text{at} \quad z^* = 0. \quad (2.23)$$

The validity of the approximation involved in (2.23) was discussed in some detail by Kibel (1963). An upper boundary condition which reflects vertically propagating waves is necessary to guarantee that the phase speed spectrum be discrete. For concreteness, we choose the "rigid lid" condition

$$w^* = 0 \quad \text{at} \quad z^* = z_{\Gamma}^* , \quad (2.24)$$

where  $z_{\Gamma}^*$  is finite. The significance of such an upper boundary condition and its implications for the application of the results of this study to the real atmosphere will be briefly discussed in chapter 4.

The boundary conditions (2.23) and (2.24) can be expressed in terms of  $\chi$  and then applied to  $Z$  as follows. First,  $w$  is expressed in terms of  $\phi$  according to  $w = (1/g)(D\phi/Dt)$  using (2.3) and the resulting expression is linearized to obtain

$$w = \frac{1}{g} \left( \chi + w^* \frac{d\bar{\phi}}{dz^*} \right) . \quad (2.25)$$

Substituting for  $w^*$  from (2.14) and using the hydrostatic relation (2.5) reduces (2.25) to the form

$$w = \frac{1}{g} \left( \chi - \frac{\bar{\Gamma}}{\Gamma} \frac{\partial \chi}{\partial z^*} \right) . \quad (2.26)$$

Then using (2.26) the lower boundary condition (2.23) may be written as

$$\frac{\partial \chi}{\partial z^*} - \frac{\Gamma}{\bar{\Gamma}} \chi = 0 \quad \text{at} \quad z^* = 0 . \quad (2.27)$$

Also, the upper boundary condition (2.24) may be expressed using (2.14) as

$$\frac{\partial \chi}{\partial z^*} = 0 \quad \text{at} \quad z^* = z_{\Gamma}^* . \quad (2.28)$$

Finally, substituting from (2.18) for  $\chi$  in (2.27) and (2.28), we see that  $Z$  must satisfy the boundary conditions

$$\frac{dZ}{dz^*} - \frac{\Gamma}{\bar{\Gamma}} Z = 0 \quad \text{at} \quad z^* = 0 \quad (2.29)$$

and

$$\frac{dZ}{dz^*} = 0 \quad \text{at} \quad z^* = z_{\Gamma}^* . \quad (2.30)$$

With the static stability  $\Gamma(z^*)$  specified as a function which is both positive and continuously differentiable for  $0 \leq z^* \leq z_T^*$ , the vertical structure equation (2.22) with the boundary conditions (2.29) and (2.30) (or any other linear homogeneous boundary conditions) forms a boundary value problem of the Sturm-Liouville type. This guarantees (Morse and Feshbach, 1953) that the phase speed spectrum is countably infinite and that the phase speeds  $c_0, c_1, \dots, c_n, \dots$  are real and can be ordered as  $c_0 > c_1 > \dots > c_n > \dots > 0$ . The corresponding vertical structure functions  $Z_n(z^*)$  then satisfy (2.22) for each  $n$ ; that is,

$$\frac{d}{dz^*} \left( \frac{e^{-z^*}}{R\Gamma} \frac{dZ_n}{dz^*} \right) + \frac{e^{-z^*}}{c_n^2} Z_n = 0, \quad n = 0, 1, 2, \dots \quad (2.31)$$

In Appendix B it is shown that the  $Z_n(z^*)$  may be made to satisfy the orthonormality condition

$$\int_0^{z_T^*} Z_n(z^*) Z_m^\dagger(z^*) e^{-z^*} dz^* = \delta_{mn}, \quad (2.32)$$

where the dagger (+) denotes complex conjugation and  $\delta_{mn}$  is the Kronecker delta. It can also be shown (Titchmarsh, 1962) that the vertical structure functions form a complete set, in the sense that any sufficiently smooth function of  $z^*$  which satisfies the boundary conditions (2.29) and (2.30) may be represented as a unique series combination of the  $Z_n(z^*)$ .

The properties of the vertical structure functions discussed above allow the tendency equation (2.17) to be solved as follows. First, we expand  $\chi(\underline{x}, z^*, t)$  in terms of the  $Z_n(z^*)$  as

$$\chi(\underline{x}, z^*, t) = \sum_{n=0}^{\infty} \chi_n(\underline{x}, t) Z_n(z^*), \quad (2.33)$$

where the coefficients  $X_n(x, t)$  in this series will be referred to as horizontal structure functions. Substituting (2.33) into (2.17) we obtain

$$\sum_{n=0}^{\infty} \left\{ \left[ \left( \frac{\partial^2}{\partial t^2} + f^2 \right) X_n \right] \left[ e^{z^*} \frac{d}{dz^*} \left( \frac{e^{-z^*}}{R\Gamma} \frac{dZ_n}{dz^*} \right) \right] + Z_n \nabla^2 X_n \right\} = 0 . \quad (2.34)$$

Using (2.31) we can write (2.34) in the form

$$\sum_{n=0}^{\infty} \left( \frac{\partial^2 X_n}{\partial t^2} + f^2 X_n - c_n^2 \nabla^2 X_n \right) Z_n = 0 . \quad (2.35)$$

Then to show that the coefficient of  $Z_n$  in this series vanishes identically for each  $n$ , we multiply (2.35) by  $Z_m^\dagger(z^*)e^{-z^*}$  and integrate from  $z^*=0$  to  $z^*=z_T^*$  and use the orthonormality property (2.32) of the  $Z_n$  to obtain

$$\frac{\partial^2 X_n}{\partial t^2} + f^2 X_n - c_n^2 \nabla^2 X_n = 0 , \quad n = 0, 1, 2, \dots , \quad (2.36)$$

where we have replaced  $m$  by  $n$  as a final step. Thus the horizontal structure functions  $X_n(x, t)$  appearing in (2.33) are found by solving the horizontal structure equation (2.36) for each  $n$ .

Equation (2.36) is identical to the one obtained for the problem of geostrophic adjustment in the divergent barotropic model (i.e., the shallow water equations) on an  $f$ -plane, with the phase speed of a pure gravity wave in that model replaced by the "phase speed"  $c_n$ . Thus the constant  $c_n$  corresponds to the phase speed of a pure gravity wave (i.e., the short wavelength limit) with vertical structure  $Z_n(z^*)$  in the stratified atmosphere. This is the motivation behind the choice of the form and name for the separation constant in (2.20). In the literature the phase speed  $c_n$  is often expressed in terms of an

"equivalent depth"  $h_n$  defined by  $c_n^2 = gh_n$ , following Taylor (1936) who was the first to discuss the existence of these vertical modes in a general context.

Once we have solved (2.31) and (2.36) for  $Z_n(z^*)$  and  $X_n(x, t)$ , respectively, these solutions may be combined according to (2.33) to obtain  $\chi(x, z^*, t)$ . The other physical fields of interest can then be obtained by substituting (2.33) into (2.14) and (2.26) and making use of (2.7b), (2.7d), (2.10), (2.31) and the definition of  $\chi$ . In this manner we obtain the following series representations:

$$\delta(x, z^*, t) = - \sum_{n=0}^{\infty} \frac{X_n(x, t)}{c_n^2} Z_n(z^*), \quad (2.37)$$

$$\zeta(x, z^*, t) = f \sum_{n=0}^{\infty} \frac{Y_n(x, t)}{c_n^2} Z_n(z^*) + \zeta(x, z^*, 0), \quad (2.38)$$

$$\Phi'(x, z^*, t) = \sum_{n=0}^{\infty} Y_n(x, t) Z_n(z^*) + \Phi'(x, z^*, 0), \quad (2.39)$$

$$T'(x, z^*, t) = \frac{1}{R} \sum_{n=0}^{\infty} Y_n(x, t) \frac{dZ_n(z^*)}{dz^*} + T'(x, z^*, 0), \quad (2.40)$$

$$w^*(x, z^*, t) = - \frac{1}{R\Gamma(z^*)} \sum_{n=0}^{\infty} X_n(x, t) \frac{dZ_n(z^*)}{dz^*}, \quad (2.41)$$

$$w(x, z^*, t) = \frac{1}{g} \sum_{n=0}^{\infty} X_n(x, t) \left[ Z_n(z^*) - \frac{\bar{T}(z^*)}{\Gamma(z^*)} \frac{dZ_n(z^*)}{dz^*} \right]. \quad (2.42)$$

Here

$$T'(x, z^*, 0) = \frac{1}{R} \frac{\partial}{\partial z^*} [\Phi'(x, z^*, 0)] \quad (2.43)$$

and we have introduced the additional horizontal structure functions  $Y_n(\underline{x}, t)$  defined by

$$Y_n(\underline{x}, t) \equiv \int_0^t X_n(\underline{x}, \tau) d\tau, \quad n = 0, 1, 2, \dots \quad (2.44)$$

The horizontal velocity field  $\underline{v}(\underline{x}, z^*, t)$  can be obtained from  $\delta(\underline{x}, z^*, t)$  and  $\zeta(\underline{x}, z^*, t)$  using (2.11) and (2.12); the details of this calculation will depend on the horizontal coordinate system chosen.

It can be seen from (2.38)-(2.40) that initial conditions are needed on  $\zeta$ ,  $\Phi'$ , and  $T'$ , in addition to those on  $X_n$  and  $\partial X_n / \partial t$  required for the solution of (2.36). All of these initial conditions can be easily obtained as follows. We assume that the initial wind  $\underline{v}(\underline{x}, z^*, 0)$  and perturbation temperature  $T'(\underline{x}, z^*, 0)$  are specified, as is consistent with the original system of equations (2.7). Then  $\Phi'(\underline{x}, z^*, 0)$  is obtained from  $T'(\underline{x}, z^*, 0)$  by integrating (2.43) in  $z^*$ , and  $\zeta(\underline{x}, z^*, 0)$  is obtained from  $\underline{v}(\underline{x}, z^*, 0)$  using (2.12). Also, from (2.11) and (2.9) we have

$$\delta(\underline{x}, z^*, 0) = \nabla \cdot [\underline{v}(\underline{x}, z^*, 0)] \quad (2.45)$$

and

$$\frac{\partial \delta}{\partial t}(\underline{x}, z^*, 0) = f\zeta(\underline{x}, z^*, 0) - \nabla^2[\Phi'(\underline{x}, z^*, 0)] \quad (2.46)$$

To relate these expressions to the initial conditions which are needed on  $X_n$ , we multiply (2.37) by  $Z_m^\dagger(z^*)e^{-z^*}$  and integrate from  $z^* = 0$  to  $z^* = z_T^*$  to obtain

$$\chi_n(\underline{x}, t) = -c_n^2 \int_0^{z_T^*} \delta(\underline{x}, z^*, t) Z_n^\dagger(z^*) e^{-z^*} dz^*, \quad (2.47)$$

where we have replaced  $m$  by  $n$  as a final step. Then evaluating (2.47) and its time derivative at  $t=0$  and substituting from (2.45) and (2.46) we obtain

$$\chi_n(\underline{x}, 0) = -c_n^2 \int_0^{z_T^*} \nabla \cdot [\underline{v}(\underline{x}, z^*, 0)] Z_n^\dagger(z^*) e^{-z^*} dz^* \quad (2.48)$$

and

$$\frac{\partial \chi_n}{\partial t}(\underline{x}, 0) = -c_n^2 \int_0^{z_T^*} \left\{ f_\zeta(\underline{x}, z^*, 0) - \nabla^2 [\Phi'(\underline{x}, z^*, 0)] \right\} Z_n^\dagger(z^*) e^{-z^*} dz^*. \quad (2.49)$$

The initial conditions (2.48) and (2.49) allow us to solve (2.36) for  $\chi_n(\underline{x}, t)$ . In the next section we show how this solution may be derived.

### 2.3 Solution of the horizontal structure equation by Fourier transforms

A solution of the horizontal structure equation (2.36) was first presented by Obukhov (1949). In that study the equations of motion were averaged in the vertical, and as a result the coefficient of the last term of (2.36) was defined differently than the phase speed  $c_n$  defined above. In this section we show how Obukhov's solution of the horizontal structure equation may be obtained by the method of Fourier transforms. This method of solution helps to clarify some aspects of the adjustment process.

For this derivation it is convenient to use the rectangular coordinates  $(x, y)$  in the horizontal, in which (2.36) becomes

$$\left( \frac{\partial^2}{\partial t^2} + f^2 \right) \chi_n(x, y, t) - c_n^2 \left( \frac{\partial^2}{\partial x^2} + \frac{\partial^2}{\partial y^2} \right) \chi_n(x, y, t) = 0 . \quad (2.50)$$

Now for any function  $\psi(x, y)$  we define the Fourier transform (denoted by a tilde) as

$$\tilde{\psi}(k, \ell) = \frac{1}{2\pi} \int_{-\infty}^{\infty} \int_{-\infty}^{\infty} \psi(x, y) e^{i(kx + \ell y)} dx dy . \quad (2.51)$$

This transform exists, and satisfies the inversion theorem

$$\psi(x, y) = \frac{1}{2\pi} \int_{-\infty}^{\infty} \int_{-\infty}^{\infty} \tilde{\psi}(k, \ell) e^{-i(kx + \ell y)} dk d\ell , \quad (2.52)$$

if  $\psi(x, y)$  is piecewise continuously differentiable in both  $x$  and  $y$  and absolutely integrable over all  $x$  and  $y$  (Sneddon, 1972). We assume that  $\chi_n(x, y, t)$  satisfies these conditions. This is reasonable because as a physical field it should be suitably smooth, and as a perturbation quantity it must vanish outside a region of finite horizontal extent at any finite time if the perturbation is of finite horizontal extent initially and propagates outward at a finite speed. Then transforming (2.50) according to (2.51) we obtain

$$\left( \frac{\partial^2}{\partial t^2} + f^2 \right) \tilde{\chi}_n(k, \ell, t) = \frac{c_n^2}{2\pi} \int_{-\infty}^{\infty} \int_{-\infty}^{\infty} \left( \frac{\partial^2}{\partial x^2} + \frac{\partial^2}{\partial y^2} \right) \chi_n(x, y, t) e^{i(kx + \ell y)} dx dy . \quad (2.53)$$

Splitting the last term of (2.53) into terms involving  $\partial^2 \chi_n / \partial x^2$  and  $\partial^2 \chi_n / \partial y^2$  and integrating these by parts twice in  $x$  and  $y$  as appropriate leads to

$$\begin{aligned}
& \left( \frac{\partial^2}{\partial t^2} + f^2 \right) \tilde{\chi}_n(k, \ell, t) + \frac{c_n^2(k^2 + \ell^2)}{2\pi} \int_{-\infty}^{\infty} \int_{-\infty}^{\infty} \chi_n(x, y) e^{i(kx + \ell y)} dx dy \\
&= \frac{c_n^2}{2\pi} \int_{-\infty}^{\infty} \left[ \left( \frac{\partial \chi_n}{\partial x} - ik \chi_n \right) e^{ikx} \right]_{x=-\infty}^{x=+\infty} e^{i\ell y} dy \\
&+ \frac{c_n^2}{2\pi} \int_{-\infty}^{\infty} \left[ \left( \frac{\partial \chi_n}{\partial y} - i\ell \chi_n \right) e^{i\ell y} \right]_{y=-\infty}^{y=+\infty} e^{ikx} dx .
\end{aligned} \tag{2.54}$$

The conditions already assumed on  $\chi_n(x, y, t)$  are sufficient to force the terms on the right-hand side of (2.54) to vanish; then using (2.51) to simplify the last term on the left-hand side, (2.54) reduces to

$$\frac{\partial^2 \tilde{\chi}_n}{\partial t^2}(k, \ell, t) + [f^2 + c_n^2(k^2 + \ell^2)] \tilde{\chi}_n(k, \ell, t) = 0 . \tag{2.55}$$

The general solution of (2.55) may be written as

$$\chi_n(k, \ell, t) = A_n(k, \ell) e^{i\nu_n t} + B_n(k, \ell) e^{-i\nu_n t} , \tag{2.56}$$

where

$$\nu_n(k, \ell) \equiv [f^2 + c_n^2(k^2 + \ell^2)]^{1/2} . \tag{2.57}$$

Taking the inverse transform of (2.56) according to (2.52) we obtain

$$\begin{aligned}
\chi_n(x, y, t) &= \frac{1}{2\pi} \int_{-\infty}^{\infty} \int_{-\infty}^{\infty} A_n(k, \ell) e^{-i(kx + \ell y - \nu_n t)} dk d\ell \\
&+ \frac{1}{2\pi} \int_{-\infty}^{\infty} \int_{-\infty}^{\infty} B_n(k, \ell) e^{-i(kx + \ell y + \nu_n t)} dk d\ell .
\end{aligned} \tag{2.58}$$

In the form (2.58) the solution can be seen to consist of a superposition of traveling waves, with wavenumbers  $k$  and  $\ell$  in the  $x$  and  $y$  directions, frequencies  $\nu_n(k, \ell)$  and amplitudes  $A_n(k, \ell)$  and  $B_n(k, \ell)$ . These amplitudes may be related to the initial conditions by evaluating (2.56) and its time derivative at  $t=0$ , obtaining

$$\tilde{X}_n(k, \ell, 0) = A_n(k, \ell) + B_n(k, \ell) \quad (2.59a)$$

and

$$\frac{\partial \tilde{X}_n}{\partial t}(k, \ell, 0) = i\nu_n [A_n(k, \ell) - B_n(k, \ell)] . \quad (2.59b)$$

Solving (2.59) for  $A_n$  and  $B_n$  yields

$$A_n(k, \ell) = \frac{1}{2} \left[ \tilde{X}_n(k, \ell, 0) + \frac{1}{i\nu_n} \frac{\partial \tilde{X}_n}{\partial t}(k, \ell, 0) \right] \quad (2.60a)$$

and

$$B_n(k, \ell) = \frac{1}{2} \left[ \tilde{X}_n(k, \ell, 0) - \frac{1}{i\nu_n} \frac{\partial \tilde{X}_n}{\partial t}(k, \ell, 0) \right] . \quad (2.60b)$$

Substituting from (2.60) in (2.58) we obtain, after some manipulation,

$$\begin{aligned} X_n(x, y, t) &= \frac{1}{2\pi} \int_{-\infty}^{\infty} \int_{-\infty}^{\infty} \tilde{X}_n(k, \ell, 0) \cos(\nu_n t) e^{-i(kx + \ell y)} dk d\ell \\ &+ \frac{1}{2\pi} \int_{-\infty}^{\infty} \int_{-\infty}^{\infty} \left[ \frac{\partial \tilde{X}_n}{\partial t}(k, \ell, 0) \right] \frac{\sin(\nu_n t)}{\nu_n} e^{-i(kx + \ell y)} dk d\ell . \end{aligned} \quad (2.61)$$

Since

$$\frac{\partial}{\partial t} \left[ \frac{\sin(\nu_n t)}{\nu_n} \right] = \cos(\nu_n t) ,$$

we may write (2.61) as

$$\begin{aligned}
X_n(x, y, t) = \frac{\partial}{\partial t} & \left\{ \frac{1}{2\pi} \int_{-\infty}^{\infty} \int_{-\infty}^{\infty} \tilde{X}_n(k, \ell, 0) \frac{\sin(v_n t)}{v_n} e^{-i(kx+\ell y)} dk d\ell \right\} \\
& + \frac{1}{2\pi} \int_{-\infty}^{\infty} \int_{-\infty}^{\infty} \left[ \frac{\partial \tilde{X}_n}{\partial t}(k, \ell, 0) \right] \frac{\sin(v_n t)}{v_n} e^{-i(kx+\ell y)} dk d\ell .
\end{aligned} \tag{2.62}$$

By a straightforward application of ordinary one-dimensional Fourier transforms from tables such as Erdelyi et al. (1954) we can derive the inverse transform

$$\begin{aligned}
& \frac{1}{2\pi} \int_{-\infty}^{\infty} \int_{-\infty}^{\infty} \frac{\sin \{ [f^2 + c_n^2 (k^2 + \ell^2)]^{1/2} t \}}{[f^2 + c_n^2 (k^2 + \ell^2)]^{1/2}} e^{-i(kx+\ell y)} dk d\ell \\
= & \left\{ \begin{array}{ll} \frac{\text{sgn}(t)}{c_n} \frac{\cos[(f/c_n)(c_n^2 t^2 - x^2 - y^2)^{1/2}]}{(c_n^2 t^2 - x^2 - y^2)^{1/2}}, & x^2 + y^2 < c_n^2 t^2 \\ 0, & x^2 + y^2 > c_n^2 t^2 \end{array} \right\} \tag{2.63}
\end{aligned}$$

where

$$\text{sgn}(t) = \left\{ \begin{array}{ll} +1, & t > 0 \\ -1, & t < 0 \end{array} \right\} .$$

Using (2.63) and the definition of  $v_n$  (2.51) we can apply the convolution theorem

$$\begin{aligned}
\frac{1}{2\pi} \int_{-\infty}^{\infty} \int_{-\infty}^{\infty} \tilde{F}(k, \ell) \tilde{G}(k, \ell) e^{-i(kx+\ell y)} dk d\ell = \\
\frac{1}{2\pi} \int_{-\infty}^{\infty} \int_{-\infty}^{\infty} F(x', y') G(x-x', y-y') dx' dy'
\end{aligned}$$

to (2.62) to obtain

$$\begin{aligned}
X_n(x, y, t) = & \frac{\partial}{\partial t} \left\{ \frac{\text{sgn}(t)}{2\pi c_n} \iint X_n(x-x', y-y', 0) \frac{\cos[(f/c_n)(c_n^2 t^2 - x'^2 - y'^2)^{1/2}]}{(c_n^2 t^2 - x'^2 - y'^2)^{1/2}} dx' dy' \right\} \\
& + \frac{\text{sgn}(t)}{2\pi c_n} \iint \left[ \frac{\partial X_n}{\partial t}(x-x', y-y', 0) \right] \frac{\cos[(f/c_n)(c_n^2 t^2 - x'^2 - y'^2)^{1/2}]}{(c_n^2 t^2 - x'^2 - y'^2)^{1/2}} dx' dy', \quad (2.64)
\end{aligned}$$

where the region of integration in both terms is the disk  $x'^2 + y'^2 \leq c_n^2 t^2$ . It is convenient to introduce the polar coordinates  $(\rho, \theta)$  defined by

$$x' = -\rho \cos \theta, \quad y' = -\rho \sin \theta.$$

Then (2.64) may be written as

$$\begin{aligned}
X_n(x, y, t) = & \frac{\partial}{\partial t} \left\{ \frac{\text{sgn}(t)}{2\pi c_n} \int_0^{2\pi} \int_0^{|c_n t|} X_n(x+\rho \cos \theta, y+\rho \sin \theta, 0) \frac{\cos[(f/c_n)(c_n^2 t^2 - \rho^2)^{1/2}]}{(c_n^2 t^2 - \rho^2)^{1/2}} \rho d\rho d\theta \right\} \\
& + \frac{\text{sgn}(t)}{2\pi c_n} \int_0^{2\pi} \int_0^{|c_n t|} \left[ \frac{\partial X_n}{\partial t}(x+\rho \cos \theta, y+\rho \sin \theta, 0) \right] \frac{\cos[(f/c_n)(c_n^2 t^2 - \rho^2)^{1/2}]}{(c_n^2 t^2 - \rho^2)^{1/2}} \rho d\rho d\theta. \quad (2.65)
\end{aligned}$$

This is the solution obtained by Obukhov (1949). As discussed in the preceding section the functions  $X_n(x, y, 0)$  and  $(\partial X_n / \partial t)(x, y, 0)$  can be obtained from the initial conditions. Thus the formal solution of the transient adjustment problem is complete.

#### 2.4 Potential vorticity and the final adjusted state

The transient solution derived above allows us to examine the state of the atmosphere at any finite time  $t$  during the adjustment process. The state of the atmosphere after the adjustment process is

complete is also of interest, and may be easily obtained without computing any of the intermediate states. To accomplish this, we first derive the potential vorticity equation by eliminating the divergence  $\delta$  between (2.10) and (2.15), obtaining

$$\frac{\partial}{\partial t} \left[ \zeta + fe^{z^*} \frac{\partial}{\partial z^*} \left( \frac{e^{-z^*}}{R\Gamma} \frac{\partial \Phi'}{\partial z^*} \right) \right] = 0 . \quad (2.66)$$

This equation implies that the potential vorticity

$$\Omega(\underline{x}, z^*) \equiv \zeta(\underline{x}, z^*, t) + fe^{z^*} \frac{\partial}{\partial z^*} \left[ \frac{e^{-z^*}}{R\Gamma} \frac{\partial \Phi'}{\partial z^*} (\underline{x}, z^*, t) \right] \quad (2.67)$$

is independent of time. Now if the final state (i.e., the state of the atmosphere in the limit as  $t \rightarrow \infty$ ) is assumed to be in geostrophic balance we have

$$f\zeta(\underline{x}, z^*, \infty) = \nabla^2 \Phi'(\underline{x}, z^*, \infty) . \quad (2.68)$$

Then evaluating (2.67) at  $t=0$  and  $t=\infty$  and making use of (2.68) and the fact that  $\Omega(\underline{x}, z^*)$  is constant in time we obtain

$$\begin{aligned} & \frac{1}{f} \nabla^2 \Phi'(\underline{x}, z^*, \infty) + fe^{z^*} \frac{\partial}{\partial z^*} \left[ \frac{e^{-z^*}}{R\Gamma} \frac{\partial \Phi'}{\partial z^*} (\underline{x}, z^*, \infty) \right] \\ & = \zeta(\underline{x}, z^*, 0) + fe^{z^*} \frac{\partial}{\partial z^*} \left[ \frac{e^{-z^*}}{R\Gamma} \frac{\partial \Phi'}{\partial z^*} (\underline{x}, z^*, 0) \right] . \end{aligned} \quad (2.69)$$

Given initial conditions on  $\zeta$  and  $\Phi'$ , (2.69) may be solved for the geopotential field of the final adjusted state, and the corresponding vorticity field may be obtained from (2.68). The assumption of geostrophic balance in the final state implies that the divergence and vertical motion fields vanish as  $t \rightarrow \infty$ . It should be noted from (2.69) that the final adjusted state is independent of the initial divergence and vertical motion, so that if only the divergent part of the wind is

perturbed initially the atmosphere will eventually adjust back to a state of rest. This is consistent with the results of Schubert et al. (1980) for the divergent barotropic model.

To solve (2.69) we first eliminate the vertical structure by making use of the eigenfunction expansions already developed. Substituting for  $\Phi'(\underline{x}, z^*, \infty)$  in (2.69) from (2.39) leads to

$$\sum_{n=0}^{\infty} \left\{ \frac{1}{\bar{f}} \nabla^2 Y_n(\underline{x}, \infty) Z_n(z^*) + f Y_n(\underline{x}, \infty) e^{z^*} \frac{d}{dz^*} \left[ \frac{e^{-z^*}}{R\Gamma} \frac{dZ_n(z^*)}{dz^*} \right] \right\} \quad (2.70)$$

$$= \zeta(\underline{x}, z^*, 0) - \frac{1}{\bar{f}} \nabla^2 \Phi'(\underline{x}, z^*, 0) .$$

Using the vertical structure equation (2.31) we can reduce (2.70) to the form

$$\sum_{n=0}^{\infty} \left[ \nabla^2 Y_n(\underline{x}, \infty) - \frac{f^2}{c_n^2} Y_n(\underline{x}, \infty) \right] Z_n(z^*) = f \zeta(\underline{x}, z^*, 0) - \nabla^2 \Phi'(\underline{x}, z^*, 0) . \quad (2.71)$$

Then replacing  $n$  by  $m$  in (2.71), multiplying by  $Z_n^\dagger(z^*) e^{-z^*}$ , integrating from  $z^* = 0$  to  $z^* = z_T^*$  and making use of the orthogonality relationship (2.32) results in

$$\nabla^2 Y_n(\underline{x}, \infty) - \frac{f^2}{c_n^2} Y_n(\underline{x}, \infty) = - \frac{1}{c_n^2} \frac{\partial X_n}{\partial t}(\underline{x}, 0) , \quad n = 0, 1, 2, \dots , \quad (2.72)$$

where the right-hand side is given by (2.49) and measures the initial departure from geostrophy for mode  $n$ .

The method of Fourier transforms can now be used to solve (2.72); the details of this approach are much the same as in section 2.3 and therefore will not be repeated here. Taking the transform of (2.72) yields

$$-(k^2 + \ell^2) \tilde{Y}_n(k, \ell, \infty) - \frac{f^2}{c_n^2} \tilde{Y}_n(k, \ell, \infty) = -\frac{1}{c_n^2} \frac{\partial \tilde{X}_n}{\partial t}(k, \ell, 0),$$

which may be solved for  $\tilde{Y}_n(k, \ell, \infty)$  to obtain

$$\tilde{Y}_n(k, \ell, \infty) = [f^2 + c_n^2 (k^2 + \ell^2)]^{-1} \frac{\partial \tilde{X}_n}{\partial t}(k, \ell, 0). \quad (2.73)$$

Then taking the inverse transform of (2.73) with the help of the convolution theorem and the inverse transform

$$\begin{aligned} \frac{1}{2\pi} \int_{-\infty}^{\infty} \int_{-\infty}^{\infty} [f^2 + c_n^2 (k^2 + \ell^2)]^{-1} e^{-i(kx + \ell y)} dk d\ell \\ = \frac{1}{c_n^2} K_0 \left[ \frac{|f|}{c_n} (x^2 + y^2)^{1/2} \right], \end{aligned}$$

where  $K_0$  is the modified Bessel function of the second kind of order zero, we obtain

$$\begin{aligned} Y_n(x, y, \infty) = \\ \frac{1}{2\pi c_n^2} \int_{-\infty}^{\infty} \int_{-\infty}^{\infty} \left[ \frac{\partial \tilde{X}_n}{\partial t}(x-x', y-y', 0) \right] K_0 \left[ \frac{|f|}{c_n} (x'^2 + y'^2)^{1/2} \right] dx' dy'. \end{aligned} \quad (2.74)$$

Finally, defining the polar coordinates  $(\rho, \theta)$  by

$$x' = -\rho \cos \theta, \quad y' = -\rho \sin \theta,$$

(2.74) may be written as

$$Y_n(x, y, \infty) = \frac{1}{2\pi c_n^2} \int_0^{2\pi} \int_0^{\infty} \left[ \frac{\partial \tilde{X}_n}{\partial t}(x + \rho \cos \theta, y + \rho \sin \theta, 0) \right] K_0 \left( \frac{|f| \rho}{c_n} \right) \rho d\rho d\theta. \quad (2.75)$$

This completes the formal solution for the final adjusted state. The similarity which can be seen between (2.65) and (2.75) will be made use of in the next section, in which we evaluate the general solution of the adjustment problem obtained above.

### 3. EXPERIMENTS

This chapter describes a series of experiments in which the general solution derived in section 2 is evaluated for different initial conditions. The choice of the basic state is discussed in section 3.1, where the vertical structure equation is solved for the phase speeds and vertical structure functions. In section 3.2 we describe the numerical evaluation of the general solution for axisymmetric initial conditions. Results of simple experiments are presented in section 3.3 and discussed in section 3.4.

#### 3.1 Basic state, phase speeds and vertical structure functions

The basic state chosen for this study is one with constant static stability  $\Gamma$ . This basic state is simple enough to allow the vertical structure equation to be solved analytically and yet is a reasonable first approximation to the real atmosphere, as we shall see. By integrating (2.8) with  $\Gamma$  held constant we obtain the basic state temperature profile

$$\bar{T}(z^*) = (T_0 - T_\infty) e^{-\kappa z^*} + T_\infty, \quad (3.1)$$

where  $T_0$  is the basic state surface temperature and  $T_\infty \equiv \Gamma/\kappa$  is the limit of  $\bar{T}(z^*)$  as  $z^* \rightarrow \infty$ . The corresponding basic state geopotential, obtained from (3.1) by integrating the hydrostatic equation (2.5), is

$$\bar{\Phi}(z^*) = R \left[ \frac{T_0 - T_\infty}{\kappa} (1 - e^{-\kappa z^*}) + T_\infty z^* \right]. \quad (3.2)$$

For the results reported here the value  $z_T^* = 2.313$  was used, which placed the rigid lid at  $p = 100$  mb (assuming a surface pressure of 1010 mb). A least-squares procedure was used to determine appropriate

values of  $\Gamma$  and  $T_0$  by minimizing the sum of the squares of the deviations of the temperature profile (3.1) from an observational sounding at discrete pressure levels. Using the data of Jordan (1958) for the mean summertime (June-September) temperature sounding for the West Indies area the values  $\Gamma = 23.79 \text{ K}$  and  $T_0 = 302.53 \text{ K}$  were obtained. The observational sounding and the temperature profile (3.1) evaluated with these values of  $\Gamma$  and  $T_0$  are shown for comparison in Fig. 1.

With the constant static stability basic state the vertical structure equation (2.31) reduces to

$$\frac{d}{dz^*} \left( e^{-z^*} \frac{dZ_n}{dz^*} \right) + \frac{R\Gamma}{c_n} e^{-z^*} Z_n = 0 . \quad (3.3)$$

To solve this equation we first define  $W_n(z^*)$  by

$$Z_n(z^*) = e^{z^*/2} W_n(z^*) . \quad (3.4)$$

With this substitution (3.3) becomes

$$\frac{d^2 W_n}{dz^{*2}} - \mu_n^2 W_n = 0 , \quad (3.5)$$

where

$$\mu_n^2 \equiv \frac{1}{4} - \frac{R\Gamma}{c_n} ,$$

and the boundary conditions (2.29) and (2.30) reduce to

$$\left. \begin{aligned} \frac{dW_n}{dz^*} + \eta W_n &= 0 \quad \text{at} \quad z^* = 0 \\ \frac{dW_n}{dz^*} + \frac{1}{2} W_n &= 0 \quad \text{at} \quad z^* = z_T^* , \end{aligned} \right\} \quad (3.6)$$

and

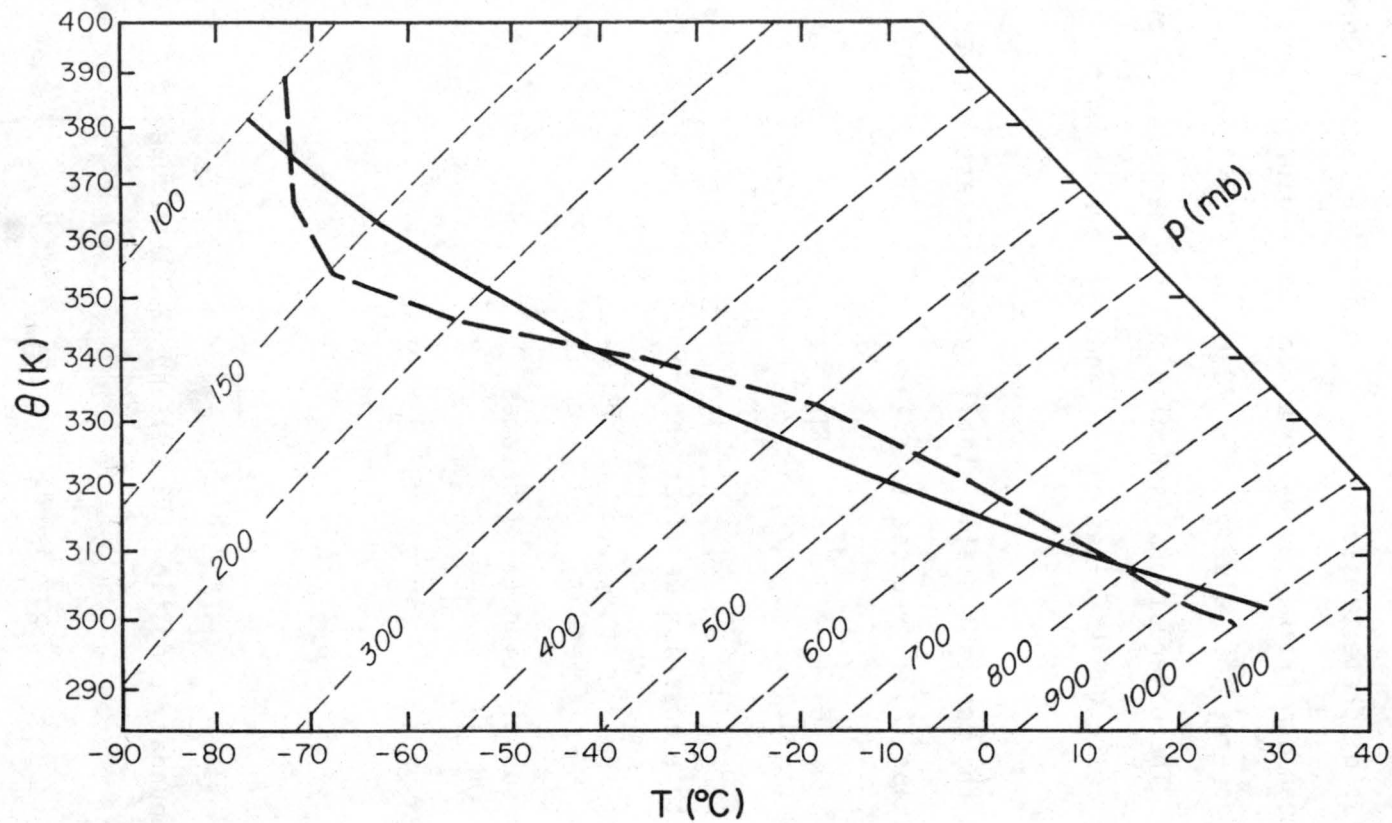


Figure 1. Tephigram comparing the model temperature profile with an observational sounding. The solid curve is the constant static stability profile (3.1) with  $\Gamma = 23.79$  K and  $T_0 = 302.53$  K. The dashed curve is the mean summertime (June-September) temperature sounding for the West Indies area reported by Jordan (1958).

where  $\eta \equiv \frac{1}{2} - \frac{\Gamma}{T_0}$ . We now investigate the solution of (3.5) with the boundary conditions (3.6) for three cases distinguished by the sign of  $\mu_n^2$ .

Case 1:  $\mu_n^2 > 0$ . In this case the general solution of (3.5) may be written in the form

$$W_n(z^*) = A \sinh(\mu_n z^*) + B \cosh(\mu_n z^*), \quad (3.7)$$

where

$$\mu_n = \left( \frac{1}{4} - \frac{R\Gamma}{c_n^2} \right)^{1/2} \quad (3.8)$$

and A and B are constants. The boundary conditions (3.6) then imply that

$$\mu_n A + \eta B = 0 \quad (3.9a)$$

and

$$\mu_n [A \cosh(\mu_n z_T^*) + B \sinh(\mu_n z_T^*)] + \frac{1}{2} [A \sinh(\mu_n z_T^*) + B \cosh(\mu_n z_T^*)] = 0 \quad (3.9b)$$

Writing (3.9) in matrix form as

$$\begin{bmatrix} \mu_n & \eta \\ \mu_n \cosh(\mu_n z_T^*) + \frac{1}{2} \sinh(\mu_n z_T^*) & \mu_n \sinh(\mu_n z_T^*) + \frac{1}{2} \cosh(\mu_n z_T^*) \end{bmatrix} \begin{bmatrix} A \\ B \end{bmatrix} = \begin{bmatrix} 0 \\ 0 \end{bmatrix}$$

and noting that for non-trivial solutions the determinant of the coefficient matrix must vanish we find that in the case where  $\mu_n^2 > 0$  the phase speeds  $c_n$  must satisfy the transcendental equation

$$\left( \frac{R\Gamma_0}{c_n^2} - \frac{1}{2} \right) \sinh(\mu_n z_T^*) = \mu_n \cosh(\mu_n z_T^*) \quad (3.10)$$

It can be shown that if  $z_T^* > (z_T^*)_{\text{crit}} \equiv 4\Gamma/(T_0 - 2\Gamma)$  then (3.10) has precisely one root  $c_0$  with  $c_0^2 > 4R\Gamma$ , and that if  $z_T^* \leq (z_T^*)_{\text{crit}}$  then (3.10) has no roots with  $\mu_n^2 > 0$ . Thus (3.10), along with (3.8), defines the one phase speed  $c_0$  in the case where  $z^* > (z_T^*)_{\text{crit}}$ . An approximate value for  $c_0$ , obtained by assuming that  $c_0^2 \gg 4R\Gamma$  and therefore setting  $\mu_0 = \frac{1}{2}$  in (3.10), is given by

$$c_0 \approx \left[ \left( 1 - e^{-z_T^*} \right) RT_0 \right]^{1/2}. \quad (3.11)$$

The vertical structure function corresponding to  $c_0$  is found from (3.7) and (3.4) to be

$$Z_0(z^*) = [A \sinh(\mu_0 z^*) + B \cosh(\mu_0 z^*)] e^{z^*/2}. \quad (3.12)$$

The constants  $A$  and  $B$  may be determined by substituting (3.12) into the normalization condition (2.32) and using the lower boundary condition (3.9a). The end result, after much algebra, is

$$Z_0(z^*) = \hat{Z}_0 [\mu_0 \cosh(\mu_0 z^*) - \eta \sinh(\mu_0 z^*)] e^{z^*/2}, \quad (3.13)$$

where

$$\hat{Z}_0^2 = 2\mu_0 \frac{c_0^2}{R\Gamma} \quad (3.14)$$

$$\times [(\mu_0^2 + \eta^2) \sinh(\mu_0 z_T^*) \cosh(\mu_0 z_T^*) - 2\mu_0 \eta \sinh^2(\mu_0 z_T^*) + (\mu_0^2 - \eta^2) \mu_0 z_T^*]^{-1}$$

This vertical mode has an exponential behavior in the vertical; it is referred to as the external mode and its existence depends on the fact that  $w^*$  is allowed to vary at the lower boundary.

Case 2:  $\mu_n^2 < 0$ . In this case we let  $\lambda_n^2 = -\mu_n^2$  and write the general solution of (3.5) in the form

$$W_n(z^*) = C \sin(\lambda_n z^*) + D \cos(\lambda_n z^*) , \quad (3.15)$$

where

$$\lambda_n = \left( \frac{R\Gamma}{c_n^2} - \frac{1}{4} \right)^{1/2} \quad (3.16)$$

and  $C$  and  $D$  are constants. The boundary conditions (3.6) then imply that

$$\lambda_n C + \eta D = 0 \quad (3.17a)$$

and

$$\lambda_n [C \cos(\lambda_n z_T^*) - D \sin(\lambda_n z_T^*)] + \frac{1}{2} [(\sin(\lambda_n z_T^*) + D \cos(\lambda_n z_T^*))] = 0 . \quad (3.17b)$$

Writing (3.17) in matrix form as

$$\begin{bmatrix} \lambda_n & \eta \\ \lambda_n \cos(\lambda_n z_T^*) & -\lambda_n \sin(\lambda_n z_T^*) \\ + \frac{1}{2} \sin(\lambda_n z_T^*) & + \frac{1}{2} \cos(\lambda_n z_T^*) \end{bmatrix} \begin{bmatrix} C \\ D \end{bmatrix} = \begin{bmatrix} 0 \\ 0 \end{bmatrix}$$

and again noting that for non-trivial solutions the determinant of the coefficient matrix must vanish we find that in the case where  $\mu_n^2 < 0$  the phase speeds  $c_n$  must satisfy

$$\left( \frac{R\Gamma_0}{c_n^2} - \frac{1}{2} \right) \sin(\lambda_n z_T^*) = \lambda_n \cos(\lambda_n z_T^*) . \quad (3.18)$$

It can be shown that (3.18) has solutions  $c_n$  ( $n=1, 2, 3, \dots$ ) with

$$\frac{4R\Gamma}{[2(n+1)\pi/z_T^*]^2 + 1} < c_n^2 < \frac{4R\Gamma}{(2n\pi/z_T^*)^2 + 1} ,$$

and that if  $z_T^* < (z_T^*)_{\text{crit}}$  then (3.18) also has one solution  $c_0$  with

$$\frac{4R\Gamma}{(2\pi/z_T^*)^2 + 1} < c_0^2 < 4R\Gamma .$$

Thus (3.18), along with (3.16), defines a countably infinite set of phase speeds  $c_n$ . For large  $n$ ,  $c_n$  may be approximated by

$$c_n \approx (R\Gamma)^{1/2} \frac{z_T^*}{n\pi} . \quad (3.19)$$

The vertical structure functions which correspond to these phase speeds are found from (3.15) and (3.4) to be

$$Z_n(z^*) = [C \sin(\lambda_n z^*) + D \cos(\lambda_n z^*)] e^{z^*/2} . \quad (3.20)$$

Evaluating the constants  $C$  and  $D$  by substituting (3.20) into the normalization condition (2.32) and using the lower boundary condition (3.17a) we obtain

$$Z_n(z^*) = \hat{Z}_n [\lambda_n \cos(\lambda_n z^*) - \eta \sin(\lambda_n z^*)] e^{z^*/2} , \quad (3.21)$$

where

$$\hat{Z}_n^2 = 2\lambda_n \frac{c_n^2}{R\Gamma} \quad (3.22)$$

$$\times [(\lambda_n^2 - \eta^2) \sin(\lambda_n z_T^*) \cos(\lambda_n z_T^*) - 2\lambda_n \eta \sin^2(\lambda_n z_T^*) + (\lambda_n^2 + \eta^2) \lambda_n z_T^*]^{-1} .$$

These modes exhibit an oscillatory behavior in the vertical and are referred to as internal modes. They correspond to waves which propagate vertically, with  $\lambda_n$  as a type of vertical wavenumber.

Case 3:  $\mu_n^2 = 0$ . In this case the general solution of (3.5) is

simply

$$W_n(z^*) = w_0 + w_1 z^* , \quad (3.23)$$

where  $w_0$  and  $w_1$  are constants. By applying the boundary conditions (3.6) to (3.23) it can be easily shown that for a non-trivial solution we must have  $z_T^* = (z_T^*)_{\text{crit}}$ . Now  $\mu_n^2 = 0$  implies that  $c_n^2 = 4R\Gamma$ , so  $c_0 = (4R\Gamma)^{1/2}$  is a phase speed of a vertical mode if and only if

$z_T^* = (z_T^*)_{\text{crit}}$ , thus filling the gap between cases 1 and 2. The corresponding vertical structure function, found by substituting (3.23) into (3.4) and applying the normalization and lower boundary conditions, is

$$Z_0(z^*) = \hat{Z}_0 (1 - \eta z^*) e^{z^*/2}$$

where

$$\hat{Z}_0^2 = \frac{c_0^2}{R\Gamma} \left\{ z_T^* \left[ 1 - \eta z_T^* + \frac{1}{3} (\eta z_T^*)^2 \right] \right\}^{-1}.$$

This mode represents a transition of the lowest order mode from an external type to an internal type as  $z_T^*$  goes from greater than  $(z_T^*)_{\text{crit}}$  to less than  $(z_T^*)_{\text{crit}}$ .

For the particular basic state described earlier with  $z_T^* = 2.313$ ,  $\Gamma = 23.79\text{K}$  and  $T_0 = 302.53\text{K}$  we find that  $(z_T^*)_{\text{crit}} = 0.373$  so the above results imply that this atmosphere has an external mode with phase speed  $c_0 > (4R\Gamma)^{1/2}$  satisfying (3.10) and a countably infinite set of internal modes with phase speeds  $c_n$  ( $n=1, 2, 3, \dots$ ) satisfying (3.18) with  $(4R\Gamma)^{1/2} > c_1 > c_2 > \dots$ . The values of the phase speeds determined by solving (3.10) and (3.18) numerically are presented in the second column of Table 1 for the external mode and the first ten internal modes. The corresponding approximate values determined from (3.11) and (3.19) appear in the third column of the same Table. The vertical structure functions for the external mode and the first four internal modes are shown in Fig. 2. These phase speeds and vertical structure functions were used in the calculations described in the following sections.

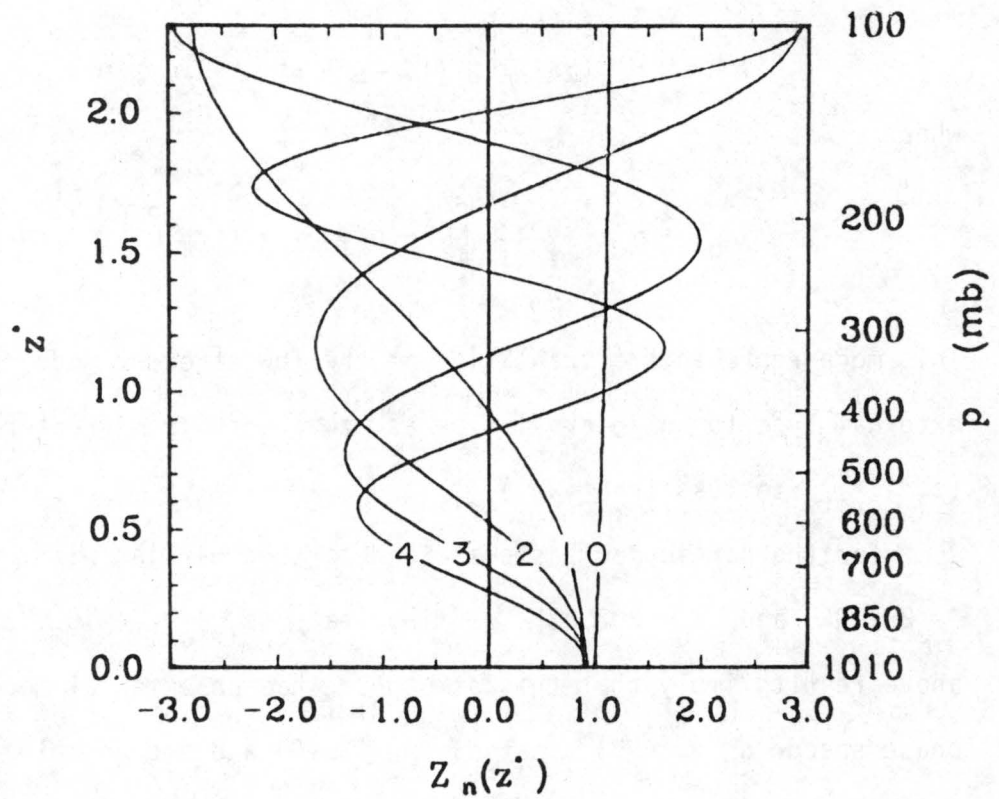


Figure 2. Vertical structure functions for the constant static stability atmosphere for  $n=0, 1, 2, 3, 4$  as labelled.

n	$c_n$ (ms <sup>-1</sup> )	
	exact	approximate
0	287.00	279.70
1	56.28	60.84
2	29.79	30.42
3	20.09	20.28
4	15.13	15.21
5	12.13	12.17
6	10.12	10.14
7	8.68	8.69
8	7.59	7.60
9	6.75	6.76
10	6.08	6.08

Table 1. Exact and approximate values of the phase speeds of the constant static stability atmosphere.

### 3.2 Numerical evaluation of the solution for axisymmetric perturbations

In the numerical evaluation of the solution derived in chapter 2 it is convenient to make certain assumptions about the initial conditions. First, in section 2.4 it was shown that the final adjusted state is independent of the initial divergence. Thus, at least in a dry model where there can be no interaction between the vertical motion field of propagating waves and a moisture field, the initial divergence is not of such fundamental importance as the initial vorticity and geopotential. Therefore, we shall consider here only initial conditions with zero divergence. With this assumption (2.48) implies that  $X_n(x,0) = 0$  for all  $n$  so that the first term of (2.65) vanishes.

Second, since we are primarily interested in the effects of vertical stratification on the adjustment process, we will assume that the initial perturbations are axisymmetric. The invariance of the f-plane model with respect to rotations in the horizontal about the origin then implies that all fields will remain axisymmetric at all

times so we can use axisymmetric cylindrical coordinates  $(r, z^*)$ , where  $r = (x^2 + y^2)^{1/2}$ . In this coordinate system (2.11) and (2.12) simplify to

$$\text{and } \left. \begin{aligned} \delta &= \frac{\partial(ru)}{r\partial r} \\ \zeta &= \frac{\partial(rv)}{r\partial r} \end{aligned} \right\} \quad (3.24)$$

where  $u(r, z^*, t)$  and  $v(r, z^*, t)$  are the radial and tangential components of the horizontal wind  $\underline{v}(r, z^*, t)$ , respectively.

Finally, we will assume that the horizontal and vertical structure of the initial conditions are separable; in particular, we assume that

$$\begin{bmatrix} v(r, z^*, 0) \\ \phi'(r, z^*, 0) \end{bmatrix} = \begin{bmatrix} \hat{v}(r) \\ \hat{\phi}(r) \end{bmatrix} D(z^*) \quad , \quad (3.25)$$

so that the initial  $v$  and  $\phi'$  fields have the same vertical structure. This assumption leads to a considerable simplification in the evaluation of the solution, as will be shown below. In this study we will investigate initial conditions in the vorticity and geopotential fields separately, so the form of (3.25) will not be particularly limiting.

With the above assumptions (2.49) easily reduces to

$$\frac{\partial X_n}{\partial t}(r, 0) = c_n^2 D_n \psi(r) \quad , \quad (3.26)$$

where

$$D_n \equiv \int_0^{z_T^*} D(z^*) Z_n^+(z^*) e^{-z^*} dz^* \quad (3.27)$$

is the projection of the vertical structure of the initial conditions onto vertical mode  $n$  and

$$\psi(r) \equiv \frac{d}{rdr} \left[ r \frac{d\hat{\phi}(r)}{dr} \right] - f \frac{d}{rdr} [r\hat{v}(r)] \quad (3.28)$$

measures the departure of the initial conditions from geostrophic balance. Substituting (3.26) into (2.65) and (2.75) and using (2.44) we obtain

$$\begin{aligned} X_n(r,t) &= D_n F_n(r,t) , \\ Y_n(r,t) &= D_n G_n(r,t) , \end{aligned} \quad (3.29)$$

where, for  $t < \infty$ ,

$$\begin{aligned} F_n(r,t) &= \text{sgn}(t) \frac{c_n}{2\pi} \int_0^{2\pi} \int_0^{|c_n t|} \psi[(r^2 + \rho^2 + 2r\rho \cos \theta)^{1/2}] \\ &\quad \times \frac{\cos[(f/c_n)(c_n^2 t^2 - \rho^2)^{1/2}]}{(c_n^2 t^2 - \rho^2)^{1/2}} \rho d\rho d\theta , \end{aligned} \quad (3.30)$$

$$G_n(r,t) = \int_0^t F_n(r,\tau) d\tau , \quad (3.31)$$

and, for  $t = \infty$ ,

$$F_n(r,\infty) = 0 , \quad (3.32)$$

$$G_n(r,\infty) = \frac{1}{2\pi} \int_0^{2\pi} \int_0^\infty \psi[(r^2 + \rho^2 + 2r\rho \cos \theta)^{1/2}] K_0 \left( \frac{|f|\rho}{c_n} \right) \rho d\rho d\theta . \quad (3.33)$$

To put these results in a form more suitable for numerical calculation we first eliminate the singularity in the integrand in (3.30) at  $\rho = |c_n t|$  by the substitution

$$s = \frac{(c_n^2 t^2 - \rho^2)^{1/2}}{c_n |t|}$$

and then reverse the order of integration in (3.30) and (3.31), obtaining

$$F_n(r,t) = c_n^2 t \int_0^1 I[c_n |t| (1-s^2)^{1/2}, r] \cos(fts) ds \quad (3.34)$$

and

$$G_n(r,\infty) = \int_0^\infty I(\rho,r) K_0 \left[ \frac{|\rho|}{c_n} \right] \rho d\rho, \quad (3.35)$$

where, after appropriate manipulations,

$$I(\rho,r) = \frac{1}{\pi} \int_0^\pi \psi[(r^2 + \rho^2 + 2r\rho \cos\theta)^{1/2}] d\theta. \quad (3.36)$$

Finally, by substituting (2.37) and (2.38) into (3.24) and using (3.29) we find that the horizontal wind components may be written in the form

$$\left. \begin{aligned} u(r,z^*,t) &= \sum_{n=0}^{\infty} D_n U_n(r,t) Z_n(z^*) \\ v(r,z^*,t) &= \sum_{n=0}^{\infty} D_n V_n(r,t) Z_n(z^*) + \hat{v}(r) D(z^*) \end{aligned} \right\} \quad (3.37)$$

where  $U_n$  and  $V_n$  are related to  $F_n$  and  $G_n$  by

$$\text{and} \quad \left. \begin{aligned} \frac{\partial}{r\partial r} [rU_n(r,t)] &= - \frac{F_n(r,t)}{c_n^2} \\ \frac{\partial}{r\partial r} [rV_n(r,t)] &= f \frac{G_n(r,t)}{c_n^2} \end{aligned} \right\} \quad (3.38)$$

The above results, along with (2.37)-(2.43), express the solution of the geostrophic adjustment problem in terms of the four functions  $F_n$ ,  $G_n$ ,  $U_n$  and  $V_n$ , each of which depends on the phase speeds  $c_n$  and the quantity  $\psi(r)$  defined by (3.28). In all but the most trivial cases the calculation of these four functions will involve numerical integrations, some of which will be quite time consuming. However, the above form of the solution allows us to compute values of  $F_n$ ,  $G_n$ ,

$U_n$  and  $V_n$  once and store them, and then use these results to compute the solution for any initial conditions which result in the same  $\psi$ . In particular, the same values of these functions can be used for any vertical structure of the initial conditions. This fact leads to a considerable savings in the time required to compute the solution.

For the results presented in the next section the functions  $F_n$ ,  $G_n$ ,  $U_n$  and  $V_n$  were evaluated numerically for a finite number of phase speeds  $c_n$  ( $n=0, 1, \dots, N$ ) as follows. Due to the large range of values of  $c_n$  each vertical mode was treated independently. Discrete points  $r_i$  ( $i=0, 1, \dots, I$ ) and  $t_k$  ( $k=0, 1, \dots, K$ ) in space and time were chosen with  $0=r_0 < r_1 < \dots < r_I$  and  $0=t_0 < t_1 < \dots < t_K$ . At each  $t_k$ ,  $F_n(r_i, t_k)$  was evaluated for all  $i$  according to (3.34) using an adaptive quadrature routine employing Gauss-type quadrature formulas;  $G_n(r_i, \infty)$  was also evaluated in the same way from (3.35). The inner integral (3.36) was evaluated using 32-point Gauss-Legendre quadrature in all cases. The asymptotic form derived in Appendix C was used to check the calculation of  $F_n$ . To obtain  $G_n(r_i, t_k)$ , (3.29) was evaluated as follows. First,  $G_n(r_i, t_0) = G_n(r_i, 0)$  was set to zero for all  $i$ . Then for each  $t_k$  in succession,  $F_n(r_i, t)$  was integrated from  $t_{k-1}$  to  $t_k$  and the result added to  $G_n(r_i, t_{k-1})$  to yield  $G_n(r_i, t_k)$ . Simpson's rule was used to perform this integration for modes which had phase speeds small enough that it could give sufficient accuracy. For the faster-moving modes values of  $F_n$  at additional time points between  $t_{k-1}$  and  $t_k$  had to be computed; in order to minimize the number of additional evaluations of  $F_n$  and at the same time utilize the values  $F_n(r_i, t_{k-1})$  and  $F_n(r_i, t_k)$  already computed, these additional points

were chosen according to the panel Lobatto quadrature rule (Abramowitz and Stegun, 1964) with up to 10 points and as many panels as necessary to achieve the desired accuracy. Finally,  $U_n(r_i, t_k)$  and  $V_n(r_i, t_k)$  were computed for all  $i$  at each  $k$  by integrating (3.38) using Simpson's rule; for this reason the  $r_i$  were chosen to be equally spaced.

Having computed and stored  $F_n$ ,  $G_n$ ,  $U_n$  and  $V_n$  as described above, the vertical structure of the initial conditions was projected onto the vertical modes by evaluating (3.27) using the adaptive quadrature routine. The resulting coefficients  $D_n$  were then used in the superposition of the various horizontal and vertical structure functions according to (2.37)-(2.42) and (3.37), with the infinite series approximated by finite sums from  $n=0$  to  $n=N$ . The results of these calculations for various initial conditions are presented in the next section.

### 3.3 Results

In this section we present the results of eight simple experiments with the solution to the geostrophic adjustment problem described above. For these experiments we choose

$$\psi(r) = \psi_0 \left( \frac{r^2}{a^2} - 1 \right) e^{-r^2/a^2} \quad (3.39)$$

with  $a = 150$  km, and set  $N = 30$  so that the external mode and 30 internal modes are considered. The value  $4.988 \times 10^{-5} \text{ s}^{-1}$  is used for the Coriolis parameter  $f$ , corresponding to a latitude of  $20^\circ\text{N}$ .

#### 3.3.1 experiment 1: initial condition in the mass field

With no initial vorticity (i.e.,  $\hat{v}(r) = 0$ ), (3.39) corresponds to an initial condition in the mass field with horizontal structure given

by

$$\hat{\Phi}(r) = \hat{\Phi}_0 e^{-r^2/a^2} \quad (3.40)$$

and  $\psi_0 = 4 \hat{\Phi}_0 / a^2$ . With this interpretation of  $\psi(r)$ ,  $a$  is the horizontal e-folding width of the perturbation. We consider five experiments with this initial condition, each having a different vertical structure.

In experiment 1a the initial condition consists of a bubble of warm air in the lower troposphere as shown in Fig. 3<sup>1</sup>. The initial perturbation temperature field is shown in Fig. 3a and has a vertical structure defined so that the bubble is confined between pressure levels  $p_L = 900$  mb and  $p_U = 700$  mb, with a maximum value (at  $r = 0$ ) of  $1.0^\circ\text{C}$  at  $p_C = 800$  mb. The corresponding perturbation geopotential field is defined so that it vanishes at  $p = p_C$ , implying that an initially unbalanced pressure gradient force exists throughout the depth of the model as shown in Fig. 3b.

The time evolution of this initial condition is depicted in Figs. 4-9. In these figures the upper plot (a) shows the perturbation temperature  $T'$  (solid contours, with dotted contours for negative values) and the radial and vertical components  $ru e^{-z^*}$  and  $w^* e^{-z^*}$  of the mass flux associated with the secondary circulation generated in the  $r, z^*$ -plane (vector representation); the lower plot (b) shows the tangential wind  $v$  (solid contours) and the perturbation geopotential  $\Phi'$  (dashed contours). The initially unbalanced pressure gradient force gives rise to a region of inflow below the bubble and a region of outflow above it, generating strong rising motion in the center of the

<sup>1</sup>In experiments where the upper portion of the atmosphere is essentially unaffected by the adjustment process, for the sake of clarity only the lower portion of the atmosphere is shown in the Figures.

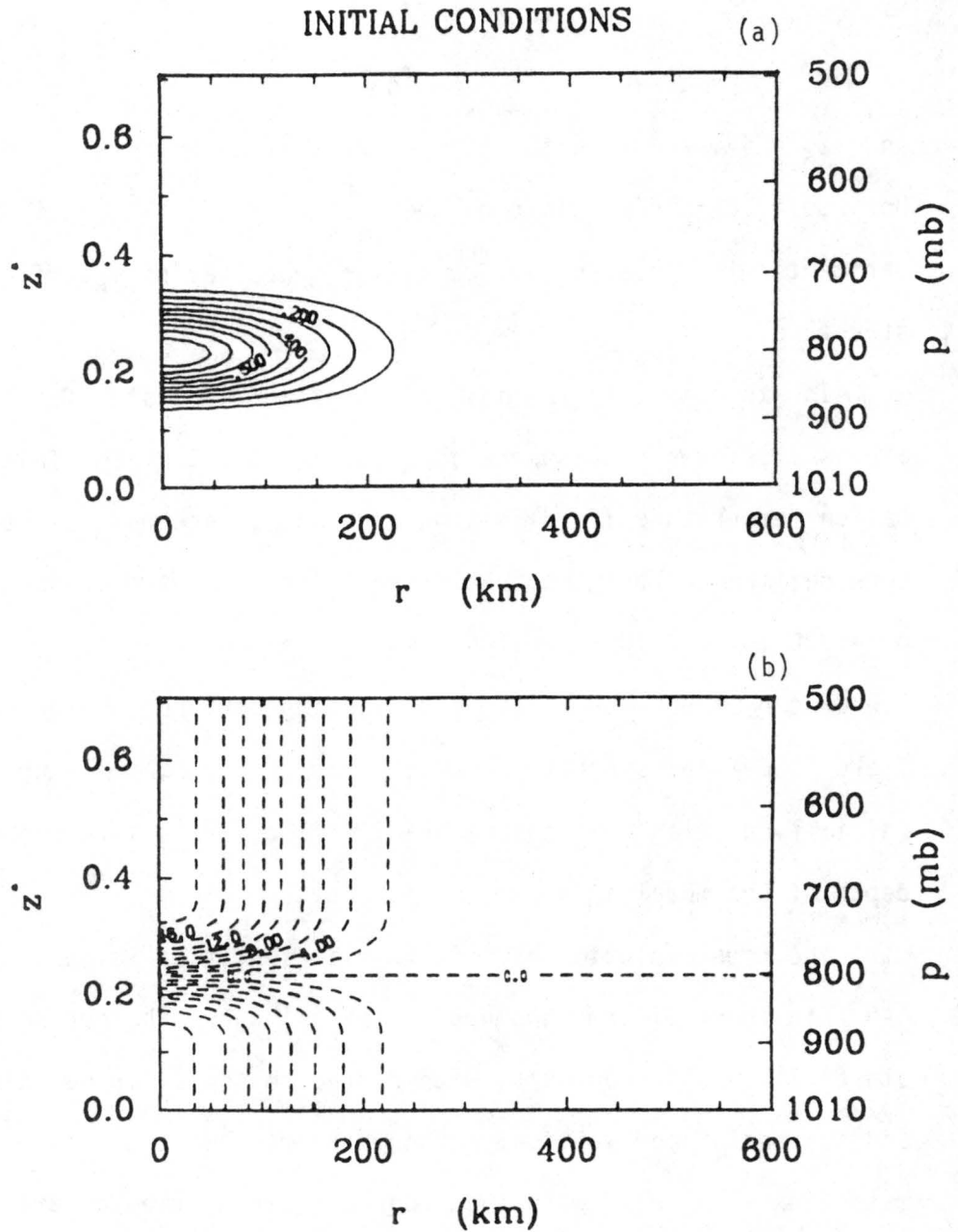


Figure 3. Initial conditions for experiment 1a. Part (a) is the perturbation temperature  $T'(r, z^*, 0)$  with contour interval  $0.1^\circ\text{C}$ . Part (b) is the perturbation geopotential  $\phi'(r, z^*, 0)$  with contour interval  $2.0 \text{ m}^2 \text{ s}^{-2}$ . The vertical coordinate is  $z^*$  with the corresponding pressure  $p$  shown on the scale on the right.

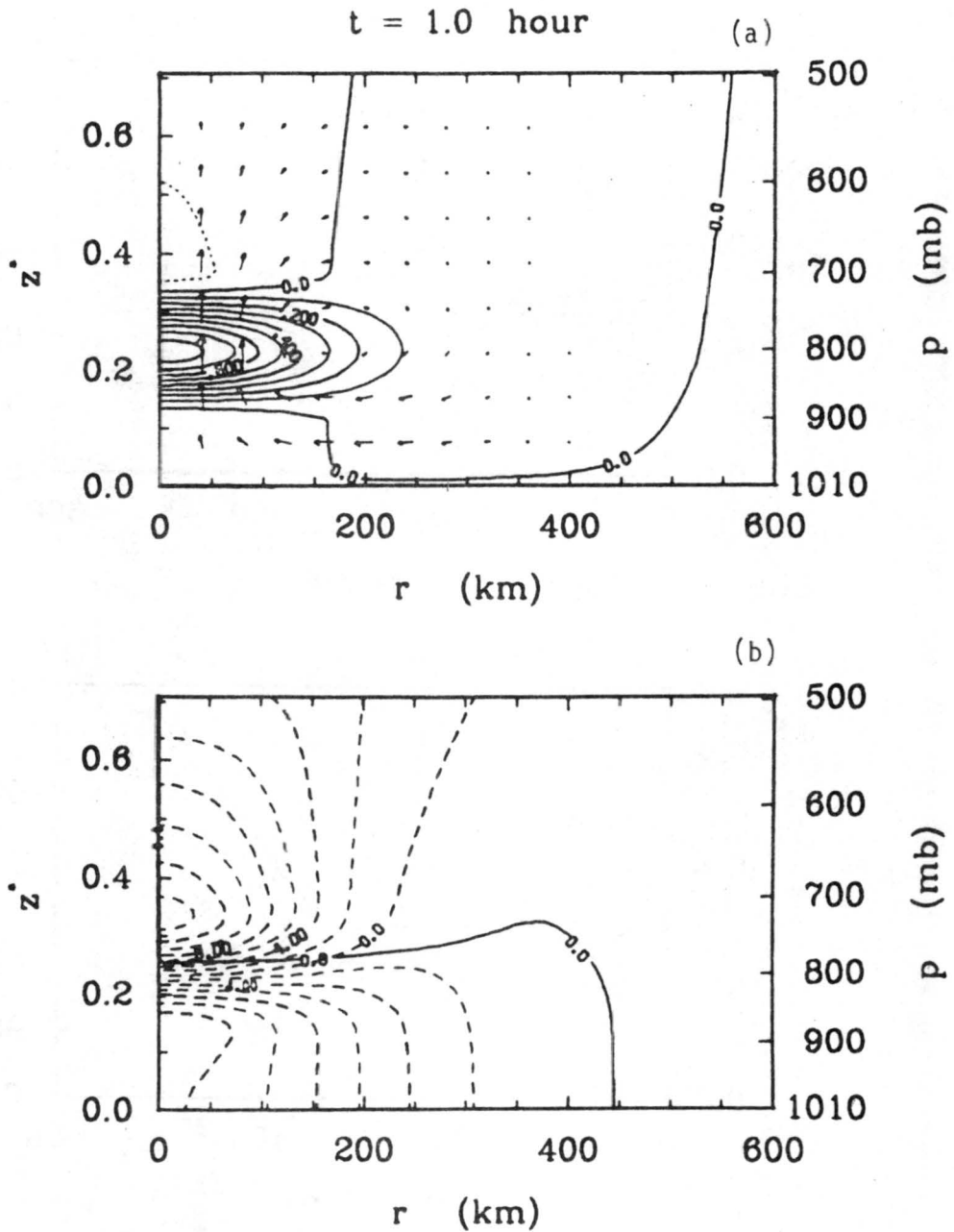


Figure 4. Transient state of the atmosphere at  $t=1.0$  hour for experiment 1a. Part (a) is the perturbation temperature  $T'(r, z^*, t)$ , with contour interval  $0.1^\circ\text{C}$  and dotted lines for negative values, and the secondary circulation  $u'e^{-z^*}$ ,  $w'e^{-z^*}$  with the vertical component scaled by  $5 \times 10^{10}$ . Part (b) is the tangential wind  $v(r, z^*, t)$  (solid lines) with contour interval  $0.1 \text{ ms}^{-1}$  and the perturbation geopotential  $\phi'(r, z^*, t)$  (dashed lines) with contour interval  $2.0 \text{ m}^2\text{s}^{-2}$ .

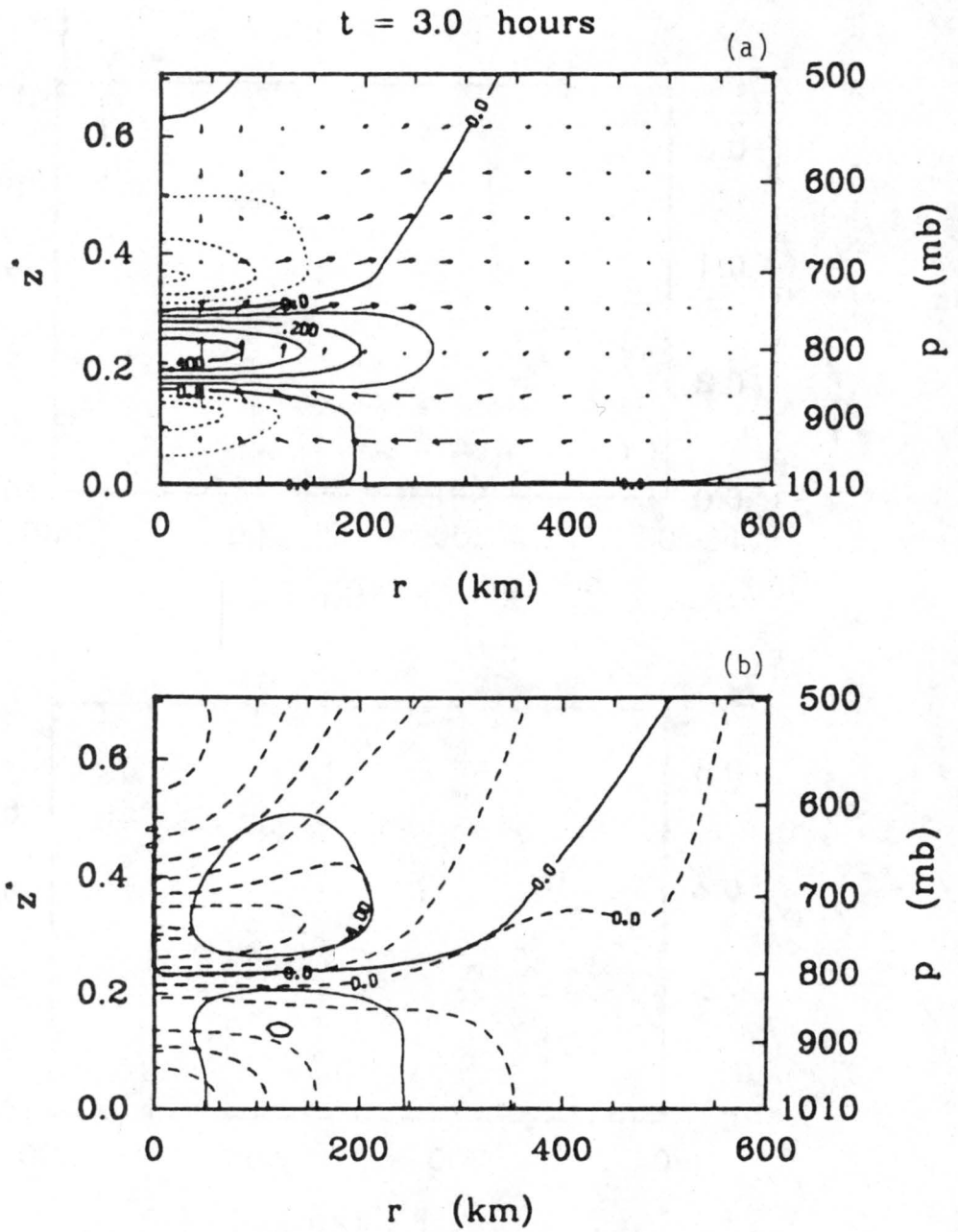


Figure 5. Same as Figure 4 but for  $t = 3.0$  hours.

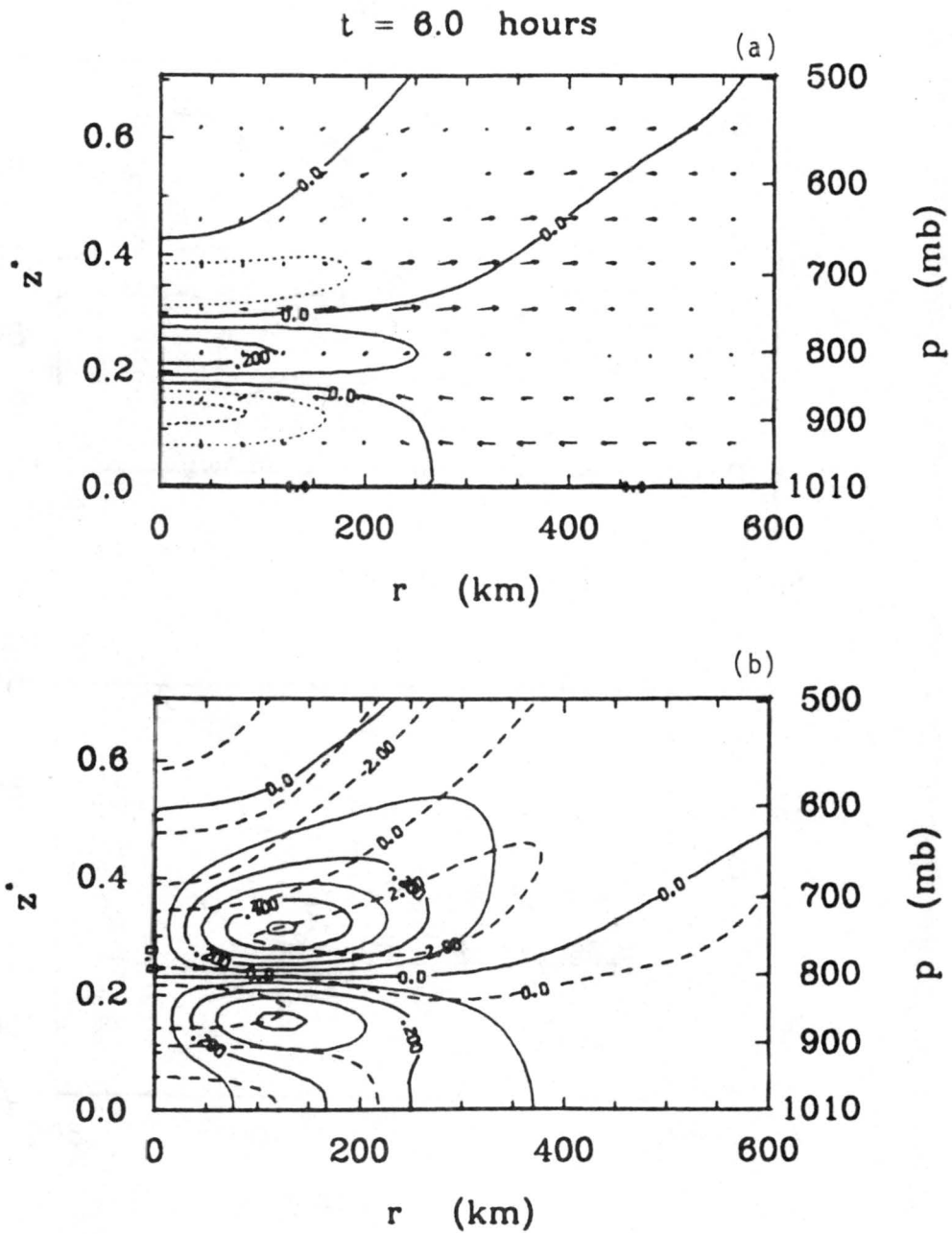


Figure 6. Same as Figure 4 but for  $t = 6.0$  hours .

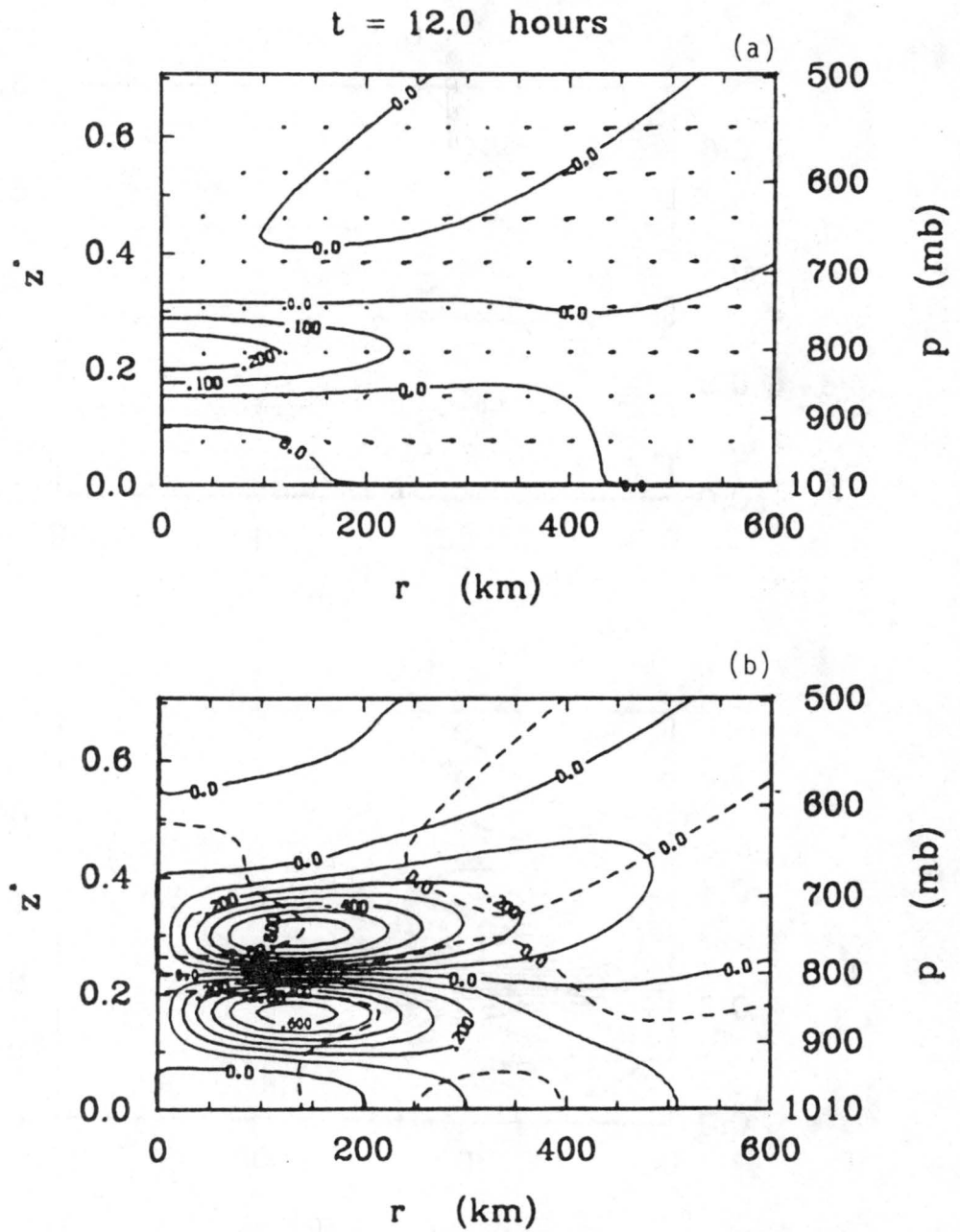


Figure 7. Same as Figure 4 but for  $t = 12.0$  hours .

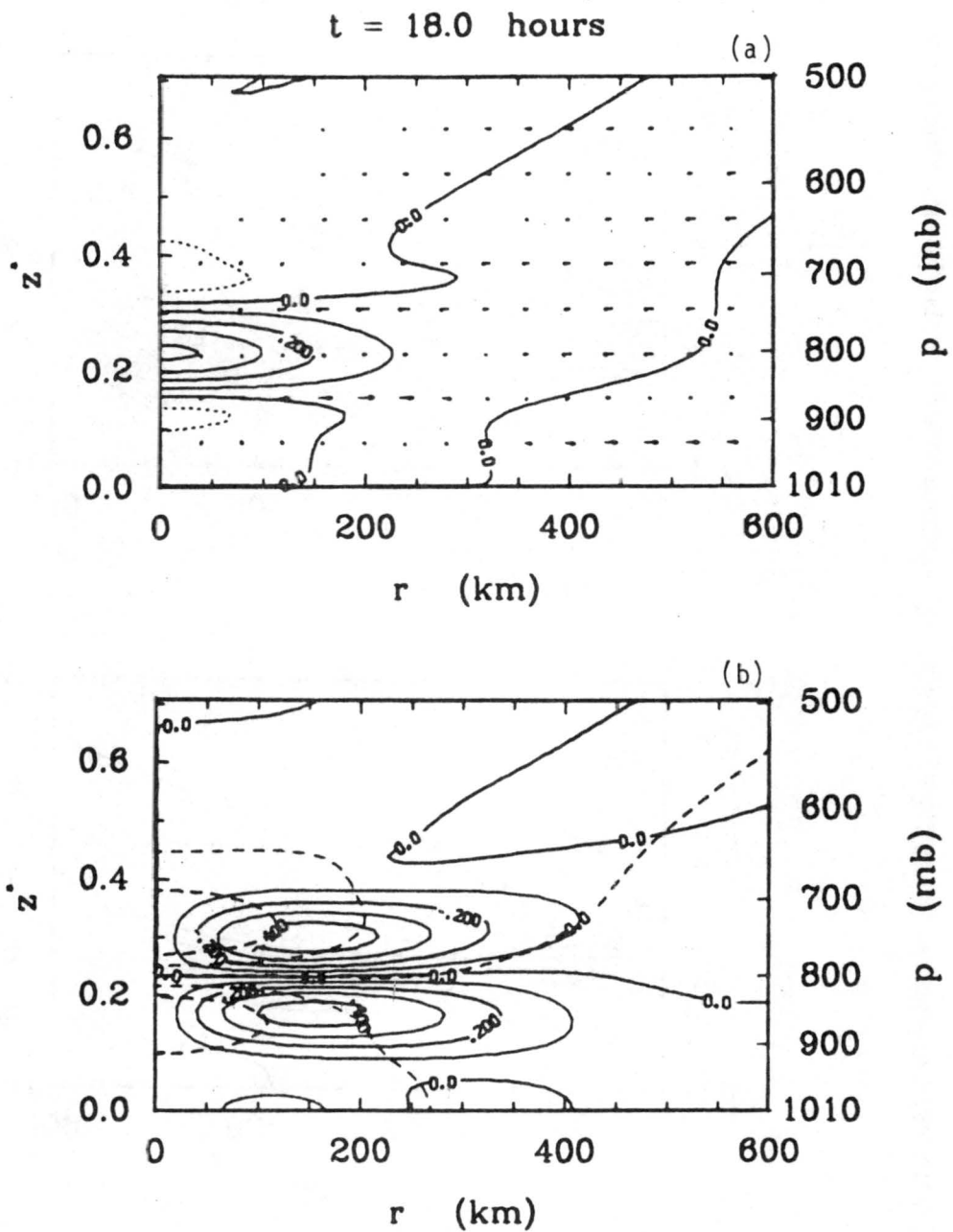


Figure 8. Same as Figure 4 but for  $t = 18.0$  hours .

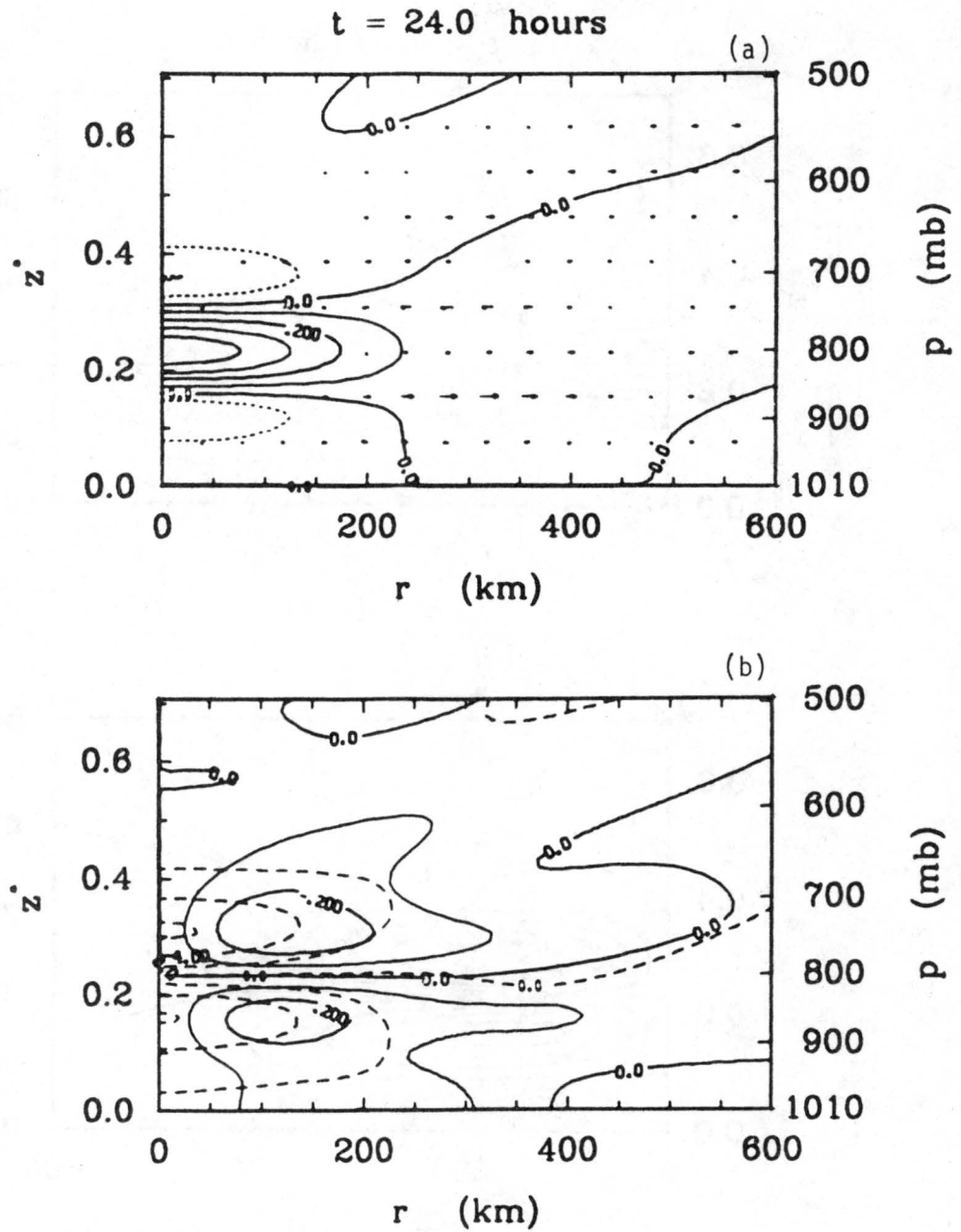


Figure 9. Same as Figure 4 but for  $t = 24.0$  hours .

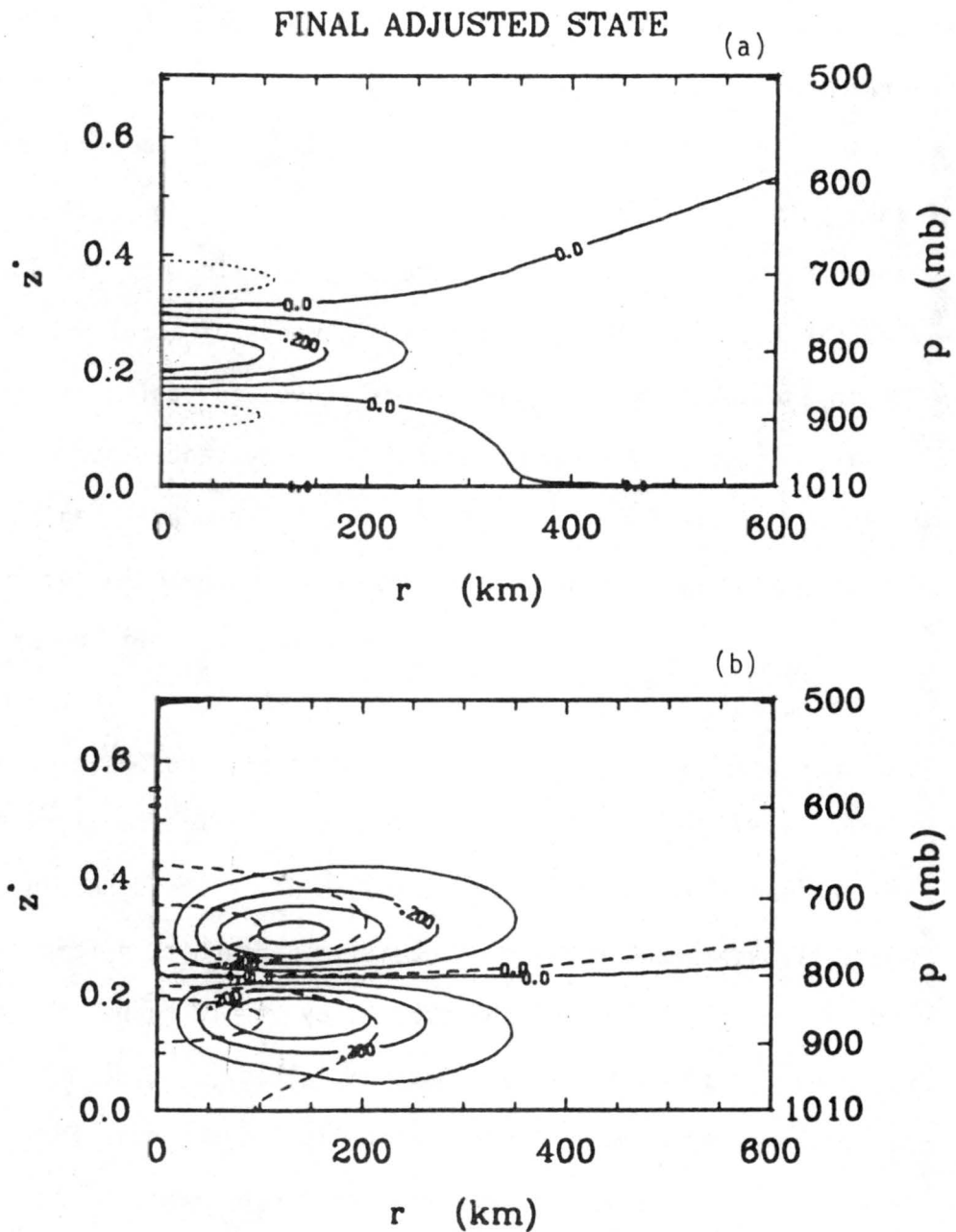


Figure 10. Final adjusted state for experiment 1a. Part (a) is the perturbation temperature  $T'(r, z^*, \infty)$  with contour interval  $0.1^\circ\text{C}$  and dotted lines for negative values. Part (b) is the tangential wind  $v(r, z^*, \infty)$  (solid lines) with contour interval  $0.1 \text{ ms}^{-1}$  and the perturbation geopotential  $\Phi'(r, z^*, \infty)$  (dashed lines) with contour interval  $2.0 \text{ m}^2\text{s}^{-2}$ .

bubble by mass continuity, as shown in Fig. 4. This rising motion reaches a maximum value of  $w^*e^{-z^*} \approx 2 \times 10^{-6} \text{ s}^{-1}$  at  $t = 1.5$  hours, corresponding to  $\omega = Dp/Dt \approx -7.5 \text{ mb/hr}$ . As the secondary circulation develops the Coriolis force acts on it to produce a broad region of weak cyclonic flow below the bubble with anticyclonic flow above. This tangential wind pattern has become better defined by  $t = 3$  hours as shown in Fig. 5, with maximum cyclonic winds of about  $0.2 \text{ m s}^{-1}$  at 900 mb and weaker anticyclonic winds above. By this time the adiabatic cooling produced by the rising motion in the center has reduced the amplitude of the warm bubble by 50% and has produced regions of cool air above and below it. The accompanying decrease in horizontal pressure gradients is reflected in the decrease in amplitude of the secondary circulation; at  $t = 6.0$  hours the rising motion in the center has vanished as shown in Fig. 6. The tangential winds have developed considerably by this time with the anticyclone now slightly stronger than the cyclone. During the next six hours weak subsidence in the center gradually warms the regions of negative perturbation temperatures above and below what is left of the bubble; by  $t = 12$  hours the tangential winds have increased to their maximum values ( $\approx 0.65 \text{ m s}^{-1}$ ) and have become somewhat more confined vertically, as shown in Fig. 7. The next twelve hours see a general reversal of these trends as the temperature field warms slightly in the center and the winds decrease in strength, as shown in Figs. 8 and 9. The magnitudes of these changes are smaller now, however, as the atmosphere has reached a quasi-balanced state.

The final adjusted state for experiment 1a is shown in Fig. 10. We see that the initial bubble of  $1.0^\circ\text{C}$  amplitude has resulted in a final perturbation temperature in the same location with a maximum of

0.4°C and cool regions with perturbation temperatures of about -0.15°C above and below. The final geostrophic wind pattern consists of a cyclone centered at  $r \approx 130$  km and  $p \approx 850$  mb with an anticyclone above it centered at  $p \approx 750$  mb. The maximum winds in this final state ( $\approx 0.40 \text{ m s}^{-1}$  in the cyclone and  $\approx 0.43 \text{ m s}^{-1}$  in the anticyclone) are about 19% of the maximum geostrophic winds of the initial state

The initial conditions for experiment 1b are identical to those of experiment 1a, except the warm bubble has been moved to the middle troposphere with  $p_L = 650$  mb,  $p_C = 550$  mb and  $p_U = 450$  mb as shown in Fig. 11. The transient adjustment in this case is qualitatively similar to the previous case; the main difference is that the secondary circulation developed in the early stages of the adjustment process is somewhat stronger, with maximum rising motions  $\omega \approx -8.7$  mb/hr. Consequently, the initial temperature field weakens more, resulting in less wind being developed. The final adjusted state, depicted in Fig. 12, has a maximum perturbation temperature of about 0.3°C; the final winds in this case are about 12% of the maximum initial geostrophic wind.

In experiment 1c we move the initial bubble to the upper troposphere, with  $p_L = 400$  mb,  $p_C = 300$  mb and  $p_U = 200$  mb as shown in Fig. 13. The secondary circulation during the adjustment process in this experiment is again slightly stronger, with the maximum rising motion reaching  $\omega \approx -9.4$  mb/hr. The final state shown in Fig. 14 indicates that the initial 1.0°C bubble has decreased in amplitude to about 0.16°C; the final winds in this case are about 5% of the maximum initial geostrophic wind.

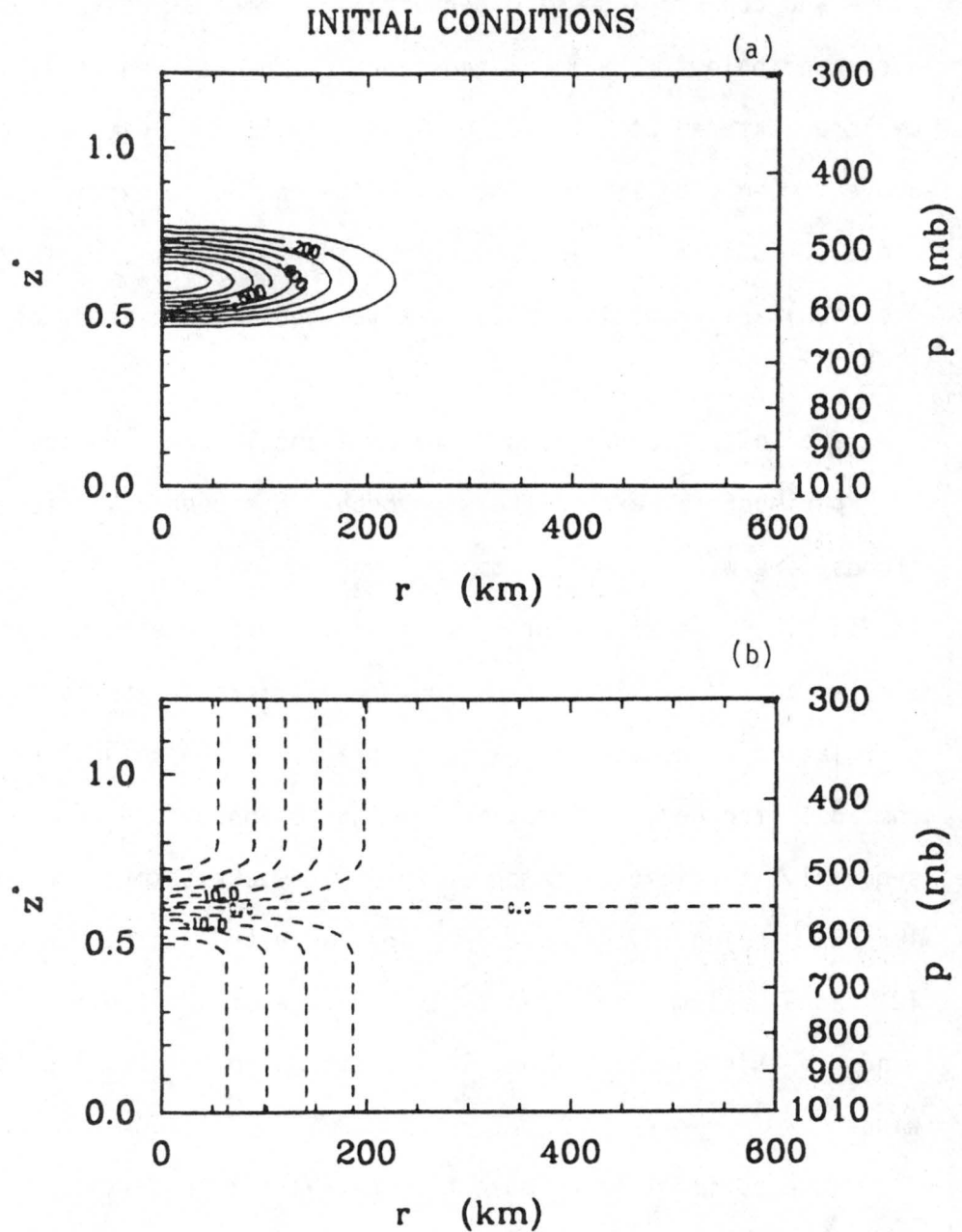


Figure 11. Initial conditions for experiment 1b. Part (a) is the perturbation temperature  $T'(r, z^*, 0)$  with contour interval  $0.1^\circ\text{C}$ . Part (b) is the perturbation geopotential  $\Phi'(r, z^*, 0)$  with contour interval  $5.0 \text{ m}^2\text{s}^{-2}$ .

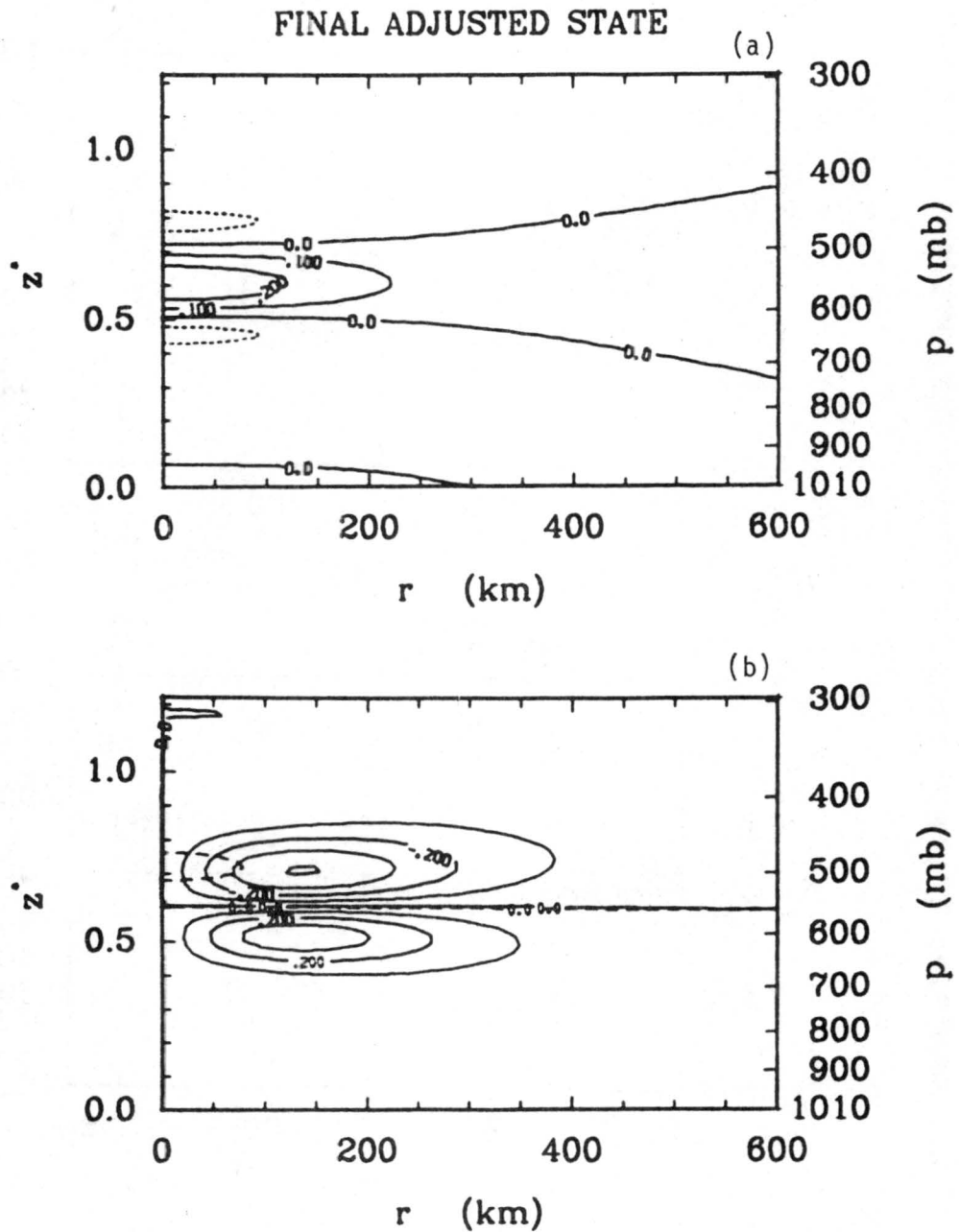


Figure 12. Final adjusted state for experiment 1b. Part (a) is the perturbation temperature  $T'(r, z^*, \infty)$  with contour interval  $0.1^\circ\text{C}$  and dotted lines for negative values. Part (b) is the tangential wind  $v(r, z^*, \infty)$  (solid lines) with contour interval  $0.1 \text{ m s}^{-1}$  and the perturbation geopotential  $\Phi'(r, z^*, \infty)$  (dashed lines) with contour interval  $5.0 \text{ m}^2 \text{ s}^{-2}$ .

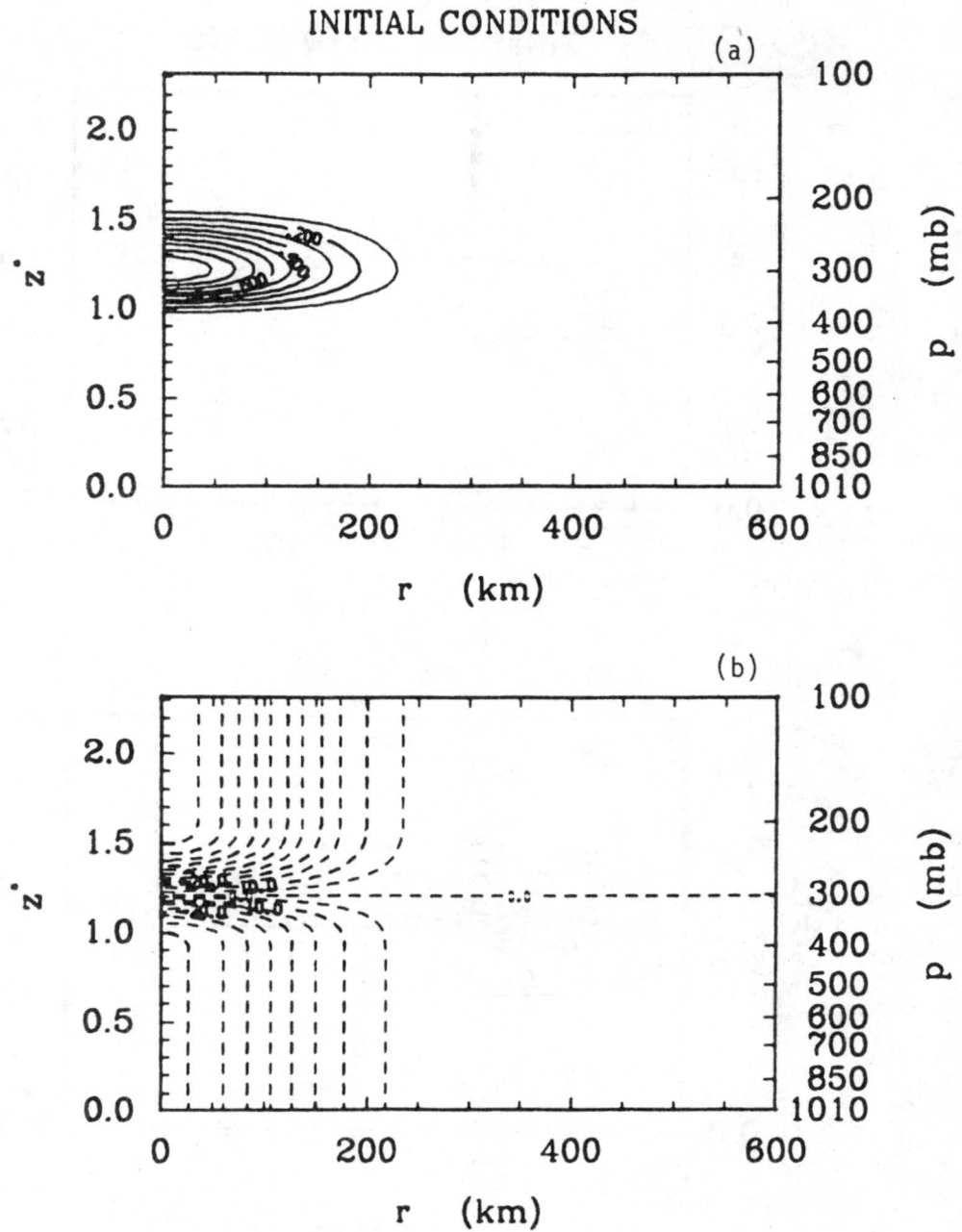


Figure 13. Initial conditions for experiment 1c. Part (a) is the perturbation temperature  $T'(r, z^*, 0)$  with contour interval  $0.1^\circ\text{C}$ . Part (b) is the perturbation geopotential  $\phi'(r, z^*, 0)$  with contour interval  $5.0 \text{ m}^2\text{s}^{-2}$ .

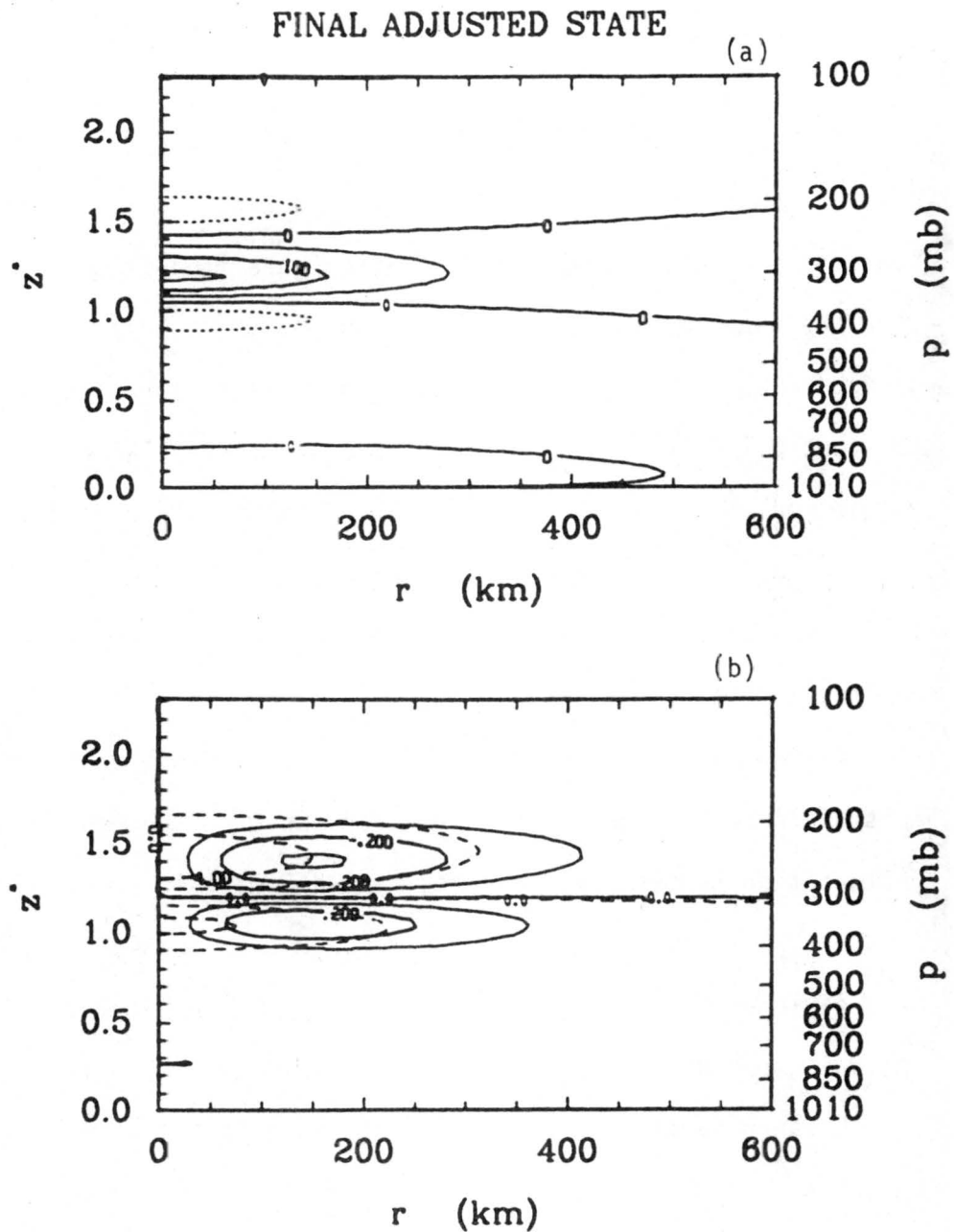


Figure 14. Final adjusted state for experiment 1c. Part (a) is the perturbation temperature  $T'(r, z^*, \infty)$  with contour interval  $0.05^\circ\text{C}$  and dotted lines for negative values. Part (b) is the tangential wind  $v(r, z^*, \infty)$  (solid lines) with contour interval  $0.1 \text{ ms}^{-1}$  and the perturbation geopotential  $\Phi'(r, z^*, \infty)$  (dashed lines) with contour interval  $2.0 \text{ m}^2\text{s}^{-2}$ .

In the final example of an initial condition in the temperature field to be considered here, experiment 1d, the warm bubble is expanded to fill most of the troposphere, with  $p_L = 900$  mb,  $p_C = 550$  mb and  $p_U = 200$  mb as shown in Fig. 15. The transient adjustment for this case is similar to that of the preceding experiments in its general features, but the secondary circulation generated is much stronger, with the maximum rising motion reaching  $\omega \approx -25$  mb/hr. The resulting strong adiabatic cooling reduces the maximum perturbation temperature to about  $0.1^\circ\text{C}$  in only three hours and the tangential wind consequently reaches only about  $0.25 \text{ m s}^{-1}$ . The final adjusted state, shown in Fig. 16, has a maximum perturbation temperature of only  $0.08^\circ\text{C}$  and a tangential wind pattern with maximum winds of only about 1% of the maximum initial geostrophic wind.

In the model considered here it is also possible to perturb the mass field by setting  $\phi'(r, z^*, 0)$  constant in  $z^*$ , so the initial perturbation temperature vanishes, but allowing it to vary in the horizontal. In experiment 1e we use this type of initial condition in the mass field with  $\hat{\phi}(r)$  given by (3.40); with  $\hat{\phi}_0 = -100 \text{ m}^2 \text{ s}^{-2}$  the initial geopotential field is as shown in Fig. 17. This initial condition can be interpreted as lowering the height of the 1010 mb surface by about 10 m and corresponds to a surface pressure drop of about 1.15 mb in a corresponding model in actual height coordinates. The transient adjustment of the mass field in this case occurs very quickly, with the maximum perturbation geopotential decreasing by a factor of 100 within the first three hours and the maximum perturbation temperature adjusting to within 2% of its final value in only a half an hour. In contrast, the tangential wind takes somewhat longer to develop and undergoes a slow, damped oscillation toward the final state as in

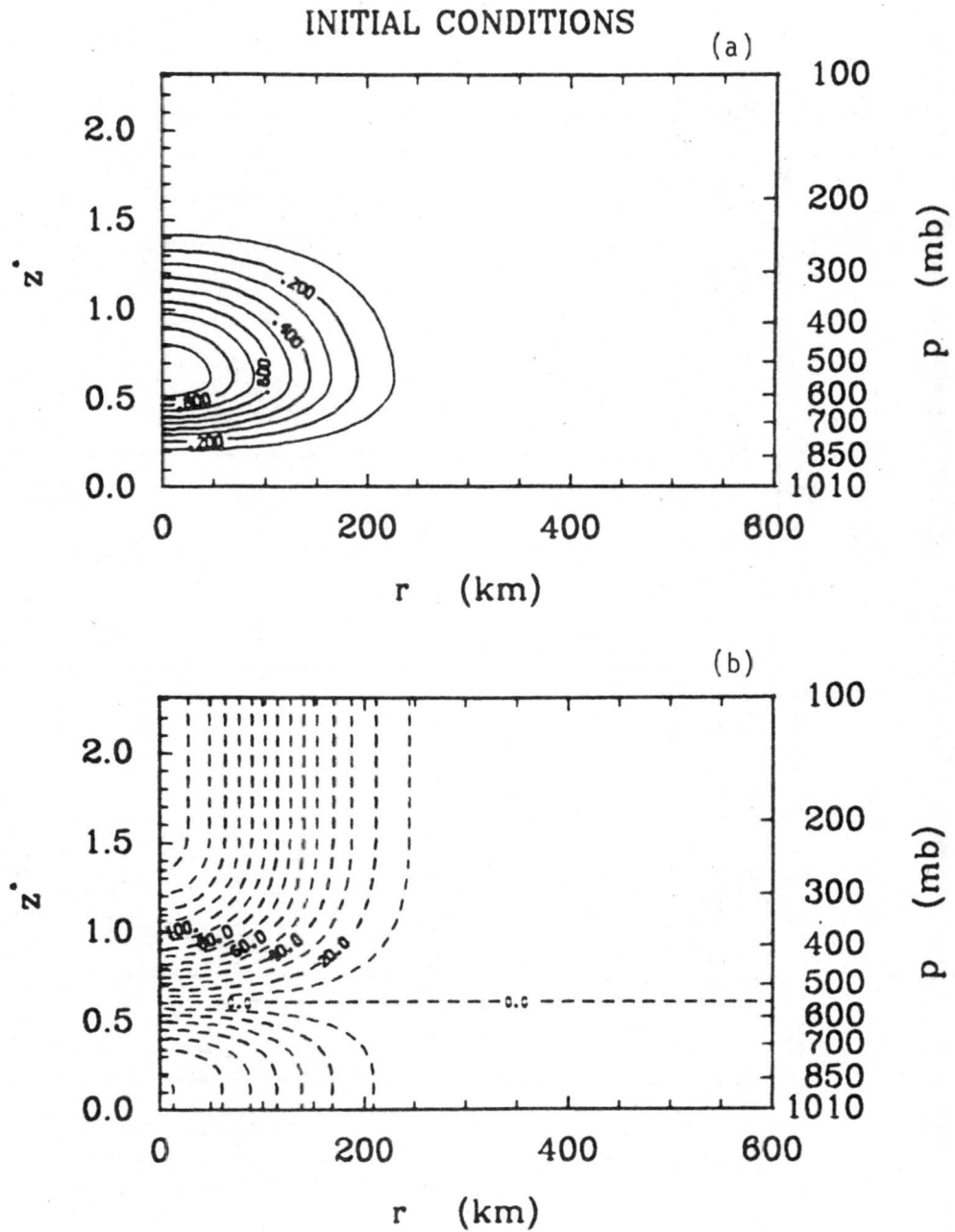


Figure 15. Initial conditions for experiment 1d. Part (a) is the perturbation temperature  $T'(r, z^*, 0)$  with contour interval  $0.1^\circ\text{C}$ . Part (b) is the perturbation geopotential  $\phi'(r, z^*, 0)$  with contour interval  $10.0 \text{ m}^2 \text{ s}^{-2}$ .

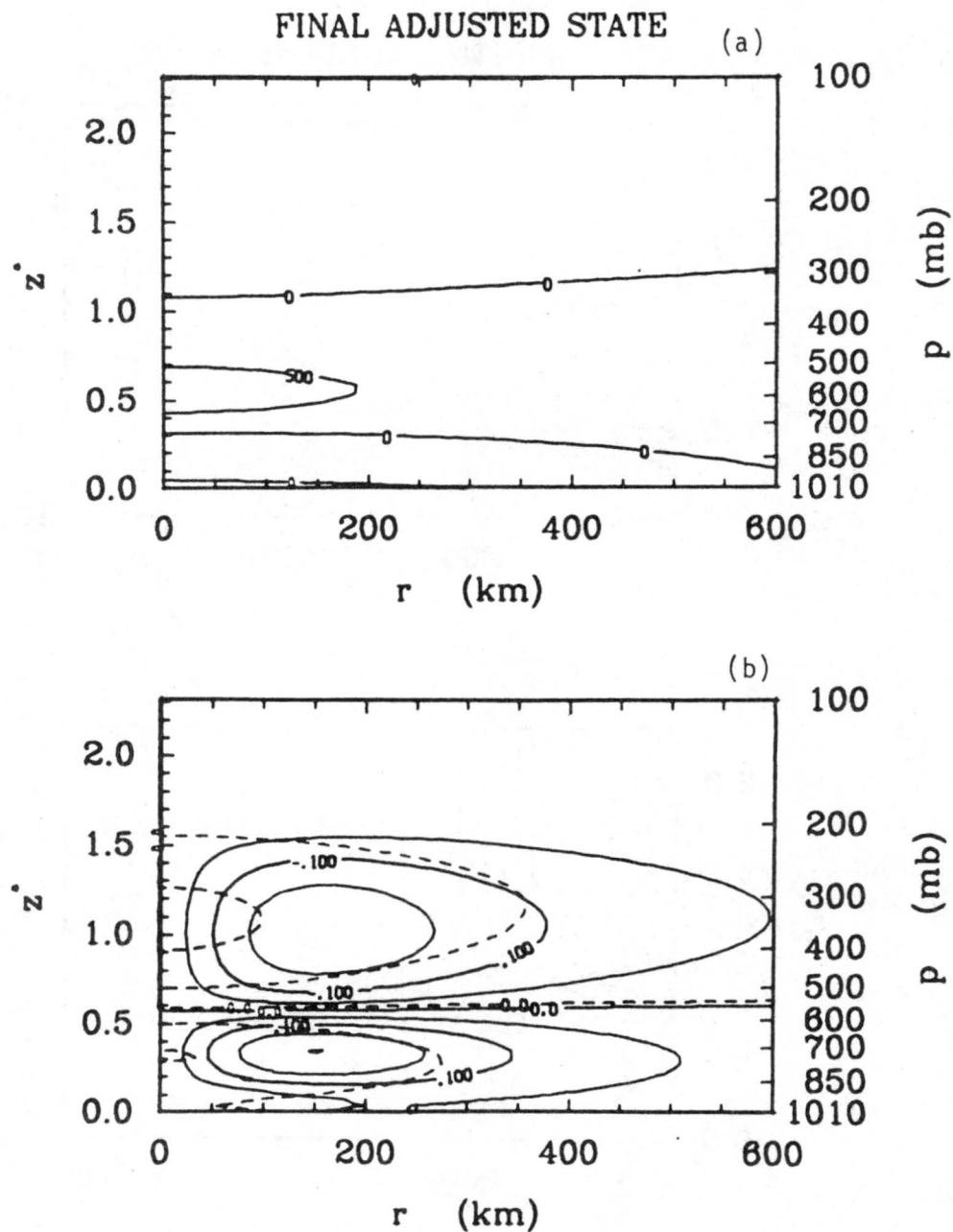


Figure 16. Final adjusted state for experiment 1d. Part (a) is the perturbation temperature  $T'(r, z^*, \infty)$  with contour interval  $0.05^\circ\text{C}$  and dotted lines for negative values. Part (b) is the tangential wind  $v(r, z^*, \infty)$  (solid lines) with contour interval  $0.05 \text{ ms}^{-1}$  and the perturbation geopotential  $\phi'(r, z^*, \infty)$  (dashed lines) with contour interval  $2.0 \text{ m}^2\text{s}^{-2}$ .

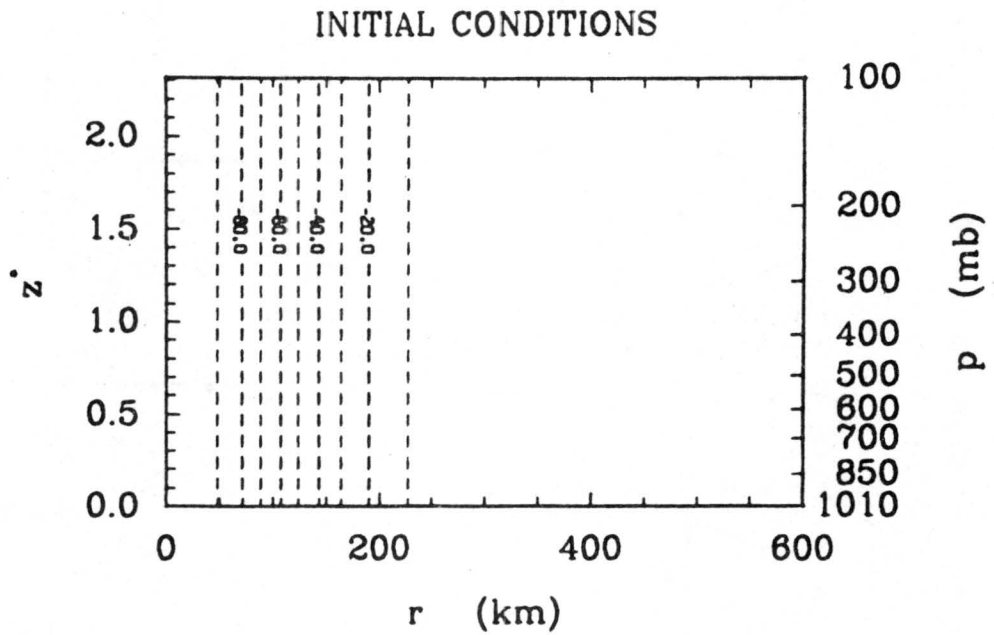


Figure 17. Initial condition in the perturbation geopotential  $\phi'(r, z^*, 0)$  for experiment 1e. The contour interval is  $10.0 \text{ m}^2 \text{ s}^{-2}$ .

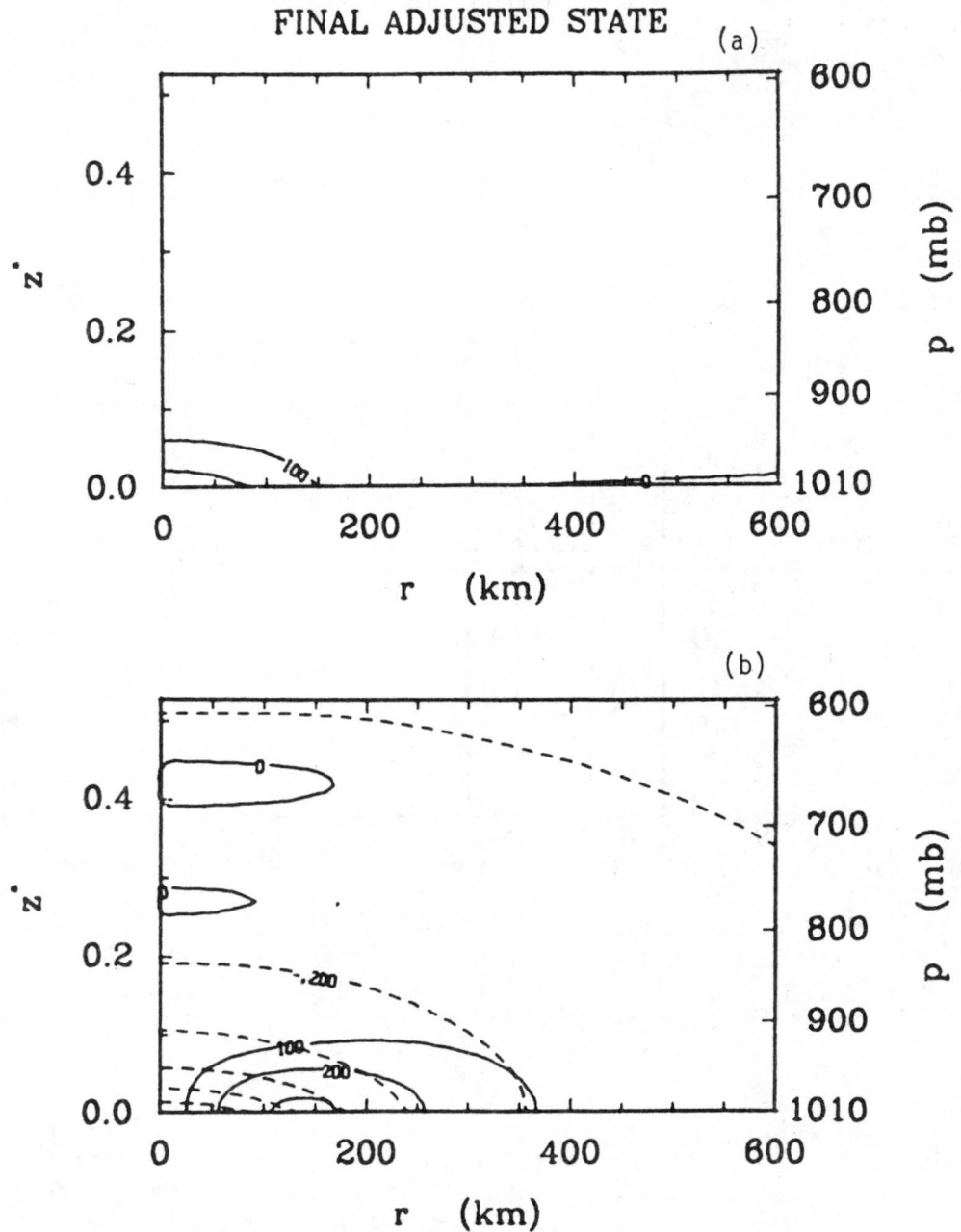


Figure 18. Final adjusted state for experiment 1e. Part (a) is the perturbation temperature  $T'(r, z^*, \infty)$  with contour interval  $0.01^\circ\text{C}$  and dotted lines for negative values. Part (b) is the tangential wind  $v(r, z^*, \infty)$  (solid lines) with contour interval  $0.01 \text{ ms}^{-1}$  and the perturbation geopotential  $\phi'(r, z^*, \infty)$  (dashed lines) with contour interval  $0.1 \text{ m}^2\text{s}^{-2}$ . Note that the  $z^*$ -scale has been changed from that of Figure 17.

experiment 1a. The final adjusted state is shown in Fig. 18, where it can be seen that essentially all of the initial disturbance has been carried away during the adjustment process, leaving behind a balanced state with a maximum perturbation temperature of only  $0.027^{\circ}\text{C}$ . The final winds, while concentrated at the surface as could be expected, are only about 0.3% of their initial geostrophic values.

### 3.3.2 experiment 2: initial condition in the vorticity field

With no initial perturbation geopotential (i.e.,  $\hat{\phi}(r) = 0$ ), (3.39) corresponds to an initial condition in the rotational part of the wind field with the horizontal structure of the tangential wind given by

$$\hat{v}(r) = \hat{v}_0 \left( \frac{r}{a} \right) e^{-r^2/a^2} \quad (3.41)$$

and  $\psi_0 = 2 f \hat{v}_0 / a$ . The maximum tangential wind occurs at  $r = a/\sqrt{2}$  (again we pick  $a = 150$  km). The corresponding vorticity field has horizontal structure

$$\hat{\zeta}(r) = \frac{2\hat{v}_0}{a} \left( 1 - \frac{r^2}{a^2} \right) e^{-r^2/a^2},$$

so that with this interpretation of  $\psi(r)$ ,  $a$  is the radius of vanishing relative vorticity, with positive vorticity for  $r < a$  and negative vorticity for  $r > a$ . We consider three experiments with this initial condition, each having a different vertical structure.

In experiment 2a the initial vertical structure of the tangential wind is defined so that the disturbance is confined to the layer 650-450 mb in the vertical, with a maximum wind of  $1 \text{ m s}^{-1}$  at  $r = 106$  km and  $p = 550$  mb. This initial tangential wind pattern is shown in Fig. 19; the initial perturbation temperature and geopotential are zero.

The time evolution of this initial condition is depicted in Figs. 20-25. The initially unbalanced Coriolis force produces a region of

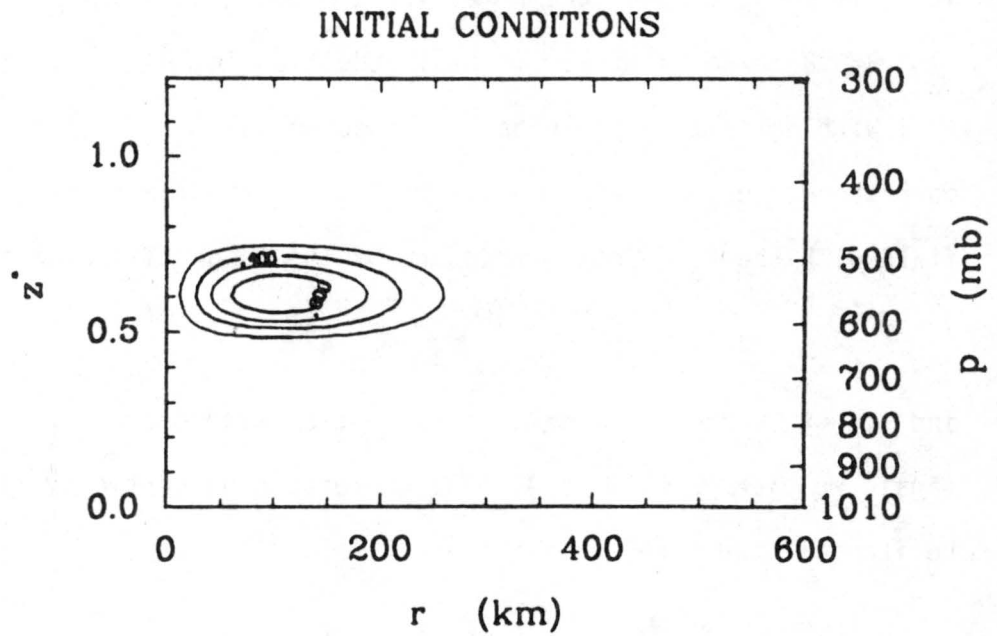


Figure 19. Initial condition in the tangential wind  $v(r, z^*, 0)$  for experiment 2a. The contour interval is  $0.2 \text{ ms}^{-1}$ .

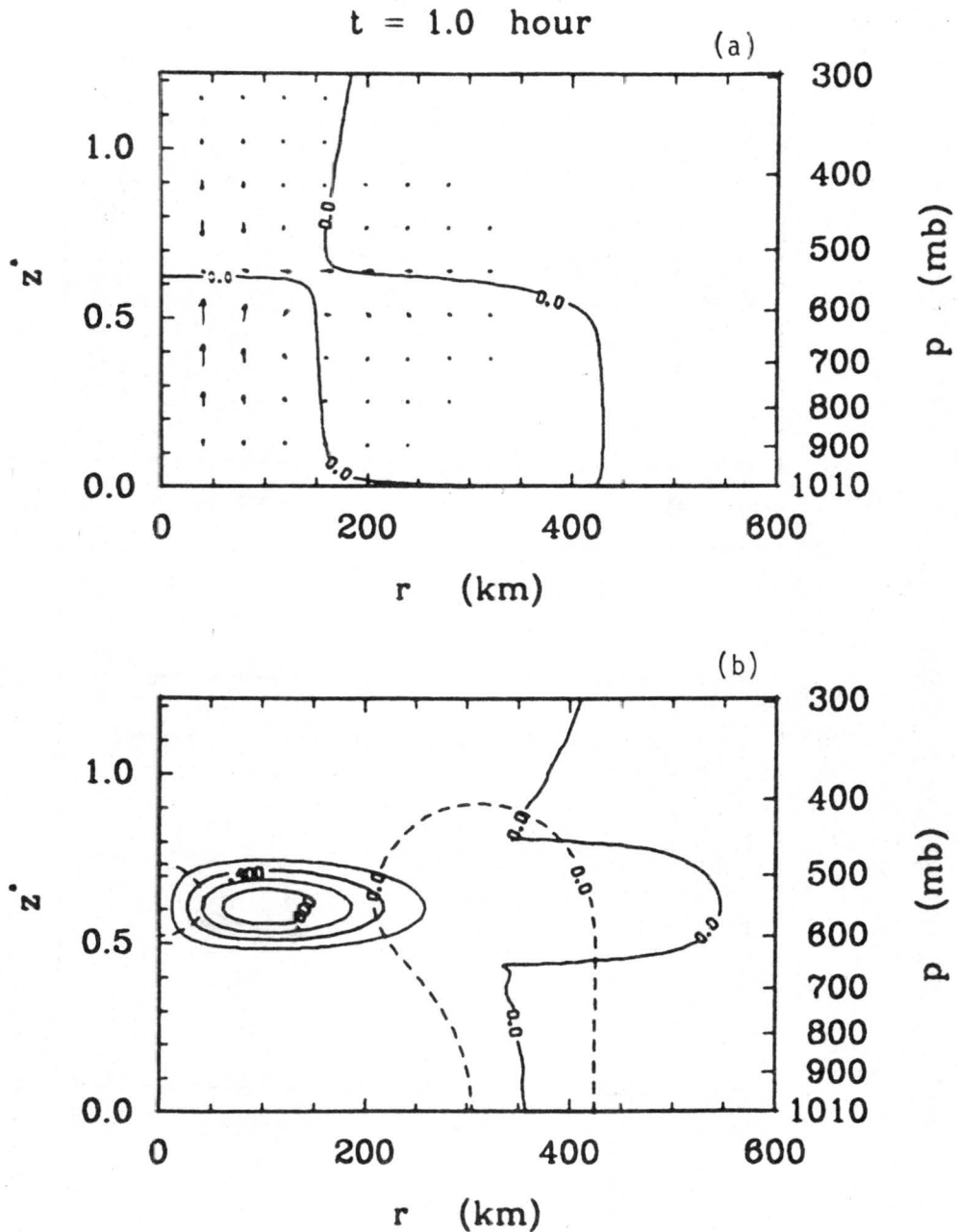


Figure 20. Transient state of the atmosphere at  $t=1.0$  hour for experiment 2a. Part (a) is the perturbation temperature  $T'(r, z^*, t)$  with contour interval  $0.05^\circ\text{C}$  and dotted lines for negative values, and the secondary circulation  $ue^{-z^*}$ ,  $w^*e^{-z^*}$  with the vertical component scaled by  $1 \times 10^{11}$ . Part (b) is the tangential wind  $v(r, z^*, t)$  (solid lines) with contour interval  $0.2 \text{ ms}^{-1}$  and the perturbation geopotential  $\phi'(r, z^*, t)$  (dashed lines) with contour interval  $2.0 \text{ m}^2\text{s}^{-2}$ .

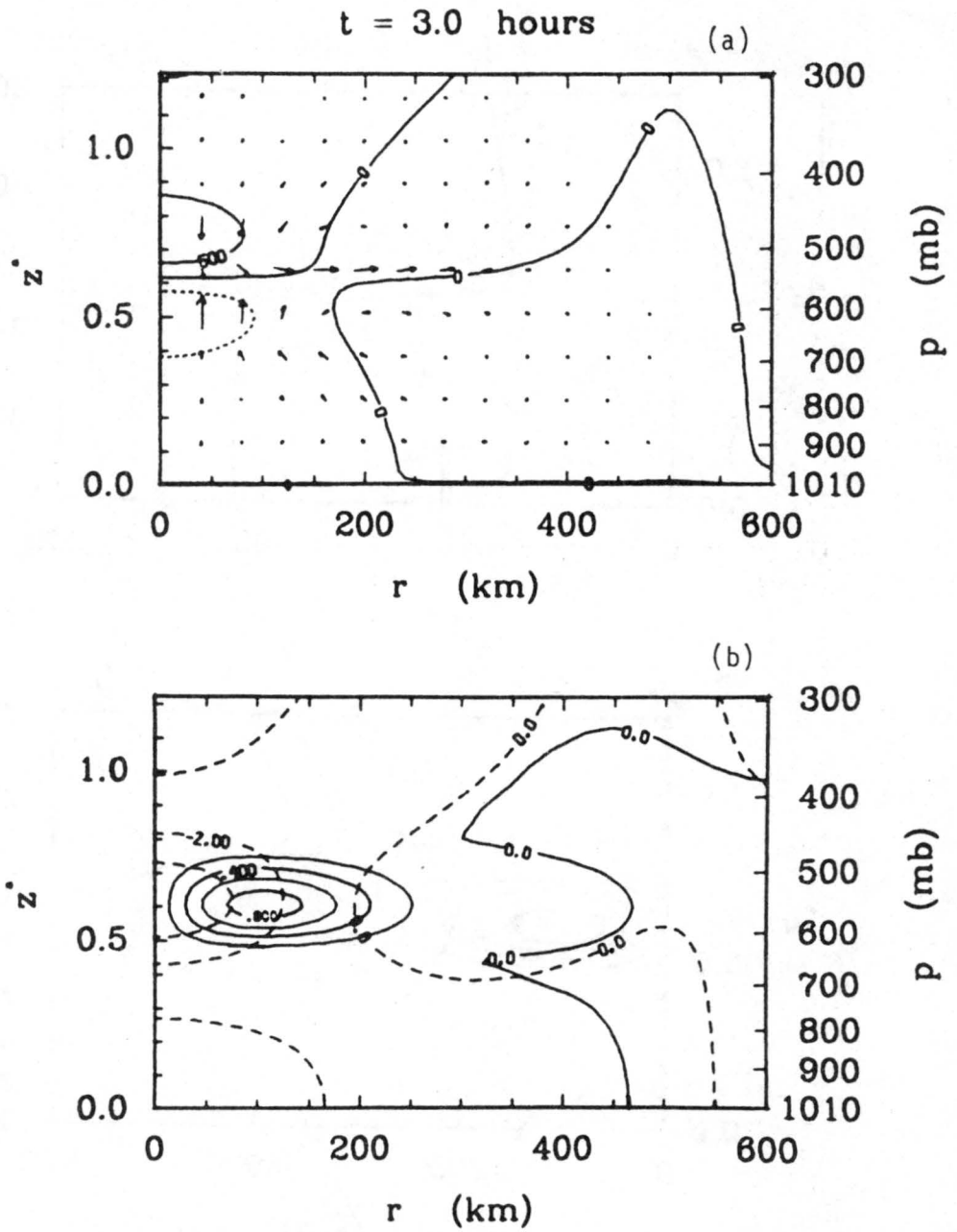


Figure 21. Same as Figure 20 but for  $t = 3.0$  hours.

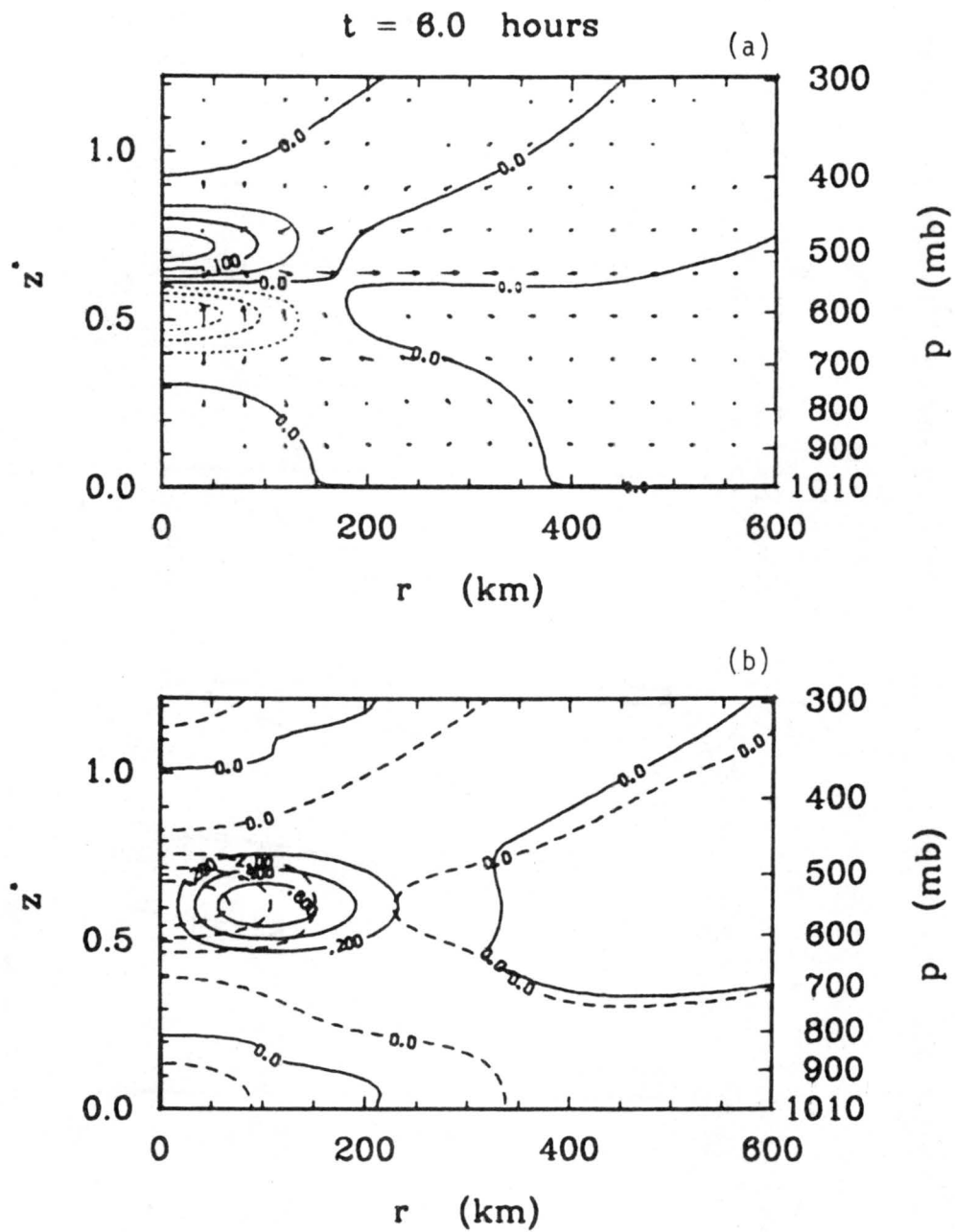


Figure 22. Same as Figure 20 but for  $t = 6.0$  hours .

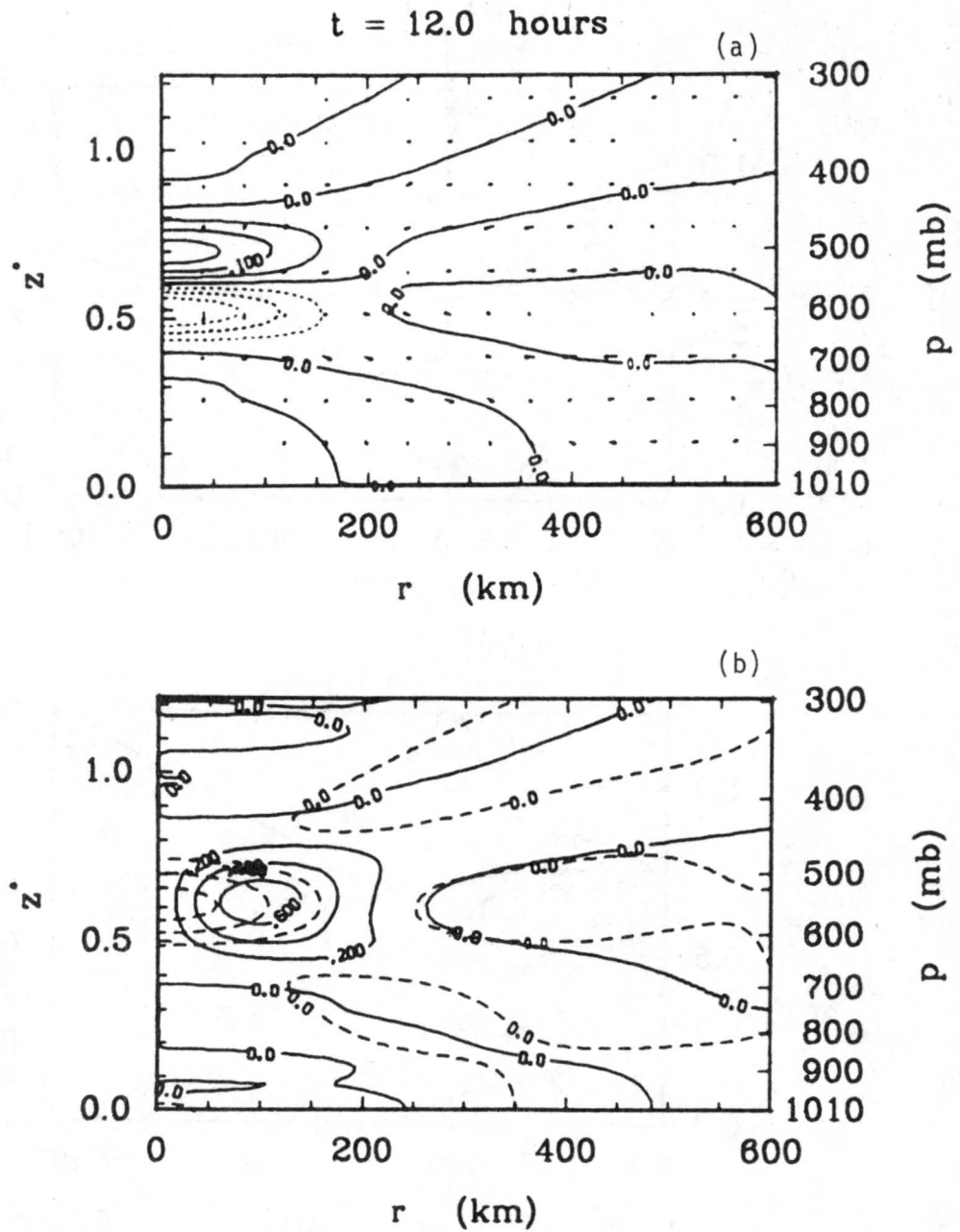


Figure 23. Same as Figure 20 but for  $t = 12.0$  hours.

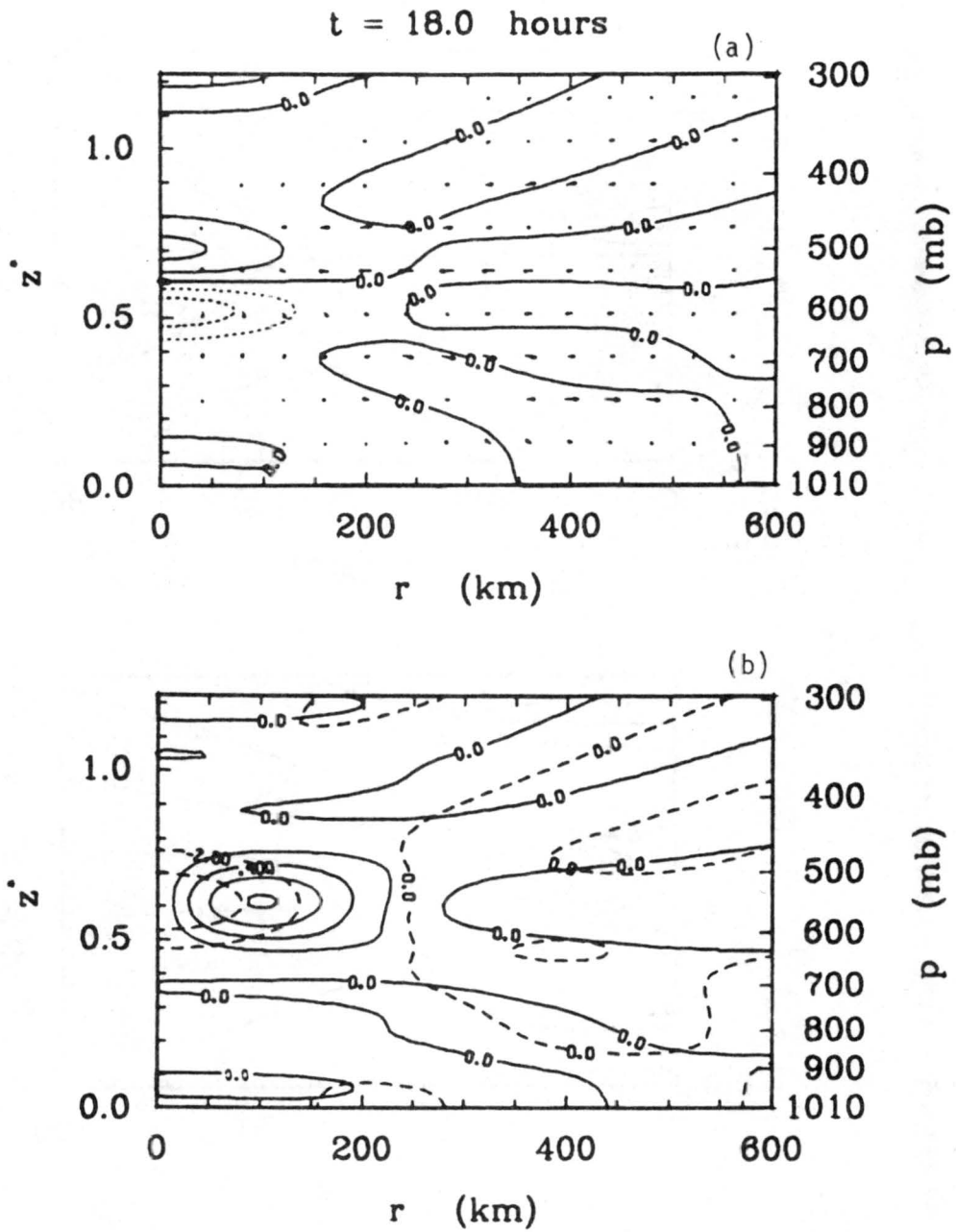


Figure 24. Same as Figure 20 but for  $t = 18$  hours .

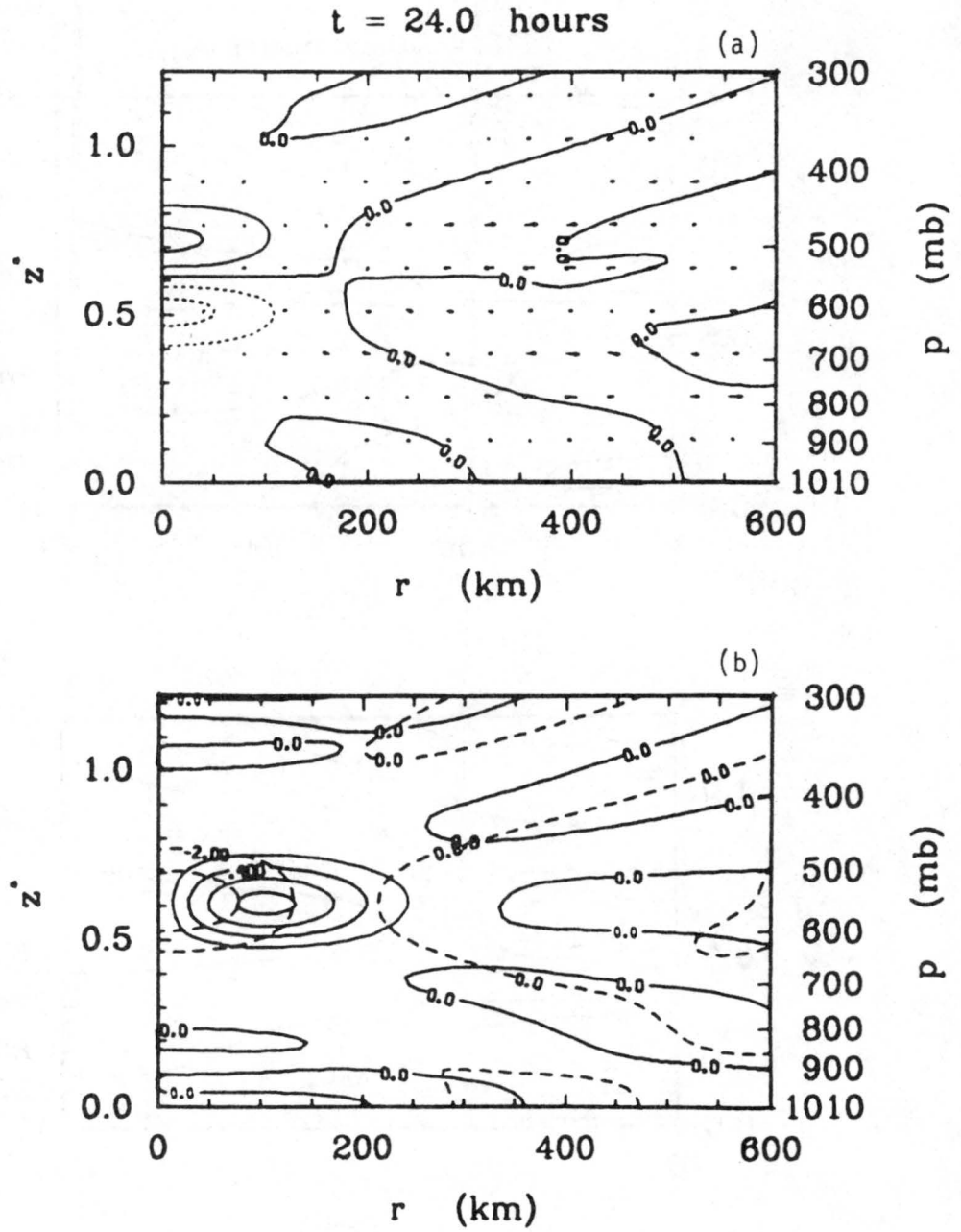


Figure 25. Same as Figure 20 but for  $t = 24$  hours .

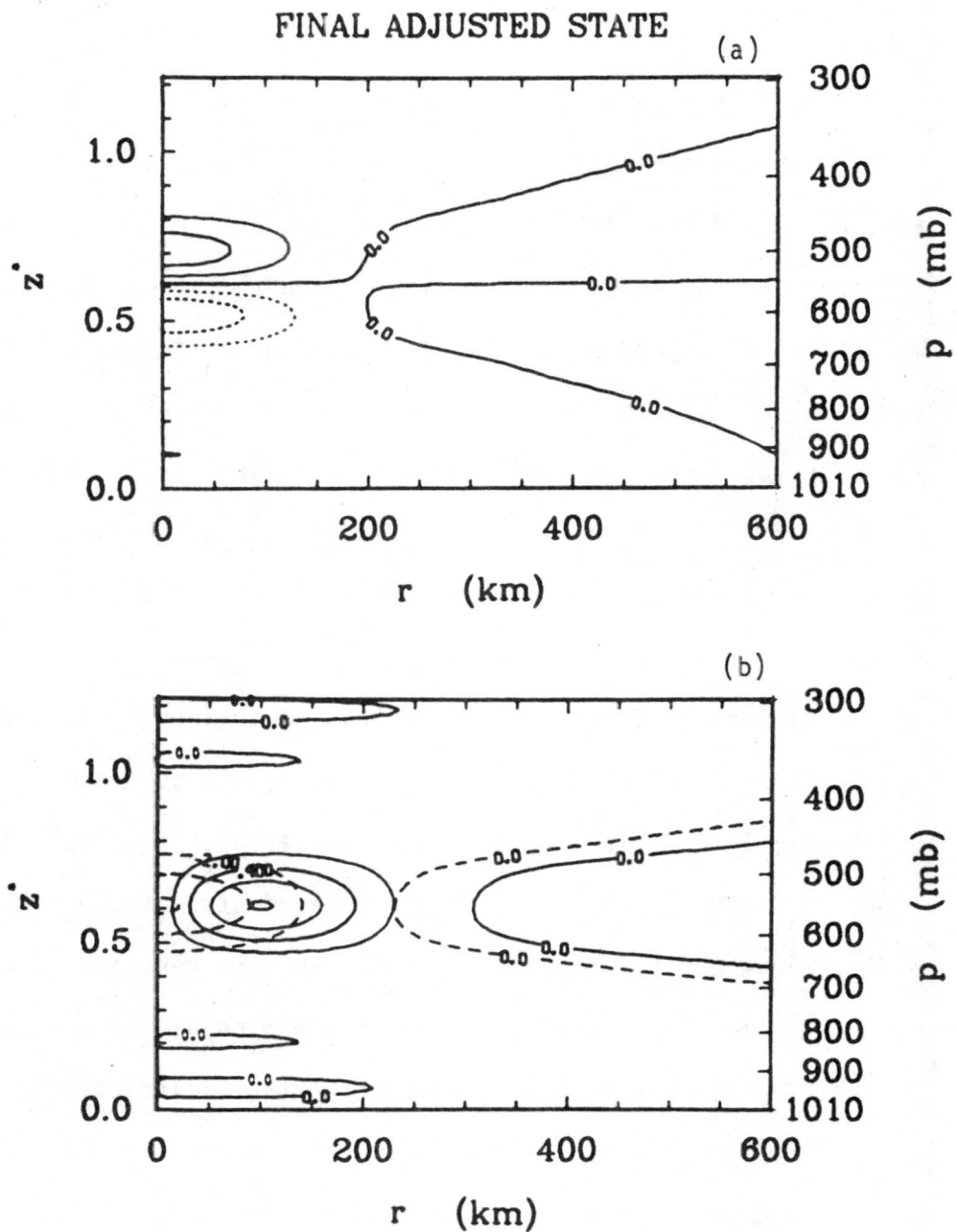


Figure 26. Final adjusted state for experiment 2a. Part (a) is the perturbation temperature  $T'(r, z^*, \infty)$  with contour interval  $0.05^\circ\text{C}$  and dotted lines for negative values. Part (b) is the tangential wind  $v(r, z^*, \infty)$  (solid lines) with contour interval  $0.2 \text{ ms}^{-1}$  and the perturbation geopotential  $\phi'(r, z^*, \infty)$  (dashed lines) with contour interval  $2.0 \text{ m}^2\text{s}^{-2}$ .

outflow in the region of the initial vortex by  $t = 1.0$  hour as shown in Fig. 20. This outflow generates vertical convergence at  $r = 0$  at the same level, as required by mass continuity, and the associated rising and sinking motions begin to cool the atmosphere below  $p = 550$  mb in the center and warm it above. By  $t = 3.0$  hours this secondary circulation has already reached its maximum strength (about 1.0 mb/hr rising motion and 0.86 mb/hr sinking motion) and has generated temperature perturbations on the order of  $0.1^\circ\text{C}$  in the center as shown in Fig. 21. The horizontal component of the secondary circulation reaches a maximum strength of  $rue^{-z^*} \approx 2.2 \times 10^4 \text{ m}^2 \text{ s}^{-1}$  after four hours, corresponding to a radial wind  $u \approx 0.23 \text{ m s}^{-1}$  at  $r \approx 180 \text{ km}$  and  $p \approx 550 \text{ mb}$ . As the Coriolis force acts on this radial flow it produces a slight weakening of the initial vortex, so that by  $t = 6.0$  hours the maximum tangential wind has been reduced by 23% as shown in Fig. 22. The temperature perturbations in the center peak at about  $0.2^\circ\text{C}$  around nine hours and the vortex reaches a minimum strength of about  $0.7 \text{ m s}^{-1}$  an hour later. The secondary circulation then reverses itself so that by  $t = 12.0$  hours the radial wind in the region of the vortex is directed inward, as shown in Fig. 23. Figures 24 and 25 indicate that the changes which occur during the next twelve hours are relatively small; the atmosphere has reached a quasi-balanced state.

The final adjusted state for experiment 2a is shown in Fig. 26. The initial vortex has been reduced in strength by about 20% and a region of weak anticyclonic flow has been generated in the same layer outside of  $r = 300 \text{ km}$ . The corresponding perturbation temperature field shows a cool central region of amplitude  $-0.14^\circ\text{C}$  at  $p = 600 \text{ mb}$  with a similar warm region above it at  $p = 500 \text{ mb}$ . The final

geopotential depression at the center is approximately 70% of its initial geostrophic value.

In experiment 2b we consider a different vertical structure for the wind perturbation (3.41). As shown in Fig. 27 this wind pattern consists of a low-level cyclone centered at 850 mb and an upper-level anti-cyclone centered at 250 mb; the maximum winds are  $1 \text{ m s}^{-1}$  at  $r = 106 \text{ km}$  in both regions and the wind vanishes at the surface,  $p = 550 \text{ mb}$  and the top of the atmosphere. The initial thermodynamic fields are again taken to be zero. The secondary circulation generated in this experiment is more complicated than that of the previous experiment, with the largest vertical motions being about  $1.7 \text{ mb/hr}$ , occurring in the lower atmosphere. The final adjusted state shown in Fig. 28 indicates that the intensity of the low-level cyclone has decreased by about 10% during the adjustment process while the upper-level anti-cyclone has changed by only about 3%. A warm region has been generated in the middle troposphere with cool regions above and below; the final perturbation geopotential values at  $r = 0$  are roughly 95% and 85% of the corresponding initial geostrophic values in the upper and lower atmosphere, respectively.

As a final example of a wind perturbation we consider an initial wind field which is constant in the vertical; thus the initial condition for experiment 2c consists of a tangential wind field which is given by (3.41) at all levels. No figures are presented for this experiment because for all practical purposes the initial and final winds are identical. The final perturbation geopotential field is essentially the same as the corresponding initial geostrophic geopotential; the geopotential depression in the center of  $8.7 \text{ m}^2 \text{ s}^{-2}$  corresponds to

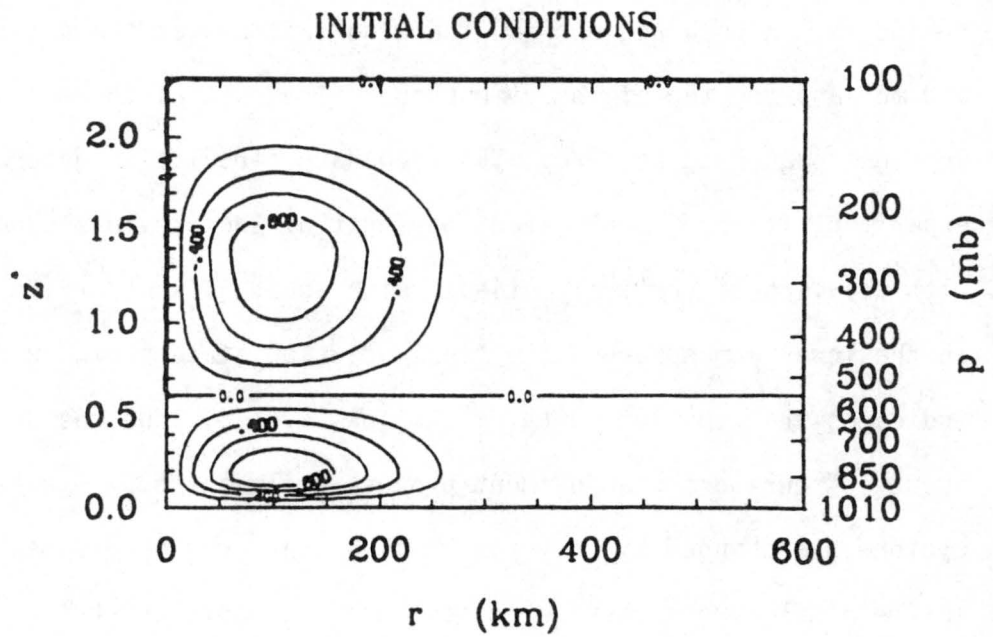


Figure 27. Initial condition in the tangential wind  $v(r, z^*, 0)$  for experiment 2b. The contour interval is  $0.2 \text{ ms}^{-1}$ .

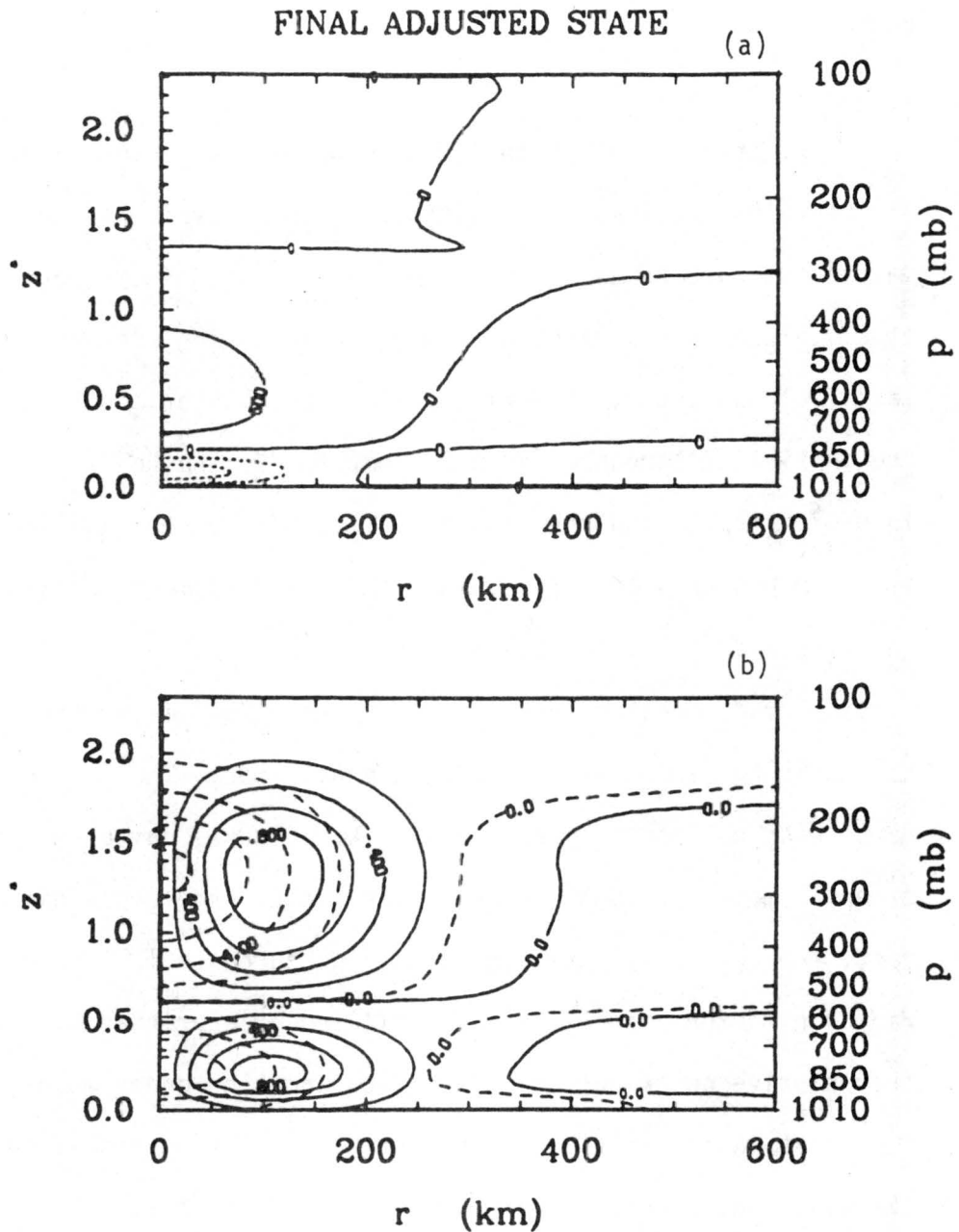


Figure 28. Final adjusted state for experiment 2b. Part (a) is the perturbation temperature  $T'(r, z^*, \infty)$  with contour interval  $0.05^\circ\text{C}$  and dotted lines for negative values. Part (b) is the tangential wind  $v(r, z^*, \infty)$  (solid lines) with contour interval  $0.2 \text{ ms}^{-1}$  and the perturbation geopotential  $\Phi'(r, z^*, \infty)$  (dashed lines) with contour interval  $2.0 \text{ m}^2 \text{ s}^{-2}$ .

lowering the central surface pressure by 0.1 mb in a model in height coordinates.

### 3.4 Discussion

The manner in which the adjustment process depends on the vertical structure of the initial conditions in the experiments described above may be interpreted as follows. As is generally known (e.g. Schubert et al., 1980), in a barotropic model with a single phase speed  $c$  the mass field adjusts to the wind field when the horizontal scale  $a$  of the initial disturbance is small compared to the Rossby radius of deformation  $c/f$ , and the wind field adjusts to the mass field when  $a$  is large compared to  $c/f$ . In the stratified model considered here there is a distinct radius of deformation  $c_n/f$  associated with each vertical mode  $n$ ; these radii range from 5754 km for the external mode to 40.65 km for the thirtieth internal mode. Thus an initial disturbance with horizontal scale  $a = 150$  km "looks" quite small to the external mode but much larger to the higher order internal modes. In fact, the horizontal scale of such a disturbance is larger than the radius of deformation  $c_n/f$  for all  $n$  greater than 8. Therefore, the relative contributions of the low and high order modes should be important in determining the extent to which the mass field adjusts to the wind field (or vice versa) in the stratified model.

Table 2 shows the coefficients of the projection of the initial conditions onto the first sixteen vertical modes as determined from (3.27) for the eight experiments described above. For each experiment the coefficients have been normalized by the value of  $D_n$  which is largest in absolute value for that experiment. The following general trends can be observed. In experiments 1a, 1b, and 1c, as the initial

n	$c_n$ ( $m\ s^{-1}$ )	$\frac{fa}{c_n}$	$D_n$ (normalized)								
			exp. 1a	exp. 1b	exp. 1c	exp. 1d	exp. 1e	exp. 2a	exp. 2b	exp. 2c	
0	287.00	0.03	1.000	-0.140	0.531	-0.319	1.000	-0.919	-0.028	1.000	
1	56.28	0.13	-0.573	1.000	1.000	1.000	0.034	-0.456	0.897	0.034	
2	29.79	0.25	-0.601	0.712	-0.094	0.492	0.010	0.272	1.000	0.010	
3	20.09	0.37	-0.556	0.285	-0.285	0.079	0.005	0.915	0.053	0.005	
4	15.13	0.49	-0.485	-0.061	0.092	-0.045	0.003	1.000	-0.113	0.003	
5	12.13	0.62	-0.398	-0.222	0.126	-0.039	0.002	0.471	-0.137	0.002	
6	10.12	0.74	-0.306	-0.198	-0.059	-0.026	0.001	-0.307	-0.207	0.001	
7	8.68	0.86	-0.213	-0.071	-0.051	-0.017	0.001	-0.823	-0.178	0.001	
8	7.59	0.99	-0.126	0.054	0.034	-0.007	0.001	-0.778	-0.152	0.001	
9	6.75	1.11	-0.051	0.108	0.021	-0.002	0.001	-0.266	-0.152	0.001	
10	6.08	1.23	0.011	0.084	-0.013	0.000	0.000	0.331	-0.135	0.000	
11	5.53	1.35	0.056	0.020	-0.008	0.001	0.000	0.631	-0.113	0.000	
12	5.07	1.48	0.084	-0.035	0.003	0.001	0.000	0.503	-0.106	0.000	
13	4.68	1.60	0.097	-0.052	0.005	0.000	0.000	0.106	-0.095	0.000	
14	4.34	1.72	0.097	-0.034	0.001	0.000	0.000	-0.264	-0.079	0.000	
15	4.05	1.85	0.087	-0.003	-0.003	0.000	0.000	-0.393	-0.070	0.000	

Table 2. Coefficients  $D_n$  of the projection of the initial vertical structure onto the first sixteen vertical modes for the eight experiments described in section 3.3. For each experiment the  $D_n$  are normalized by the value of  $D_n$  which is largest in absolute value for that experiment. The second column gives the phase speed and the third column compares the horizontal scale  $a=150$  km to the radius of deformation  $c_n/f$  for each mode.

warm bubble is moved higher in the troposphere the relative contributions of the higher order modes become smaller. When the bubble is expanded in experiment 1d to fill most of the troposphere, the relative contribution of the higher order modes is even less. For experiment 2a the fact that the initial wind is confined vertically leads to relatively large contributions from the higher order modes, while the more slowly changing initial vertical structure of experiment 2b projects more onto the lower order modes. Finally, when the initial geopotential or tangential wind is constant in the vertical as in experiments 1e and 2c the only contribution of any real significance is from the external mode. We note that these trends can be deduced from a comparison of the initial conditions with the vertical structure functions shown in Fig. 2.

Knowing the relative contributions of the various vertical modes we can interpret the results of the previous section as follows. In experiment 1a the contributions of the higher order modes are relatively important and thus in a general sense the initial disturbance does not "look" particularly small in the horizontal. Therefore, even though the mass field does tend to adjust to the initial wind field (since the initial wind is zero, this implies that the initial temperature disturbance tends to weaken considerably), a significant fraction of the initial perturbation remains in the final balanced state. In contrast, as a greater portion of the initial condition is projected onto the lower order modes in experiments 1b, 1c and 1d, the horizontal scale of the disturbance "looks" smaller in a general sense and the adjustment of the mass field to the wind field is more nearly complete. Finally, in the extreme case of experiment 1e, where practically all of the

initial condition is projected onto the external mode, the disturbance "looks" extremely small and the adjustment of the mass field to the wind field is almost total. An analogous interpretation holds for the initial wind experiments; here the adjustment of the mass field to the wind field implies that the initial wind changes very little during the adjustment process.

#### 4. CONCLUSIONS

In this study we have derived a general solution to the problem of geostrophic adjustment in a stratified atmosphere. The spectral expansion employed in the vertical has proven useful in providing a simple interpretation of the results in terms of the corresponding barotropic problem. Simple experiments have been used to illustrate the adjustment process and investigate its dependence on the vertical structure of the initial conditions.

Schubert et al. (1980) concluded from an essentially barotropic study that in the tropics the efficiency of cloud cluster scale heating in producing balanced vortex flow is very low while the efficiency of cloud cluster scale modification of the vorticity field is very high. We conclude from the results of the present study that when the vertical stratification of the atmosphere is taken into account these generalizations remain true but the efficiencies may be changed significantly. This change is generally in the direction of moderating the above conclusions; i.e., with vertical structure heating perturbations on the cloud cluster scale can be significantly more efficient and vorticity perturbations on the cloud cluster scale significantly less efficient than the simpler barotropic analysis might lead one to expect. The extent to which these efficiencies are changed depends on how the initial conditions project onto the various vertical modes. In particular, for initial conditions on the cloud cluster scale with significant contributions from the higher-order vertical modes the mass field adjusts less to the wind field than might be expected, thus increasing the efficiency of heating and decreasing the efficiency of vorticity

field modification in producing balanced vortex flow. Thus we conclude that the vertical structure of the initial conditions can have important effects on the geostrophic adjustment process.

In applying these results to the understanding of dynamical processes in the tropical atmosphere certain limitations of the approach taken here need to be recognized. First, this study assumes a constant Coriolis parameter. Second, only linear perturbations are considered, implying that the final state is in geostrophic rather than gradient balance. Third, the basic state is assumed to be at rest, which simplifies the mathematical treatment but implies that the results may be applied directly only to situations in which the mean flow is relatively weak. Fourth, the model is dry and thus the possibility of feedback between a moisture field and the vertical motion field generated in the adjustment process has been eliminated. Fifth, the effects of transient (rather than impulsive) forcing have not been included in this study. Finally, this analysis assumes a rigid lid at a finite level in the atmosphere, an upper boundary condition which does not allow for the vertical propagation of energy out of the model. This assumption will be discussed further below.

The results presented here may be extended in several ways. First, the constant static stability profile of the basic state may be replaced by a suitable temperature profile determined from observations. In this case the vertical structure equation must be solved numerically. The results of Hack and Schubert (1980) for a similar problem suggest that the effects of this change will be relatively minor. Second, energetics may be computed using a form of the Parseval relation appropriate to the spectral expansion. Third, the rigid lid upper

boundary condition may be replaced by a condition which allows for the vertical propagation of energy out of the model. As a result of such a condition the phase speed spectrum for the internal modes becomes continuous and the discrete spectral representation used here is replaced by an appropriate integral transform in the vertical. At this point in time the physical validity of various upper boundary conditions remains an open question, but a comparison of the geostrophic adjustment process with and without a lid may shed some light on this problem. The author is currently investigating the above three topics. A final topic for further study is the consideration of nonlinear effects and a non-resting basic state. This is a difficult theoretical problem and may not yield to solution by analytical methods.

## REFERENCES

- Abramowitz, M., and I.A. Stegun, 1964: Handbook of Mathematical Functions. Dover edition, 1965, Dover, New York, 1046 pp.
- Arfken, G., 1970: Mathematical Methods for Physicists, second edition. Academic Press, New York, 815 pp.
- Blumen, W., 1972: Geostrophic adjustment. Rev. Geophys. Space Phys., 10, 485-528.
- \_\_\_\_\_, and W. M. Washington, 1969: The effect of horizontal shear flow on geostrophic adjustment in a barotropic fluid. Tellus, 21, 167-176.
- Bolin, B., 1953: The adjustment of a non-balanced velocity field towards geostrophic equilibrium in a stratified fluid. Tellus, 5, 373-385.
- Cahn, A., 1945: An investigation of the free oscillations of a simple current system. J. Meteorol., 2, 113-119.
- Charney, J. G., 1948: On the scale of atmospheric motions. Geofysiske Publikasjoner, 17, 1-17.
- Eckart, C., 1960: Hydrodynamics of Oceans and Atmospheres. Pergamon Press, New York, 290 pp.
- Erdelyi, A., W. Magnus, F. Oberhettinger, and F. G. Tricomi, 1954: Tables of Integral Transforms, 2 volumes. McGraw-Hill, New York.
- Fischer, G., 1963: Über die Adaption einfacher Stromfelder in der Atmosphäre. Ber. Dent. Wetterdienstes, 12(87), 87/3-87/20.†
- Fjelsted, J. E., 1958: Ocean current as an initial value problem. Geofysiske Publikasjoner, 20, 1-24.
- Geisler, J. E., and R. E. Dickinson, 1972: The role of variable Coriolis parameter in the propagation of inertia-gravity waves during the process of geostrophic adjustment. J. Phys. Oceanogr., 2, 263-272.
- Hack, J. J. and W. H. Schubert, 1980: Lateral boundary conditions for tropical cyclone models. Submitted to Mon. Wea. Rev.
- Jacobs, S. J., and A. Wiin-Nielsen, 1966: On the stability of a barotropic basic flow in a stratified atmosphere. J. Atmos. Sci., 23, 682-687.
- Jordan, C. L., 1958: Mean soundings for the West Indies area. J. Meteorol., 15, 91-97.

- Kibel, I. A., 1963: An Introduction to the Hydrodynamical Methods of Short Period Weather Forecasting. Translation edited by R. Baker. Pergamon, New York, 375 pp.
- Lindzen, R. S., and D. Blake, 1972: Lamb waves in the presence of realistic distributions of temperature and dissipation. J. Geophys. Res., 77, 2166-2176.
- Mihaljan, J. M., 1963: The exact solution of the Rossby adjustment problem. Tellus, 15, 150-154.
- Monin, A. S., 1958: Pressure variations in a baroclinic atmosphere. Izv. Acad. Sci. USSR, Phys. Solid Earth, No. 4, 280-286.
- Morse, P. M. and H. Feshbach, 1953: Methods of Theoretical Physics, vol. I. McGraw-Hill, New York, 997 pp.
- Obukhov, A. M., 1949: On the question of geostrophic wind (in Russian), Izv. Akad. Nauk SSSR, Ser. Geograf.-Geofiz., 13, 281-306.†
- Paegle, J., 1978: The transient mass-flow adjustment of heated atmospheric circulations. J. Atmos. Sci., 35, 1678-1688.
- Phillips, N. A., 1966: The equations of motion for a shallow rotating atmosphere and the "traditional approximation". J. Atmos. Sci., 23, 626-628.
- Rossby, C.-G., 1938: On the mutual adjustment of pressure and velocity distributions in certain simple current systems, II. J. Mar. Res., 1, 239-263.
- Schubert, W. H., J. J. Hack, P. L. Silva Dias and S. R. Fulton, 1980: Geostrophic adjustment in an axisymmetric vortex. J. Atmos. Sci., 37, in press.
- Siebert, M., 1961: Atmospheric tides. Advances in Geophysics, 7, Academic Press, New York, 105-187.
- Silva Dias, P. L., and W. H. Schubert, 1979: The dynamics of equatorial mass-flow adjustment. Atmospheric Science Paper No. 312, Department of Atmospheric Science, Colorado State University, Fort Collins, Colorado. 203 pp.
- Sneddon, I. N., 1972: The Use of Integral Transforms. McGraw-Hill, New York, 539 pp.
- Taylor, G. I., 1936: The oscillations of the atmosphere. Proc. Roy. Soc., A156, 318-326.
- Titchmarsh, E. C., 1962: Eigenfunction Expansions Associated with Second Order Differential Equations, vol. I, second edition. Oxford University Press, London, 203 pp.

Whitham, G. B., 1974: Linear and Nonlinear Waves. John Wiley and Sons, New York, 636 pp.

Wiin-Nielsen, A., 1971: On the motion of various vertical modes of transient, very long waves, Part I. Beta plane approximation. Tellus, 23, 87-98.

† English translation available from S. Fulton, Department of Atmospheric Science, Colorado State University.

## APPENDIX A: The nature of the phase speed spectrum

The vertical boundary conditions (2.23) and (2.24) chosen for this study reduce the vertical structure problem (i.e., the solution of the vertical structure equation) to one of the Sturm-Liouville type. Consequently, the phase speeds form a countably infinite and hence discrete set. The nature of the phase speed spectrum with other vertical boundary conditions and its dependence on  $\Gamma(z^*)$  is the subject of this Appendix.

Let us first discuss the lower boundary condition. The condition (2.23) permits parcels of air to cross the lower boundary of the model (i.e.,  $z^*=0$ ), thus allowing an oscillation of the atmosphere as a whole in the vertical known as the external mode. It is well known (e.g., Wiin-Nielsen, 1971) that this mode is eliminated if it is required that  $w^*=0$  at the lower boundary. It can be shown that the effect of this more restrictive boundary condition on the internal modes is small.

The question of the upper boundary condition is more complicated and of greater consequence. The condition (2.24) is a perfect reflector; i.e., it does not allow vertically propagating waves to leave the model and hence traps energy in the vertical. Conceptually, any other linear homogeneous boundary condition applied at a finite level in the atmosphere will have the same effect; mathematically this implies that the corresponding phase speed spectrum is discrete. An upper boundary condition which allows energy to propagate vertically out of the model is conceptually different; this physical difference shows up in the mathematical treatment in that the phase speed spectrum may have a continuous part.

Jacobs and Wiin-Nielsen (1966) show that when the requirement of finite vertical flux of wave energy is used as an upper boundary condition for an infinite isothermal atmosphere the resulting phase speed spectrum has both a discrete and a continuous part. The discrete part is associated with the external mode (or, with  $w^* = 0$  at the lower boundary, the nondivergent barotropic mode) and the continuous part is  $0 < c^2 < 4\kappa R\bar{T}$ , corresponding to the internal modes. In studies of free atmospheric oscillations (i.e., when no forcing is considered) the continuous part of the spectrum is often eliminated by applying more restrictive upper boundary conditions, such as requiring the total kinetic energy in a column of unit cross-sectional area to be finite (Siebert, 1961). However, for initial value problems these internal modes are crucial, being the components out of which the initial conditions (minus the part projected onto the external mode, if any) are formed. The mathematical effect of allowing such a continuous spectrum is to turn the discrete eigenfunction expansion used in this study into an appropriate integral transform in the vertical.

In general the effect of the vertical stratification of the basic state as expressed by  $\Gamma(z^*)$  is to modify the phase speeds and vertical structure functions somewhat but not to change the fundamental nature of the spectrum. Two important exceptions to this statement exist. First, when  $\Gamma(z^*)$  is such that  $p \rightarrow 0$  at a finite height, the spectrum becomes discrete even when the upper boundary condition is simply that the solution remain bounded (Eckart, 1960). An atmosphere with constant lapse rate in actual height  $z$  is an example of this case (Siebert, 1961). The other case, discussed by Lindzen and Blake (1972), occurs when a thermosphere of very high temperature is included in the

model. Here the external mode may have a phase speed, determined primarily by the tropospheric temperature profile due to the density factor  $e^{-z^*}$  which appears in the vertical structure equation, which is small enough that it may have an oscillatory behavior in the upper atmosphere where the temperatures are higher. Such a wave propagates slowly in the vertical and thus an external wave in the strictest sense does not exist.

APPENDIX B: Properties of the eigenvalues and eigenfunctions

In this Appendix we show that the eigenvalues  $c_n^2$  and eigenfunctions  $Z_n(z^*)$  satisfy the following properties:

- (i) the eigenvalues  $c_n^2$  are real
- (ii) the eigenfunctions  $Z_n(z^*)$  form an orthonormal set

We note that these properties are a result of the fact that the vertical structure problem is of the Sturm-Liouville type (Arfken, 1970).

The vertical structure equation is

$$\frac{d}{dz^*} \left( \frac{e^{-z^*}}{R\Gamma} \frac{dZ_n}{dz^*} \right) + \frac{e^{-z^*}}{c_n^2} Z_n = 0 . \quad (B1)$$

Replacing  $n$  by  $m$  in (B1) and taking the complex conjugate (denoted by a dagger  $\dagger$ ) results in

$$\frac{d}{dz^*} \left( \frac{e^{-z^*}}{R\Gamma} \frac{dZ_m^\dagger}{dz^*} \right) + \frac{e^{-z^*}}{(c_m^2)^\dagger} Z_m^\dagger = 0 . \quad (B2)$$

Then multiplying (B1) by  $Z_m^\dagger$  and (B2) by  $Z_n$  and subtracting yields

$$\begin{aligned} Z_m^\dagger \frac{d}{dz^*} \left( \frac{e^{-z^*}}{R\Gamma} \frac{dZ_n}{dz^*} \right) - Z_n \frac{d}{dz^*} \left( \frac{e^{-z^*}}{R\Gamma} \frac{dZ_m^\dagger}{dz^*} \right) \\ = \left[ \frac{1}{(c_m^2)^\dagger} - \frac{1}{c_n^2} \right] Z_n Z_m^\dagger e^{-z^*} . \end{aligned} \quad (B3)$$

The left-hand side of (B3) may be rewritten to obtain

$$\frac{d}{dz^*} \left[ \frac{e^{-z^*}}{R\Gamma} \left( Z_m^\dagger \frac{dZ_n}{dz^*} - Z_n \frac{dZ_m^\dagger}{dz^*} \right) \right] = \left[ \frac{1}{(c_m^2)^\dagger} - \frac{1}{c_n^2} \right] Z_n Z_m^\dagger e^{-z^*} . \quad (B4)$$

Integrating (B4) from  $z^* = 0$  to  $z^* = z_T^*$  we obtain

$$\begin{aligned}
& \left[ \frac{e^{-z^*}}{R\Gamma} \left( Z_m^\dagger \frac{dZ_n}{dz^*} - Z_n \frac{dZ_m^\dagger}{dz^*} \right) \right]_{z^*=0}^{z^*=z_T^*} \\
& = \left[ \frac{1}{(c_m^2)^\dagger} - \frac{1}{c_n^2} \right] \int_0^{z_T^*} Z_n(z^*) Z_m^\dagger(z^*) e^{-z^*} dz^* .
\end{aligned} \tag{B5}$$

Applying the boundary conditions (2.29) and (2.30) to (B5) we find that the left-hand side vanishes so that

$$\left[ \frac{1}{(c_m^2)^\dagger} - \frac{1}{c_n^2} \right] \int_0^{z_T^*} Z_n(z^*) Z_m^\dagger(z^*) e^{-z^*} dz^* = 0 . \tag{B6}$$

Now if we set  $m=n$  in (B6) the integral term is positive so we must have  $(c_n^2)^\dagger = c_n^2$ . Thus  $c_n^2$  is real, which establishes property (i). Also, if  $m \neq n$  in (B6) and the eigenvalues  $c_m^2$  and  $c_n^2$  are distinct we obtain

$$\int_0^{z_T^*} Z_n(z^*) Z_m^\dagger(z^*) e^{-z^*} dz^* = 0 . \tag{B7}$$

Thus eigenfunctions which correspond to distinct eigenvalues are orthogonal in the sense of (B7). If any eigenvalue has two or more linearly independent eigenfunctions associated with it, they may also be made orthogonal in the sense of (B7) by means of the Gram-Schmidt orthogonalization procedure. Therefore the eigenfunctions form an orthogonal set. Since the vertical structure equation is linear the eigenfunctions are defined only to within an arbitrary multiplicative constant. We choose that constant for each  $n$  so that

$$\int_0^{z_T^*} |Z_n|^2 e^{-z^*} dz^* = 1 . \tag{B8}$$

Then we may combine (B7) and (B8) as

$$\int_0^{z_T^*} Z_n(z^*) Z_m^\dagger(z^*) e^{-z^*} dz^* = \delta_{mn} \quad , \quad (\text{B9})$$

where

$$\delta_{mn} = \begin{cases} 1 & m = n \\ 0 & m \neq n \end{cases}$$

is the Kronecker delta. Therefore the eigenfunctions  $Z_n$  form an orthonormal set, establishing property (ii).

APPENDIX C: Asymptotic solution of the horizontal structure equation

The exact solution (2.65) of the horizontal structure equation (2.36) is expressed in terms of double integrals and is therefore somewhat complicated (and time consuming) to evaluate numerically. Therefore, in this Appendix we derive an asymptotic solution by the method of stationary phase (Whitham, 1974). This asymptotic form serves as a check on the calculation of the exact solution and is useful in the numerical evaluation of the solution at large times.

The starting point for this derivation is (2.58), which we write in the form

$$\chi_n(x, y, t) = \chi_n^{(1)}(x, y, t) + \chi_n^{(2)}(x, y, t) \quad (C1)$$

where

$$\chi_n^{(1)}(x, y, t) = \frac{1}{2\pi} \int_{-\infty}^{\infty} \int_{-\infty}^{\infty} A_n(k, \ell) e^{-i(kx + \ell y - v_n t)} dk d\ell$$

and

$$\chi_n^{(2)}(x, y, t) = \frac{1}{2\pi} \int_{-\infty}^{\infty} \int_{-\infty}^{\infty} B_n(k, \ell) e^{-i(kx + \ell y + v_n t)} dk d\ell .$$

Treating  $\chi_n^{(1)}$  first, we hold  $x$ ,  $y$ , and  $t$  fixed and define

$$\sigma_n(k, \ell) = \frac{kx + \ell y}{t} - v_n(k, \ell) \quad (C2)$$

so that

$$\chi_n^{(1)}(x, y, t) = \frac{1}{2\pi} \int_{-\infty}^{\infty} \int_{-\infty}^{\infty} A_n(k, \ell) e^{-i\sigma_n(k, \ell)t} dk d\ell . \quad (C3)$$

According to the method of stationary phase, if  $A(k, \ell)$  does not vary rapidly and  $t$  is large enough, the major contributions to the integral in (C3) will be obtained near the stationary points of  $\sigma_n(k, \ell)$ ; i.e., near these points where  $\partial\sigma_n/\partial k = \partial\sigma_n/\partial \ell = 0$ . Substituting for  $v_n(k, \ell)$  in (C2) from (2.57) we find that  $\sigma_n(k, \ell)$  has the unique stationary point  $(k'_n, \ell'_n)$  given by

$$(k'_n, \ell'_n) = \text{sgn}(t) \frac{|f|}{c_n} \frac{(x, y)}{(c_n^2 t^2 - x^2 - y^2)^{1/2}} \quad (C4)$$

with corresponding frequency

$$v'_n = v_n(k'_n, \ell'_n) = \frac{c_n |ft|}{(c_n^2 t^2 - x^2 - y^2)^{1/2}} \quad (C5)$$

Then near this stationary point we approximate  $A_n(k, \ell)$  by  $A_n(k'_n, \ell'_n)$  and, using Taylor's theorem,

$$\begin{aligned} \sigma_n(k, \ell) \approx & \sigma_n(k'_n, \ell'_n) + \frac{1}{2} \left[ \frac{\partial^2 \sigma_n}{\partial k^2} \Big|_{(k'_n, \ell'_n)} (k - k'_n)^2 \right. \\ & \left. + 2 \frac{\partial^2 \sigma_n}{\partial k \partial \ell} \Big|_{(k'_n, \ell'_n)} (k - k'_n) (\ell - \ell'_n) + \frac{\partial^2 \sigma_n}{\partial \ell^2} \Big|_{(k'_n, \ell'_n)} (\ell - \ell'_n)^2 \right]. \end{aligned}$$

With these approximations, (C3) reduces to

$$\chi_n^{(1)}(x, y, t) \approx A_n(k'_n, \ell'_n) e^{-i(k'_n x + \ell'_n y - v'_n t)} E_n(x, y, t) \quad (C6)$$

where

$$\begin{aligned} E_n(x, y, t) \equiv & \frac{1}{2\pi} \int_{-\infty}^{\infty} \int_{-\infty}^{\infty} \exp \left\{ \frac{it}{2} \left[ \frac{\partial^2 v_n}{\partial k^2} \Big|_{(k'_n, \ell'_n)} (k - k'_n)^2 \right. \right. \\ & \left. \left. + 2 \frac{\partial^2 v_n}{\partial k \partial \ell} \Big|_{(k'_n, \ell'_n)} (k - k'_n) (\ell - \ell'_n) + \frac{\partial^2 v_n}{\partial \ell^2} \Big|_{(k'_n, \ell'_n)} (\ell - \ell'_n)^2 \right] \right\} dk d\ell, \end{aligned} \quad (C7)$$

having substituted for  $\sigma_n(k, \ell)$  from (C2).

The integral in (C7) has the form of an "error" integral in two dimensions and may be evaluated as follows. First, we employ vector notation to write (C7) as

$$E_n(x, y, t) = \frac{1}{2\pi} \int_{-\infty}^{\infty} \int_{-\infty}^{\infty} \exp \left[ \frac{it}{2} (M \underline{k}, \underline{k}) \right] dk d\ell, \quad (C8)$$

where

$$M \equiv \begin{bmatrix} \frac{\partial^2 v_n}{\partial k^2} & \frac{\partial^2 v_n}{\partial k \partial \ell} \\ \frac{\partial^2 v_n}{\partial \ell \partial k} & \frac{\partial^2 v_n}{\partial \ell^2} \end{bmatrix} (k_n', \ell_n')$$

$$\underline{k} \equiv \begin{bmatrix} k - k_n' \\ \ell - \ell_n' \end{bmatrix},$$

and  $(\underline{u}, \underline{v})$  represents the ordinary  $\mathbb{R}^2$  inner (dot) product  $\underline{u} \cdot \underline{v}$ .

Evaluating  $M$  using (2.57), (C4) and (C5) leads to

$$M = \frac{(c_n^2 t^2 - x^2 - y^2)^{1/2}}{c_n |ft| t^2} \begin{bmatrix} c_n^2 t^2 - x^2 & -xy \\ -xy & c_n^2 t^2 - y^2 \end{bmatrix}.$$

Now the key to simplifying (C8) is to diagonalize  $M$ . The eigenvalues of  $M$  are found to be

$$\left. \begin{aligned} \lambda_1 &= \frac{(c_n^2 t^2 - x^2 - y^2)^{3/2}}{c_n |ft| t^2} = \frac{f^2 c_n^2}{v_n'^3} \\ \lambda_2 &= \frac{(c_n^2 t^2 - x^2 - y^2)^{1/2}}{|ft|} = \frac{c_n^2}{v_n'} \end{aligned} \right\} \quad (C9)$$

and

If  $r \equiv (x^2 + y^2)^{1/2} > 0$ ,  $\lambda_1$  and  $\lambda_2$  are distinct and correspond to the unit eigenvectors

$$\tilde{v}_1 = \frac{1}{r} \begin{bmatrix} x \\ -y \end{bmatrix}$$

and

$$\tilde{v}_2 = \frac{1}{r} \begin{bmatrix} y \\ x \end{bmatrix},$$

respectively, and we can define the real, orthogonal transformation matrix  $P$  by

$$P = \begin{bmatrix} \tilde{v}_1 \rightarrow \\ \tilde{v}_2 \rightarrow \end{bmatrix} = \frac{1}{r} \begin{bmatrix} x & -y \\ y & x \end{bmatrix}.$$

If  $r = 0$  then  $\lambda_1 = \lambda_2 = (c_n/f)^2$  and we define  $P$  as the  $2 \times 2$  identity matrix. Then in both cases

$$PMP^{-1} = D = \begin{bmatrix} \lambda_1 & 0 \\ 0 & \lambda_2 \end{bmatrix}$$

so that if we define  $\underline{\alpha} = \begin{bmatrix} \alpha_1 \\ \alpha_2 \end{bmatrix}$  by  $\underline{\alpha} = P\underline{k}$ , the fact that  $P$  is real and orthogonal implies that

$$\begin{aligned} (M_{\underline{k}, \underline{k}}) &= (P^{-1} D P_{\underline{k}, \underline{k}}) \\ &= (D P_{\underline{k}, \underline{k}}) \\ &= (D \underline{\alpha}, \underline{\alpha}) \\ &= \lambda_1 \alpha_1^2 + \lambda_2 \alpha_2^2. \end{aligned}$$

Making this substitution in (C8) and noting that  $\frac{\partial(\alpha_1, \alpha_2)}{\partial(k, l)} = \det P = 1$  we obtain

$$E_n(x,y,t) = \frac{1}{2\pi} \int_{-\infty}^{\infty} \int_{-\infty}^{\infty} \exp \left[ \frac{it}{2} (\lambda_1 \alpha_1^2 + \lambda_2 \alpha_2^2) \right] d\alpha_1 d\alpha_2 . \quad (C10)$$

The transformation

$$\beta_1 = \exp \left[ -i \operatorname{sgn}(t) \frac{\pi}{4} \right] \left( \frac{|t| \lambda_1}{2} \right)^{1/2} \alpha_1 ,$$

$$\beta_2 = \exp \left[ -i \operatorname{sgn}(t) \frac{\pi}{4} \right] \left( \frac{|t| \lambda_2}{2} \right)^{1/2} \alpha_2$$

then reduces (C10) to the real "error" integral

$$E_n(x,y,t) = \frac{i}{\pi t} \cdot \frac{1}{(\lambda_1 \lambda_2)^{1/2}} \int_{-\infty}^{\infty} \int_{-\infty}^{\infty} e^{-(\beta_1^2 + \beta_2^2)} d\beta_1 d\beta_2 .$$

Using polar coordinates we easily obtain the value  $\pi$  for the double integral in this expression; finally, substituting for  $\lambda_1$  and  $\lambda_2$  from (C9) we obtain

$$E_n(x,y,t) = \frac{i|f|t}{c_n^2 t^2 - x^2 - y^2} . \quad (C11)$$

With the substitution (C11), (C6) becomes

$$X_n^{(1)}(x,y,t) \approx \frac{i|f|t A_n(k'_n, l'_n)}{c_n^2 t^2 - x^2 - y^2} e^{-i(k'_n x + l'_n y - v'_n t)} . \quad (C12)$$

An argument similar to that above shows that

$$X_n^{(2)}(x,y,t) \approx - \frac{i|f|t B_n(-k'_n, -l'_n)}{c_n^2 t^2 - x^2 - y^2} e^{i(k'_n x + l'_n y - v'_n t)} . \quad (C13)$$

Noting from (2.60) that  $B_n(-k'_n, -l'_n) = A_n^\dagger(k'_n, l'_n)$ , (C12) and (C13) imply that  $X_n^{(2)}(x,y,t) = [X_n^{(1)}(x,y,t)]^\dagger$ . Thus (C1) reduces to

$$X_n(x,y,t) \approx 2\text{Re} [X_n^{(1)}(x,y,t)] .$$

Substituting for  $X_n^{(1)}$  from (C12) and making use of (2.60a) we obtain

$$X_n(x,y,t) \approx \frac{|f|t}{c_n^2 t^2 - x^2 - y^2} \left[ \tilde{X}_n(k_n', \ell_n', 0) \sin(k_n' x + \ell_n' y - v_n' t) + \frac{1}{v_n'} \frac{\partial \tilde{X}_n}{\partial t}(k_n', \ell_n', 0) \cos(k_n' x + \ell_n' y - v_n' t) \right] .$$

Finally, substituting for  $k_n'$  and  $\ell_n'$  from (C4) and  $v_n'$  from (C5), the asymptotic form of  $X_n$  may be written as

$$X_n(x,y,t) \approx -f|t| \frac{\sin[(f/c_n)(c_n^2 t^2 - x^2 - y^2)^{1/2}]}{c_n^2 t^2 - x^2 - y^2} \tilde{X}_n(k_n', \ell_n', 0) + \frac{\text{sgn}(t)}{c_n} \frac{\cos[(f/c_n)(c_n^2 t^2 - x^2 - y^2)^{1/2}]}{(c_n^2 t^2 - x^2 - y^2)^{1/2}} \frac{\partial \tilde{X}_n}{\partial t}(k_n', \ell_n', 0) . \quad (\text{C14})$$

With the axisymmetric, non-divergent initial conditions assumed in section 3.2 the above results may be expressed as follows. First, since  $\psi(r)$  as defined by (3.28) is axisymmetric the Fourier transform and zero-order Hankel transform of  $\psi(r)$  are equivalent, so that

$$\tilde{\psi}(k, \ell) = \hat{\psi}(\hat{k}) \equiv \int_0^\infty \psi(r) J_0(\hat{k}r) r dr ,$$

where  $\hat{k} = (k^2 + \ell^2)^{1/2}$  and  $J_0$  is the Bessel function of the first kind of order zero. Then substituting (3.26) into (C14) and comparing the result with (3.29) we find that the asymptotic form of  $F_n$  is

$$F_n(r,t) \approx c_n \operatorname{sgn}(t) \frac{\cos[(f/c_n)(c_n^2 t^2 - r^2)^{1/2}]}{(c_n^2 t^2 - r^2)^{1/2}} \hat{\psi}(\hat{k}_n'), \quad (C15)$$

where, from (C4),

$$\hat{k}_n' = \frac{|f|}{c_n} \cdot \frac{r}{(c_n^2 t^2 - r^2)^{1/2}}. \quad (C16)$$

In order to use this result the initial conditions as expressed by  $\psi(r)$  must be transformed in the horizontal and evaluated at  $\hat{k}_n'$  as defined by (C16). Care should be exercised here because for some initial conditions  $\hat{\psi}(\hat{k})$  varies rapidly enough near  $\hat{k}_n'$  that the above derivation breaks down. Finally, it should be noted that the above solution is valid only for  $c_n^2 t^2 \gg r^2$  so that if  $G_n(r,t)$  is to be obtained by integrating (C15) in time, the integration must be performed from  $t = \infty$  backwards to a finite time  $t$ , making use of the final adjusted state calculation (3.33).

## APPENDIX D: Principal Symbols

A, B, C, D	constants
$A_n, B_n$	Fourier amplitudes of gravity-inertia waves
D	vertical structure of initial tangential wind and perturbation geopotential
$D_n$	projection of D onto vertical mode n
$E_n$	two-dimensional "error" integral in asymptotic solution
$F_n, G_n$	auxiliary horizontal structure functions
M	matrix of second partials of $v_n$ in asymptotic solution
P	transformation matrix in asymptotic solution
R	gas constant for dry air
T, $\bar{T}$ , T'	temperature (absolute): total, basic state, perturbation
$T_0, T_\infty$	constant static stability basic state temperature at $z^*=0$ and $z^*=\infty$
$U_n, V_n$	horizontal structure functions for wind field
$W_n$	auxiliary vertical structure function
$X_n, Y_n$	horizontal structure functions
$Z_n$	vertical structure function
$c_n$	phase speed (eigenvalue of vertical structure equation)
$c_p$	specific heat at constant pressure for dry air
f	constant Coriolis parameter
g	acceleration due to gravity
$h_n$	equivalent depth
k, $\ell$	Fourier transform parameters (horizontal wavenumbers)

$\hat{k}$	vertical unit vector; Hankel transform parameter
$p$	pressure
$p_0$	fixed surface pressure
$r$	horizontal coordinate in axisymmetric geometry
$t$	time
$u, v$	radial and tangential wind components
$\tilde{v}$	horizontal wind vector
$\hat{v}$	horizontal structure of initial tangential wind
$w$	vertical velocity in $z$ -coordinate
$w^*$	vertical velocity in $z^*$ -coordinate
$\tilde{x}$	horizontal position vector
$x, y$	horizontal coordinates in Cartesian geometry
$z$	geopotential height
$z^*$	$\equiv \ln(p_0/p)$ : log-pressure vertical coordinate
$\Gamma$	static stability in log-pressure coordinate
$\Phi, \bar{\Phi}, \Phi'$	geopotential: total, basic state, perturbation
$\hat{\Phi}$	horizontal structure of initial perturbation geopotential
$\Psi$	arbitrary function
$\Omega$	potential vorticity
$\delta$	horizontal divergence
$\delta_{mn}$	Kronecker delta
$\zeta$	vertical component of relative vorticity
$\eta$	$\equiv 1/2 - \Gamma/T_0$
$\kappa$	$\equiv R/c_p$
$\lambda_1, \lambda_2$	eigenvalues of $M$ in asymptotic solution

$\lambda_n$	$\equiv (R\Gamma/c_n^2 - 1/4)^{1/2}$ : vertical wavenumber (internal modes)
$\mu_n$	$\equiv (1/4 - R\Gamma/c_n^2)^{1/2}$ : vertical wavenumber (external mode)
$\nu_n$	$\equiv [f^2 + c_n^2 (k^2 + \ell^2)]^{1/2}$ : frequency of mode $n$
$\sigma_n$	$\equiv (kx + \ell y)/t - \nu_n$
$\chi$	local time derivative of perturbation geopotential
$\psi$	horizontal structure of initial departure from geostrophy

BIBLIOGRAPHIC DATA SHEET		1. Report No. CSU-ATSP-326	2. Recipient's Accession No.
3. Title and Subtitle  GEOSTROPHIC ADJUSTMENT IN A STRATIFIED ATMOSPHERE		5. Report Date August, 1980	
4. Author(s) Scott R. Fulton and Wayne H. Schubert		6.	
7. Performing Organization Name and Address Department of Atmospheric Science Colorado State University Foothills Campus Fort Collins, CO 80523		8. Performing Organization Rept. No. CSU-ATSP-326	
9. Sponsoring Organization Name and Address National Science Foundation		10. Project/Task/Work Unit No.	
11. Supplementary Notes		11. Contract/Grant No. ATM-7808125 ATM-8009799	
12. Abstracts		13. Type of Report & Period Covered	
<p>The geostrophic adjustment process in a compressible atmosphere with arbitrary vertical stratification is studied as an initial value problem. The governing equations are the adiabatic quasi-static equations on an f-plane linearized about a motionless basic state. A rigid lid upper boundary condition is assumed which permits the use of a discrete eigenfunction expansion in the vertical. Using Fourier transforms in the horizontal a general solution is obtained for both the transient and final states.</p> <p>The general solution is evaluated for several simple experiments with axisymmetric initial conditions in the mass and vorticity fields which have horizontal variations on the tropical cloud cluster scale. These experiments assume a basic state characterized by constant static stability in log-pressure coordinates and a Coriolis parameter corresponding to 20°N latitude. Results are presented which illustrate the nature of the transient adjustment process. Comparison of the</p>		14.	
15. Key words and Document Analysis. 17a. Descriptors			
<p>geostrophic adjustment gravity-inertia waves</p>			
17b. Identifiers/Open-Ended Terms			
<p>16. Abstract continued: initial and final states indicates that the inclusion of vertical structure does not alter the basic conclusion from previous barotropic studies that in the tropics the mass field tends to adjust to the wind field. However, it is found that the extent of this adjustment depends strongly on the vertical structure of the initial conditions. These results are interpreted in terms of the projection of the initial conditions onto the vertical modes.</p>			
17c. COSATI Field/Group			
18. Availability Statement		19. Security Class (This Report) UNCLASSIFIED	21. No. of Pages 97
		20. Security Class (This Page) UNCLASSIFIED	22. Price